2mi4

NASA TECHNICAL NOTE

NASA TN D-7509

NASA TN D-7509

EN ROUTE POSITION AND TIME CONTROL OF AIRCRAFT USING KALMAN FILTERING OF RADIO AID DATA

by Leonard A. McGee and Jay V. Christensen

Ames Research Center
Moffett Field, Calif. 94035

NATIONAL AERONAUTICS AND SPACE ADMINISTRATION • WASHINGTON, D. C. • DECEMBER 1973

1. Report No. NASA TN D-7509	2. Government Accession No.	3. Recipient's Catalog No.
4. Title and Subtitle EN ROUTE POSITION AND TIME CONTROL OF AIRCRAFT USING KALMAN FILTERING OF RADIO AID DATA		5. Report Date December 1973 6. Performing Organization Code
7. Author(s) Leonard A. McGee and Jay V. Christensen		8. Performing Organization Report No. A-3505
9. Performing Organization Name and Address Ames Research Center Moffett Field, Calif., 94035		10. Work Unit No. 115-17-01-01-00-21 11. Contract or Grant No.
12. Sponsoring Agency Name and Address National Aeronautics and Space Administration Washington, D. C. 20546		13. Type of Report and Period Covered Technical Note 14. Sponsoring Agency Code
15. Supplementary Notes		

16. Abstract

Fixed-time-of-arrival (FTA) guidance and navigation is investigated as a possible technique capable of operation within much more stringent en route separation standards and offering significant advantages in safety, higher traffic densities, and improved scheduling reliability, both en route and in the terminal areas.

This study investigates the application of FTA guidance previously used in spacecraft guidance. These FTA guidance techniques have been modified and are employed to compute the velocity corrections necessary to return an aircraft to a specified great-circle reference path in order to exercise en route time and position control throughout the entire flight. The necessary position and velocity estimates to accomplish this task are provided by Kalman filtering of data from Loran-C, VORTAC/TACAN, Doppler radar, radio or barometric altitude, and altitude rate. The guidance and navigation system was evaluated using a digital simulation of the cruise phase of supersonic and subsonic flights between San Francisco and New York City, and between New York City and London.

It was found that the fixed-time-of-arrival guidance system is capable of easily meeting the present lateral separation standards and of maintaining en route timing errors to less than 30 sec over intercontinental routes.

17. Key Words (Suggested by Author(s))	18. Distribution Statement
En route timing, fixed-time-of-arrival guidance, Kalman filtering, on-board digital computer, cruise phase, great-circle route, digital simulation	Unclassified – Unlimited

19. Security Classif. (of this report)	20. Security Classif. (of this page)	21. No. of Pages	22. Price*
Unclassified	Unclassified	101	Domestic, $4.25 Foreign, $6.75

* For sale by the National Technical Information Service, Springfield, Virginia 22151

TABLE OF CONTENTS

TABLE OF CONTENTS — CONCLUDED

SYMBOLS

d	slant range from transmitter to receiver
H	Jacobian matrix relating data-set quantities and vehicle state (2×6 matrix)
I	identity matrix with appropriate dimensions
K	weighting matrix (6×2)
LOP	line-of-position
P	covariance matrix of estimation error vector, $E(\tilde{x}\ \tilde{x}^T)$, ($6 \times 6$ matrix)
ΔP	correction to the P matrix for wander from the predicted path
P_1, P_2, P_3, P_4	3×3 submatrices of P
P^*	P transformed into altitude, along-track, cross-track coordinates
Q	covariance matrix of the data-set measurement errors (2×2 matrix)
rms	root mean square
$r(t)$	position deviation vector from the reference position at time t
R	covariance matrix of the deviation between the actual reference states, $E(xx^T)$
ΔR	correction to the R matrix following a course correction maneuver
Δs	commanded change in ground speed
S	vector from center of earth to a station on surface
SNR	signal-to-noise-ratio
t	general time argument, hr
t_k	time of the kth data-set sample
t_k^-	time of the kth data-set sample but further updating required
δt	deviation of the arrival time from the reference arrival time
$v(t)$	velocity deviation vector from its reference value
V	total velocity vector, with respect to earth-fixed coordinate frame

$\|V\|$	magnitude of V
x	deviation of state vector from reference state vector (6×1 matrix)
X	state of vector of position and velocity (6×1 matrix)
δ Δ	increment
ΔX	change in state vector (6×1 matrix)
$\Delta\psi$	commanded change in aircraft heading angle
$\Delta\theta$	commanded change in aircraft pitch angle
y	measured data-set
α	correlation decay coefficient
σ	standard deviation of subscript random variable
$\Phi(t_2, t_1)$	transition matrix relating deviation state at t_2 to deviation state at t_1

Notation Conventions

$(\dot{\ })$	first time derivative of ( ) with respect to an earth-fixed frame
$(\ddot{\ })$	second time derivative of ( )
$(\hat{\ })$	estimate of ( )
$(\tilde{\ })$	error in the estimate of ( )
E( )	expected value of ( )
$(\ )^T$	transpose of matrix ( )
$(\ )^{-1}$	inverse of matrix ( )

Subscripts

A	actual
E	estimated
ENV	envelope

k	at the kth data set
meas	measured
R	reference
REC	receiver
x	Loran-C slave station x
y	Loran-C slave station y
λ	longitude
ϕ	latitude

EN ROUTE POSITION AND TIME CONTROL OF AIRCRAFT USING KALMAN FILTERING OF RADIO AID DATA

Leonard A. McGee and Jay V. Christensen

Ames Research Center

SUMMARY

Fixed-time-of-arrival (FTA) guidance and navigation is investigated as a possible technique capable of operation within much more stringent en route separation standards and offering significant advantages in safety, higher traffic densities, and improved scheduling reliability, both en route and in the terminal areas.

Thus study investigates the application of FTA guidance previously used in spacecraft guidance. These FTA guidance techniques have been modified and are employed to compute the velocity corrections necessary to return an aircraft to a specified great-circle reference path in order to exercise en route time and position control throughout the entire flight. The necessary position and velocity estimates to accomplish this task are provided by Kalman filtering of data from Loran-C, VORTAC/TACAN, Doppler radar, radio or barometric altitude, and altitude rate. The guidance and navigation system was evaluated using a digital simulation of the cruise phase of supersonic and subsonic flights between San Francisco and New York City, and between New York City and London.

Performance is evaluated with emphasis on the ability of the system to maintain position and time control along the great-circle reference paths.

It was found that the fixed-time-of-arrival guidance system is capable of easily meeting the present lateral separation standards and of maintaining en route timing errors to less than 30 sec over intercontinental routes.

INTRODUCTION

As air traffic density steadily increases, it is important to improve accuracy in the estimation and control of aircraft position and velocity so that separation of aircraft may be reduced without increasing the risk of collision. In particular, if a reliable and accurate en route timing capability can be attained, then significant advantages in safety, higher traffic densities, air traffic control procedures, and economies associated with aircraft scheduling will result.

It is felt that on-board digital computer technology has improved to the point where advanced computer-oriented integrated systems techniques can be

considered in the improvement of aircraft navigation and guidance. The larger, more expensive jet aircraft, such as the jumbo jets and supersonic transports may well find the application of a computer-oriented system to be economically justifiable. Such a system would hold potential for improvement of the present method of arrival time control.

This study investigates the performance of a computer-oriented system which utilizes Kalman filtering of data from VORTAC/TACAN, Loran-C, a radio altimeter, a barometric altimeter, and Doppler radar for navigation. The guidance technique of this investigation is based on the well-known fixed-time-of-arrival guidance previously used successfully for midcourse guidance of spacecraft (ref. 1). This guidance technique is modified appropriately for the aircraft cruise phase guidance problem and is used by the navigation and guidance system throughout the flight to compute the necessary changes in direction and speed that will return the aircraft to a reference great-circle route and maintain the aircraft on-time throughout the entire flight. The results obtained are from a simulation on a digital computer of the cruise phase of flight for supersonic and subsonic flights between San Francisco and New York City, and between New York City and London. The necessary position and velocity estimates are provided by Kalman filtering of data from Loran-C, VORTAC/TACAN, Doppler radar, a radio altimeter, or a barometric altimeter. Error models for these subsystems are derived and discussed. The radio aids were assumed to be of the latest types with ground equipment locations currently operational along the selected routes. The following factors were included in the study: (a) attitude measurement uncertainty; (b) aircraft wander between data samples due to external disturbances; and (c) number and timing of course corrections.

Performance is evaluated with emphasis on the ability of the system to meet an established time of arrival at a fixed position. Performance is also evaluated on the basis of: (a) error in the estimation of position and velocity; (b) course correction requirements in terms of heading and velocity magnitude changes that are required; and (c) the ability of the system to control the aircraft position and velocity with respect to a selected great-circle reference route.

SYSTEM DESCRIPTION

General Description of the On-Board System

The on-board navigation and guidance system that was investigated is illustrated in figure 1. Simulated data from the sensors included random errors generated from sensor error models.

The functions carried out by the estimation and guidance system computer are receiver channel selection and sensor sampling, data filtering and estimation of the aircraft state, and course correction commands for fixed-time-of-arrival guidance. The on-board sensors sampled successively by the computer for data filtering are the Doppler radar system, which measures

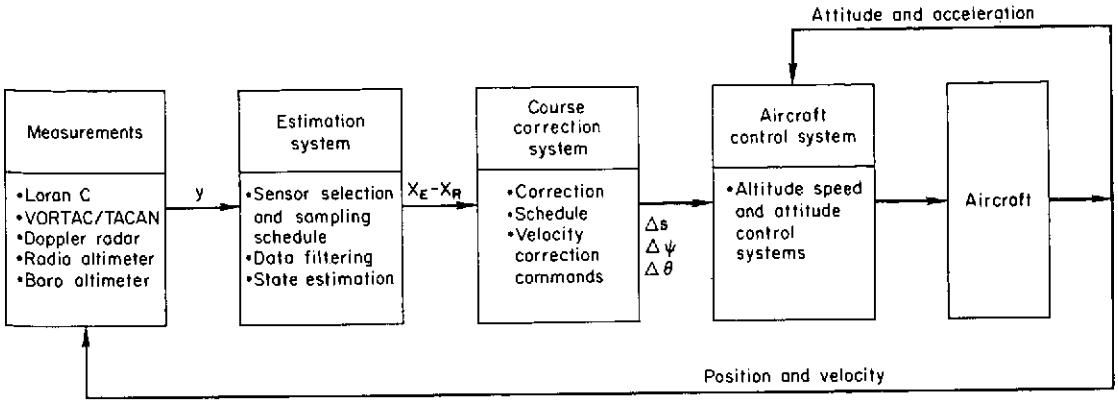

Figure 1.— The on-board navigation and guidance system.

groundspeed and drift angle, and the radio altimeter or the air-data system, both of which measure altitude and altitude rate. The computer also samples other sensors used in data filtering computations which derive their basic information from ground station radio transmissions. The Loran-C receiver is used to obtain signals from which latitude and longitude are computed by a coordinate converter. The VORTAC/TACAN receivers are used to determine the range and bearing of the aircraft relative to the selected ground station. Other on-board sensors which are not used directly by the computer in filter computations but are used by the other on-board systems are the vertical and heading references, which measure aircraft pitch, roll, and heading, and a body-mounted accelerometer, which measures longitudinal acceleration.

Also on-board is an automatic control system which is in operation continuously throughout all flights. Its functions are to: (1) change the aircraft heading in accordance with computer commands necessary to fly a great-circle course; (2) maintain heading within specified limits; (3) maintain altitude within specified limits; and (4) respond to course correction commands from the on-board computer. This system cannot fly the aircraft along a preprogrammed reference path without error because the on-board sensors on which it must rely for information are imperfect measuring devices. As a result of these imperfections and external disturbances, the aircraft will drift from the reference course to such an extent that some corrective action is necessary for both en route safety and adherence to schedule. This correction is provided by an on-board navigation system, which determines the aircraft position and velocity, and the on-board guidance system, which computes the necessary corrections to the groundspeed, altitude, and heading which will return the aircraft to the reference path. Indeed, a sufficient number of course corrections are desirable to keep the aircraft within a specified distance of the reference path, to keep it on-time, and to maintain safe separation from other aircraft.

Flight Environment

Great-circle reference routes— The great-circle reference routes between San Francisco (SF) and New York City (NYC), and between New York City and London (L), are illustrated in figure 2. This figure also shows the existing Atlantic area Loran-C stations that were used in this study.

The principal difference between these two flight paths is the type of position data that is available. For the first 75 percent of the land route from San Francisco to New York City, only VORTAC/TACAN is available. During the remaining 25 percent, both VORTAC/TACAN and Loran-C are available. Position information in the vertical direction is obtained from an on-board barometric altimeter which is part of an air-data system and is used in preference to a radio altimeter, which measures the altitude above the local terrain instead of above the mean sea level. Over the water route from New York City to London, longitude and latitude information is obtained from Loran-C exclusively, even when near New York City, because it provides more accurate information than VORTAC/TACAN. Altitude information is obtained from a radio altimeter since there are no terrain effects to consider.

Cruise conditions— The cruise phases of flight for two different aircraft are considered. Each aircraft attempts to follow a reference great-circle path from origin to destination, with a fixed-time-of-arrival at the destination. The entire reference cruise flight from origin to destination is at the specified cruise altitude and groundspeed for each aircraft. The two reference cruise conditions considered will be referred to hereafter as "supersonic" and "subsonic." The supersonic cruise conditions represent an aircraft flying at a reference groundspeed of 3,000 km/hr (1,620 knots) at 21.336 km (70,000 ft) altitude. For the subsonic cruise, the reference groundspeed is 1,000 km/hr (540 knots) and the altitude is 10.668 km (35,000 ft).

The initial and final position coordinates of the great-circle reference routes are summarized below:

	San Francisco	New York	London
Latitude	37.634° north	40.634° north	52.000° north
Longitude	122.359° west	73.783° west	1.000° west

External disturbances— The forecast wind over the originating airport was assumed arbitrarily to be 100 km/hr from 210° relative to true north. The random component was realized from a normal distribution with zero mean and with a standard deviation in both the along-track and cross-track directions of 25 km/hr. The initial heading of the aircraft was altered to "crab" the aircraft into the average wind in order to aline the ground velocity vector along the desired track; the estimated groundspeed was adjusted accordingly. In this study the aircraft was considered to have sufficient reserve power so that there would be no difficulty in adjusting the airspeed to obtain the desired groundspeed. During the remainder of the flight, the effects of random winds were brought into the problem by random time-correlated variations in the aircraft ground track, heading and velocity.

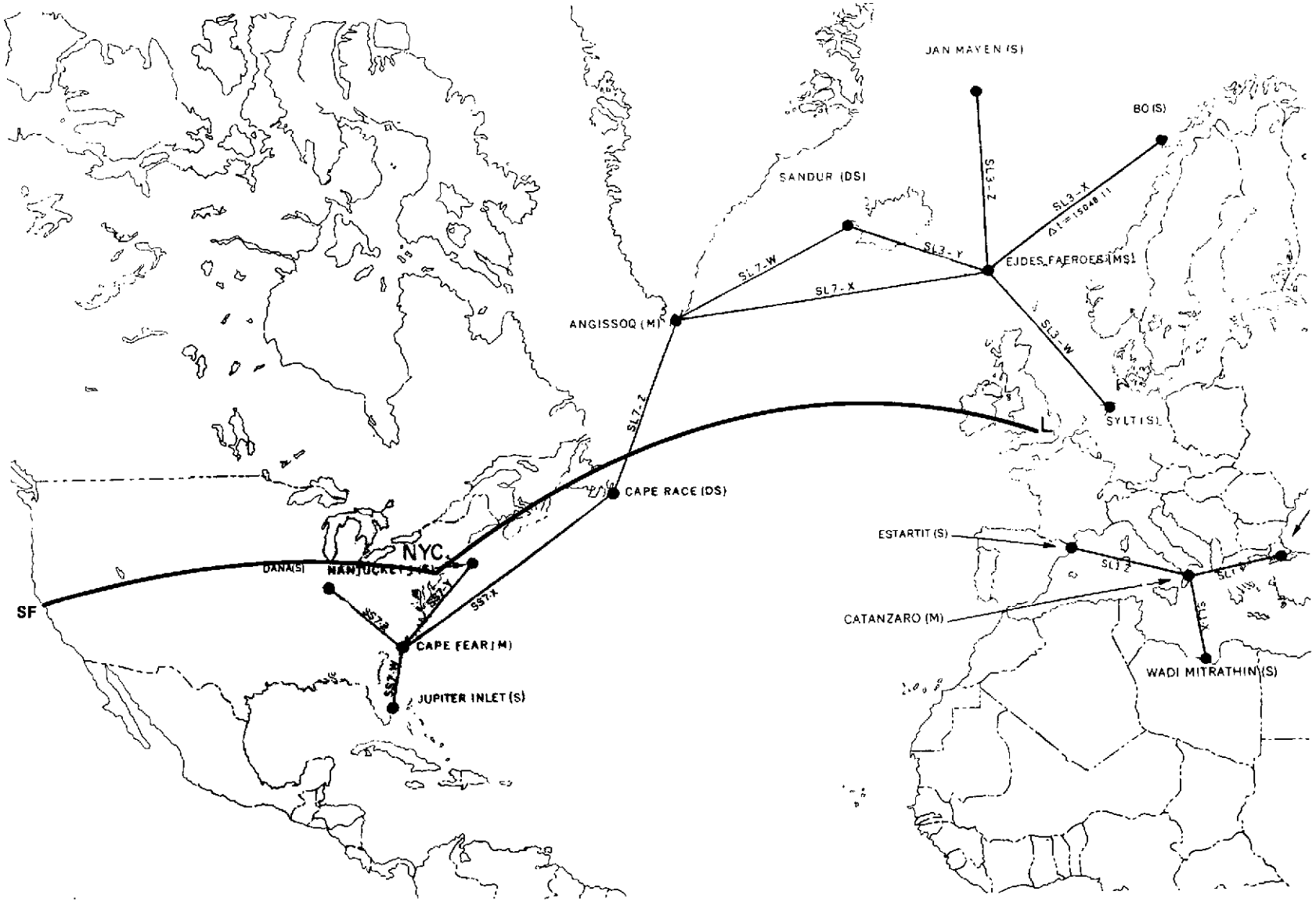

Figure 2.— DOD map showing the two flight paths and Loran-C stations.

Changes in the steady-state wind components were found by averaging the Doppler drift angle and integrating the acceleration from the body-mounted accelerometer along the aircraft longitudinal axis. The Doppler drift angle measures the angle between the ground track velocity vector and the aircraft longitudinal axis in the horizontal plane. Averaging this angle over several seconds gives an estimate of the change in the cross-track steady-state wind; this value was used by the computer to compensate for the change in aircraft heading. Similarly, integrating the output of the accelerometer (compensated for deviations from the level state) gives an estimate in the along-track change in the steady-state wind.

Desired time en route— The main objective of this study was to investigate fixed-time-of-arrival guidance and navigation. The objective of the guidance system was to fly a great-circle reference course with the en route times given in the following table.

Route	Flight time (min)	
	Subsonic	Supersonic
S.F. to N.Y.C.	250.079	83.360
N.Y.C. to London	330.066	110.022

For simplicity, a fixed sample rate was used, with adjustments to the rate when useful.

Data sampling— For the supersonic case, sensors are selected and sampled every minute except for one special case, in which the sample rate is increased to 2/min just prior to course corrections. For the subsonic case, sensors are sampled every 3 min. The sensors are sampled in a sequential pattern. A typical pattern is VORTAC/TACAN or Loran-C first; Doppler radar, second; and an altimeter, third.

The following logic was used for accepting VORTAC/TACAN and Loran-C dataset samples: slant ranges to all the stations are computed based on the aircraft's estimated position and the coordinates of the stations. For VORTAC/TACAN, the station with the minimum slant range is used if the slant range is less than 275 km (148 nmi). If the slant range is greater than 275 km, the sample is skipped. For Loran-C, the signals from three stations are required. The triad having the smallest slant range to its farthest station is selected and the position sample is accepted if: (1) the slant range is less than 2800 km (1628 nmi); and (2) the line-of-position (*LOP*) crossing angle is greater than 25°. If the slant range is greater than 2800 km, then no other station triad can meet the acceptance requirements and the sample is skipped. If the *LOP* crossing angle is less than 25°, the acceptance criteria are repeated for another station triad with the next larger slant range to its farthest station. This process is repeated until a suitable station triad is found or the sample is skipped because the slant range requirement cannot be met.

Course corrections— In selecting a course correction strategy, it was required that the strategy demonstrate effectiveness both in reducing the lateral position dispersion during flight (air corridor) and in maintaining the aircraft on-time with a reasonable amount of aircraft maneuvering. The strategy should also function satisfactorily with thresholds which must be exceeded by the commanded changes before execution would be allowed. These thresholds were imposed to reduce the probability of making course corrections which would cause greater course error than already present due to errors in executing the course correction. For the selected strategy each course correction consists of two maneuvers as illustrated in figure 3. The first maneuver at

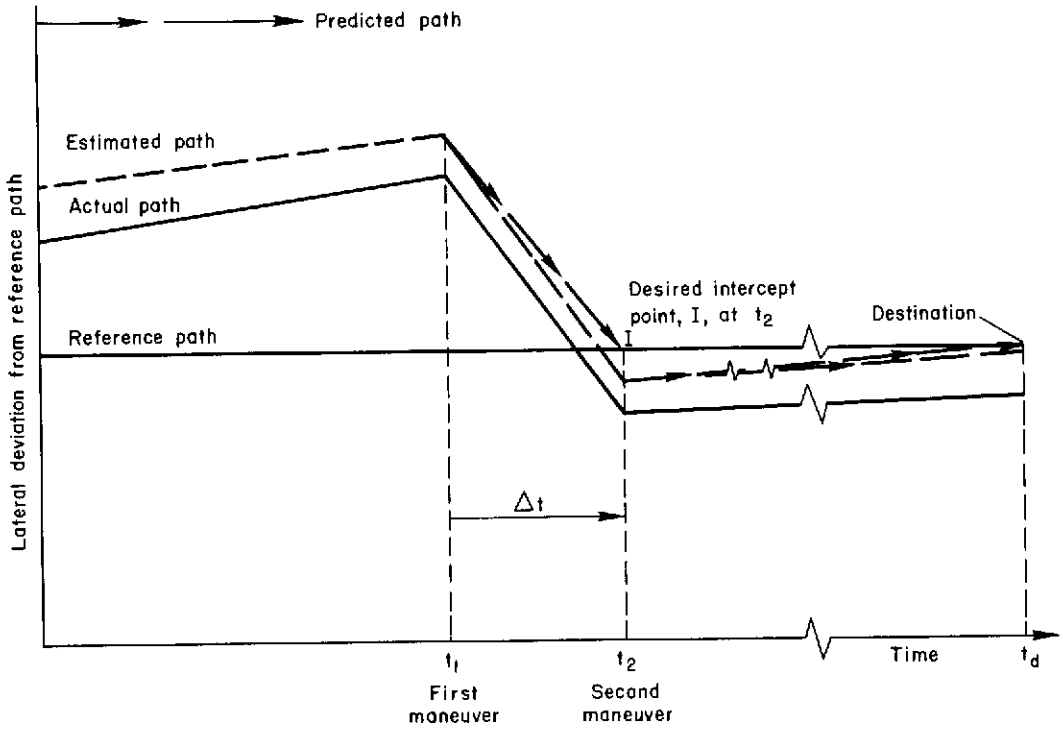

Figure 3.— Typical two-maneuver course correction.

t_1 is designed to cause the aircraft to intercept the reference flight path at point I after a fixed time Δt. The value of Δt is taken as 5 and 15 min, respectively, for the supersonic and subsonic cases. Because of external disturbances during Δt and errors in making the correction at t_1, the aircraft will not exactly reach the intercept point I at t_2. This situation is to be expected and, if the state estimate at t_2 is reasonably accurate, causes no difficulty. A second correction maneuver is made at t_2 to intercept the destination at the desired time, t_d. Again, because of control errors, navigation errors, and course correction errors, the actual path will not exactly follow the predicted path as is shown in figure 3. Even though these correction maneuvers are executed with some error, it will be shown later that

this is an effective course correction strategy capable of meeting the requirements specified.

Course corrections are implemented as a change in aircraft speed and heading. A change in altitude rate is also computed but the changes were always less than the threshold value and therefore not used.

To gain insight into the fundamental properties of the two-maneuver course correction strategy, a simplified example involving only speed and heading change will be examined. Consider sketch (a), which depicts the first maneuver of the two-maneuver strategy.

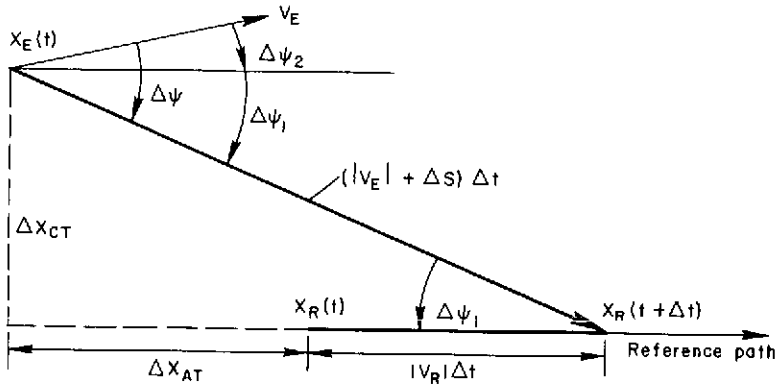

Sketch (a)

where

ΔX_{AT} along-track error

ΔX_{CT} cross-track error

V_R reference groundspeed

V_E estimated groundspeed

X_E estimated position

$\Delta\Psi$ required heading change from V_E: $\Delta\Psi_1 + \Delta\Psi_2$

Δs required change in groundspeed

Δt fixed time to intercept point

From the geometry of sketch (a):

$$(|V_E| + \Delta s)\Delta t = [(|V_R|\Delta t + \Delta X_{AT})^2 + \Delta X_{CT}^2]^{1/2}$$

$$= |V_R|\Delta t[(1 + \Delta X_{AT}/|V_R|\Delta t)^2 + (\Delta X_{CT}/|V_R|\Delta t)^2]^{1/2} \qquad (1)$$

$$\tan \Delta\psi_1 = \frac{\Delta X_{CT}}{\Delta X_{AT} + |V_R|\Delta t} = \frac{\Delta X_{CT}/|V_R|\Delta t}{1 + \Delta X_{AT}/|V_R|\Delta t} \tag{2}$$

Assuming ΔX_{AT} and $\Delta X_{CT} << |V_R|\Delta t$, then $\Delta\psi_2$ is a small angle. Using this assumption,

$$(|V_E| + \Delta s)\Delta t = |V_R|\Delta t\left[1 + \frac{\Delta X_{AT}}{|V_R|\Delta t} + \frac{\Delta X_{AT}^2 + \Delta X_{CT}^2}{(|V_R|\Delta t)^2} + \cdots\right]$$

$$\cong |V_R|\Delta t + \Delta X_{AT} + \text{higher order terms} \tag{3}$$

$$\tan \Delta\psi_1 \cong \Delta\psi_1 \cong \frac{\Delta X_{CT}}{|V_R|\Delta t} \tag{4}$$

from which

$$\Delta s \cong (|V_R| - |V_E|) + \Delta X_{AT}/\Delta t \tag{5}$$

$$\Delta\psi \cong \Delta\psi_2 + \Delta X_{CT}/V_R\Delta t \tag{6}$$

From equations (5) and (6), it is seen that the speed and heading changes each consist of two terms; the first term corrects for the current error in velocity or heading ($|V_R| - |V_E|$ or $\Delta\psi_2$) and the second term corrects for current position errors. Considering position errors to a first order approximation, the speed change, Δs, corrects the along-track (or en route timing) error and the heading change corrects the cross-track error. These are important relationships which will aid in interpreting the course correction data to be presented in a following section.

The times at which the course corrections are scheduled for the various cases are given in table 1. A fixed course correction sequence is used for

TABLE 1.— COURSE CORRECTION SCHEDULE (MIN EN ROUTE)

Course correction	Subsonic				Supersonic			
	NYC to L		SF to NYC		NYC to L		SF to NYC	
	Maneuver		Maneuver		Maneuver		Maneuver	
	First	Second	First	Second	First	Second	First	Second
1	21	36	15	30	12	17	11	16
2	48	63	60	75	42	47	38	43
3	111	126	105	120	72	77	62	67
4	156	171	150	165				
5	204	219	195	210				
6	246	261						
7	282	297						

each case to aid in comparing simulation results. Three course corrections are used on all the supersonic flights. Five course corrections are used on the subsonic San Francisco to New York City flights and seven on the subsonic New York City to London flights.

Error Models

Error models are mathematical representations of the error processes in taking measurements. These models are used in the simulation of the real (noisy) data, which are the inputs to the estimation system, and also as the statistical description of the measurement errors used in the Kalman filter state estimation computations. In many cases, accurate error models are difficult to obtain because it is usually necessary to select a representative device and contact the manufacturer for information. Often the manufacturer does not have complete information, especially if the device is new, and there is no alternative but to assume a model based only on what little data may be available.

The error models for the various subsystems are summarized in table 2 and discussed in the following text along with other models used in the simulation.

The sensors are sampled and processed by the Kalman filter state estimator; each sensor considered here provides a measurement of two quantities which are sampled simultaneously and called a data set. If the errors in the measured quantities have a bias error, it is assumed to be known to sufficient accuracy and subtracted from the particular measurement so that, in effect, the measurement errors can be considered to be Gaussian distributed random variables with a zero mean and a variance of σ^2. In order to process the measurements, a 2 × 2 covariance matrix of the measurement errors, $Q(t_k)$, must be given for the particular sensor being sampled. This covariance matrix is of the form

$$Q(t_k) = \begin{bmatrix} \sigma_1^2 & \rho_{12}\sigma_1\sigma_2 \\ \rho_{12}\sigma_1\sigma_2 & \sigma_2^2 \end{bmatrix}$$

where σ_1, σ_2, and ρ_{12} are the standard deviations and correlation, respectively, of the errors in the measurements of the two quantities in a data set.

The measurement subsystem error models are dependent upon assumptions regarding their operational characteristics. On-board equipment is assumed to be modern lightweight digital equipment using modern noise rejection techniques to improve the operational range and accuracy. The ground equipment for VORTAC/TACAN stations used in this study are assumed to have a useful range of 275 km at an altitude of 21.336 km (70,000 ft). The Loran-C ground transmitting stations are assumed to have equipment similar to that in more recently established installations.

TABLE 2.— SUMMARY OF SUBSYSTEM ERROR MODELS

Subsystem	Error model expression — Standard Deviations
Loran-C	Latitude error = f(prediction errors + instrumentation errors + coordinate converter errors + station geometry errors) Longitude error = f(prediction errors + instrumentation errors + coordinate converter errors + station geometry errors)
VORTAC/TACAN	Range error = transmitter = 0.55 km receiver = $0.055 + 0.165\times10^{-3}$ Bearing error = 1.3865° × range (km)
Doppler radar	Velocity magnitude error = $0.002\lvert V_R\rvert$ km Drift angle error = 0.2°
Radio altimeter	Altitude error = 0.030 km = 100 ft Altitude rate error = $0.5 + 0.005\lvert\dot{h}_A\rvert$ km/hr
Air data	Altitude error = 0.183 km = 600 ft Altitude rate error = $1.0 + 0.1\lvert\dot{h}_A\rvert$ km/hr
Vertical and heading reference	Short period roll, pitch, and heading errors = 0.25° Long period pitch and roll errors = 0.25° or 0.50° Long period heading errors = (0.25° or 0.50°) + 0.1°/hr
Body-mounted accelerometer	Acceleration error = 0.01 g
Altitude and attitude control system	Altitude control error = 0.183 km = 600 ft Roll control error = 2.0° Heading control error = limited to $< \pm\sqrt{2.0}°$
Speed control	Error in speed control = 5.0 km/hr

Except as noted, all values are 1 σ and based on a Gaussian distribution with a zero mean.

Loran-C— Loran-C ground transmitting station chains are arranged in geometric patterns consisting of combinations of one or more three-station triads designed to give maximum coverage to a particular area. Each triad of stations consists of two slave stations and a common master station and provides a position fix in its area of coverage. To conserve equipment, many complex station arrangements may be made in which a single station provides multiple functions, such as a double slave (DS), master-slave (MS), and so forth, in order to provide a large number of position-fixing triads.

Each master-slave pair produces synchronized pulses. At the receiver, the time difference between the arrival of two pulses (say TD_x) from one master-slave pair places the receiver on a line of constant time difference (hyperbola) called a line-of-position (*LOP*). Similarly, the time difference between the arrival of pulses from the same master and a second slave (say TD_y) places the receiver on a second *LOP*. The intersection of these two *LOP*'s is the position of the receiver. The latitude and longitude of the receiver is computed by a coordinate converter from two such time differences measured simultaneously and from position coordinates of the master and its slave stations. Maximum accuracy is obtained when the *LOP*'s crossing angle is 90° and when the groundwave propagation mode is used rather than the skywave mode, for which the signals are reflected from the ionosphere.

The accuracy of Loran-C position fixes using the groundwave propagation mode are dependent upon the following mutually independent error processes: (a) prediction errors in the groundwave propagation; (b) instrumentation errors in the ground station and in the on-board receiver; (c) coordinate converter errors; and (d) errors due to the geometrical arrangement of the master and slave stations and the aircraft.

Prediction errors arise from assumptions which must be made regarding such things as the conductivity and dielectric constants of the various media over which the groundwave must travel, uncertain earth shape, and aircraft altitude. Most of these errors can be reduced by calibration and/or compensation in the on-board computer. Therefore, in this report, the following uncertainties (1 σ) will be assumed for the prediction error sources:

1. Altitude — negligible after compensation based on estimated altitude; and

2. Earth shape and calibration uncertainty overwater and overland — 0.1 μsec (ref. 2 gives a value of 0.06 μsec over accurately surveyed land).

Instrumentation errors at the ground transmitting stations are due to inaccurate synchronization of master and slave stations. Reference 2 gives 0.02 μsec (1 σ) for this value. The on-board receiver is assumed to be able to accept instructions from the computer to select a particular station triad identified by the pulse repetition rate of the master station and two slave stations. The receiver continuously tracks the master and two slave stations so as to produce continuously two time differences. The uncertainty in the time difference measurements of the receiver depends on the signal-to-noise

ratio (SNR) of the received signals, which in turn depends on the distance from the transmitting station and the ambient noise factor. Following reference 2, the SNR is taken as

$$SNR_i = \begin{cases} 10 - \dfrac{1}{50\left(d_{\max_i} - 1300\right)}\,\text{dB} & 1300 < d_{\max} \leq 2800 \text{ km} \\ \text{greater than 10 dB} & d_{\max} < 1300 \text{ km} \end{cases} \qquad i = x,y \quad (8)$$

Here, x and y distinguish the two slave stations of the Loran-C triad and $d_{\max_i}$ is the larger of the distances (in km) to slave (i) or the master station. The SNR decreases linearly for distances greater than 1300 km and reaches the limit of receiver sensitivity (-20 dB) at 2800 km. This estimate of SNR is conservative and corresponds to an ambient noise factor of 40 dB above 1 μV, a 300 kW transmitter, and propagation across fair soil.

Following reference 3, the *rms* receiver errors in measuring TD_x and TD_y can be given by

$$(\sigma_i)_{REC} = 1.1(\sigma_i)_{ENV} \qquad i = x,y \quad (9)$$

where $(\sigma_i)_{ENV}$ is found from the expressions in the table below, in which SNR_i is the minimum master, slave (i) signal-to-noise ratio.

SNR_i; $i = x,y$	$(\sigma_i)_{ENV}$ (μsec) $i = x,y$
≥ 10 dB	0.05
< 10 dB	$+0.1957\times10^{-6}\ (SNR_i)^4$
	$-0.8338\times10^{-5}\ (SNR_i)^3$
	$+0.4069\times10^{-3}\ (SNR_i)^2$
	$-0.6128\times10^{-2}\ (SNR_i)$
	$+0.7730\times10^{-1}$

The variance of errors in the measurement of TD_x and TD_y at the receiver due to prediction, ground station, and receiver error sources are then:

$$\sigma_i^2 = (0.1)^2 + (0.02)^2 + (\sigma_i)^2_{REC} \qquad i = x,y \quad (10)$$

The coordinate converter computes latitude and longitude from the time differences TD_x and TD_y. The conversion is subject to some computation errors. Reference 4 gives some examples of conversion errors; if we assume they are typical, then the standard deviation of the latitude and longitude conversion

errors that could be expected are about 0.46" of arc (2.23×10^{-6} rad) and 0.59" of arc (2.86×10^{-6} rad), respectively.

The geometry of the station triad and the aircraft affects the uncertainties with which the two time differences TD_x and TD_y are converted to latitude and longitude. The geometrical effect is treated in appendix A where the covariance matrix, $Q_{\phi\lambda}$, is derived; this matrix relates latitude and longitude uncertainties to the total time difference variances, σ_x^2 and σ_y^2 and errors due to station-aircraft geometry. A final covariance matrix, $Q(t_k)$, that is used in the Kalman filtering of the Loran-C data sets can now be given:

$$Q(t_k) = Q_{\phi\lambda} + \begin{bmatrix} (2.23\times10^{-6})^2 & 0 \\ 0 & (2.86\times10^{-6})^2 \end{bmatrix} \tag{11}$$

The maximum usable range of Loran-C is assumed to be 2800 km. At this range, the signal-to-noise ratio is at the limit of the receiver sensitivity (-20 dB). In the event that no station triad has a maximum range less than 2800 km, the computer skips the position fix. In addition, if the line-of-position (*LOP*) crossing angle, as defined in appendix A, is less than 25° the computer attempts to use a more distant station triad.

VORTAC/TACAN— The military system TACAN operates in the UHF band. From the transmitted signals, an aircraft receiver is able to measure its magnetic bearing and slant range to the selected station. The bearing is measured by phase comparisons using coarse and fine frequencies of 15 and 135 Hz, respectively. The slant range is obtained from the Distance Measuring Equipment (DME) of TACAN, which measures the transit time of pulses sent from the aircraft to a ground transponder and return.

A VORTAC station is the colocation of a civil VHF Omnidirectional Range (VOR) station operating in the VHF band and a TACAN station operating in the UHF band. The VOR provides the same bearing information as does TACAN, but instead measures the phase difference between a 30 Hz signal whose phase is varied with magnetic heading and a reference 30 Hz signal. Slant range for the civil user is provided by the DME portion of TACAN.

Twenty-two VORTAC/TACAN stations which lie along the great-circle route from San Francisco to New York are used. The physical location of each of these stations is taken from a DOD Flight Information Publication (ref. 5) and each station is assumed to have either VORTAC or TACAN equipment. Station locations are listed in table 3. For this study it is assumed that all stations are located at sea level and have sufficient power output to be useful at 21.336 km (70,000 ft) altitude at a range of 275 km.

The on-board VORTAC/TACAN receiver is assumed to be a modern digital unit capable of rapid search, lock-on, and rapid channel switching as instructed by the on-board navigation computer. The station selection logic used in this

TABLE 3.— VORTAC/TACAN STATION LOCATIONS

Station	Latitude, north	Longitude, west
San Francisco	37°38'11"	122°21'36"
Stockton	37°50'01"	121°10'13"
Sacramento	38°26'37"	121°33'02"
Fallon NAAS	39°24'59"	118°42'10"
Wilson Creek	28°15'01"	114°23'36"
Bonneville	40°43'34"	113°45'24"
Provo	40°16'30"	111°56'23"
Myton	40°08'42"	110°07'37"
Meeker	40°04'03"	107°55'27"
Denver	39°51'39"	104°45'08"
Sidney	41°05'04"	103°06'09"
Grand Island	40°59'02"	98°18'52"
Omaha	41°10'02"	95°44'11"
Des Moines	41°26'15"	93°38'54"
Moline	41°19'16"	90°38'17"
Joliet	41°32'42"	88°19'06"
Southbend	41°46'07"	86°19'06"
Cleveland	41°21'29"	82°09'44"
Philipsburg	40°54'58"	77°59'35"
Selingsgrove	40°47'27"	76°53'04"
Yardly	40°15'12"	74°54'29"
Kennedy	40°37'50"	73°46'22"

report chooses the closest station. This process always resulted in selecting a station much closer than 275 km, yet sufficiently distant so that the aircraft was never in the "cone of confusion" above the selected station.

The same error models were used for both the VORTAC and the TACAN range and bearing measurements. These error models give the standard deviation of the error in the range and bearing measurements about a zero mean. The zero mean results from the assumption that constant receiver bias errors have been determined, that ground station bias errors versus bearing are known, and that a suitable method of correcting for them has been programmed into the on-board computer.

The *rms* range and bearing uncertainties due to transmitting station and receiver errors were taken from references 6 and 7 and are summarized below.

Measurement	Transmitter	Receiver
Range (km)	0.055 km (180 ft)	$0.055 \text{ km} + 0.16\times10^{-3} \times \text{range}$
Bearing	1.25°	0.6°

The transmitter and receiver errors are assumed to be independent random processes so that the $Q(t_k)$ matrix for VORTAC/TACAN range and bearing measurements taken simultaneously is

$$Q(t_k) = \left| \begin{array}{c|c} (0.055)^2 + (0.055 + 0.165\times10^{-3} \times \text{range})^2 & 0 \\ \hline 0 & (0.0242)^2 \end{array} \right| \qquad (12)$$

The uncertainties in range and bearing are assumed to be uncorrelated with each other and uncorrelated in time with their previous values, since the bias errors versus bearing and range are assumed to be removed by prior calibration of the ground and on-board equipment and subsequent storage of the calibration data in the on-board computer.

Doppler velocity and drift angle— The Doppler radar system assumed for this report is an on-board radar with four downward-looking pencil beams arranged much like the four legs of a draftsman's stool. The antenna radiating the four beams is space stabilized to the local vertical so that the radiation pattern on the surface below is not disturbed by rotational motions of the aircraft. By comparing the Doppler frequency shifts from each of the four beams with each other, the magnitude of the ground track velocity and the Doppler drift angle are determined continuously. The drift angle is the angle between the aircraft heading and the ground track velocity vector.

The Doppler radar system is assumed capable of operating to an altitude of 21.336 km (70,000 ft) with continuous output samples as needed by the digital computer. Velocity errors are assumed to be uncorrelated in time when the sampling interval is 30 sec or greater. The manufacturer's literature indicates that present Doppler equipment measures groundspeed with 0.2 percent *rms* uncertainty and drift angle with 0.2° *rms* uncertainty.

Because of the system mechanization, groundspeed and drift angle measurement errors are essentially uncorrelated. The Doppler drift angle measurement is combined with the current measurement of the aircraft heading to provide a measurement of ground track heading, GTH. The heading reference is in error by an amount independent of the Doppler drift angle so that the combined error in measuring the ground track heading is

$$\text{GTH } (1\ \sigma) = [(0.2)^2 + E\tilde{\psi}^2]^{1/2} \text{ deg} \qquad (13)$$

The heading reference error variance, $E\tilde{\psi}^2$, (from table 2) dominates the ground track heading standard deviation in equation (13), with the result that this measurement contributed little to the knowledge of ground track heading or, alternatively, the cross-track velocity. It does, however, provide a useful check on the performance of the automatic control system.

The matrix $Q(t_k)$ is computed as

$$Q(t_k) = \begin{bmatrix} (0.002|V_R|)^2 & 0 \\ 0 & (0.00349)^2 + E(\tilde{\psi}^2) \end{bmatrix} \qquad (14)$$

where the units are $(\text{km/hr})^2$ and $(\text{rad})^2$.

Radio altimeter— A radio altimeter is a downward-looking radar ranging system which measures the range from the aircraft to the surface below. The recent design trend is to integrate some of the functions of the radio altimeter with those of the Doppler radar. This integration allows a space stabilized antenna for the radio altimeter at low cost. The radio altimeter assumed for this report is a high power device capable of measuring altitude above the local surface, up to 21.336 km (70,000) ft). A radio altimeter was assumed only for flights overwater, since terrain effects would not have to be considered. The radio altimeter operates continuously and its output is sampled under control of the on-board digital computer. Reference 8 gives a 1 σ uncertainty of about 0.0061 km (20 ft) in the measurement of altitude for a system which has been adjusted immediately prior to the measurement. Since the system assumed here would not normally be adjusted prior to a measurement, the *rms* altitude uncertainty is taken as 0.0305 km (100 ft).

Altitude rate is obtained from the radio altimeter by measuring the Doppler shift in the carrier frequency, which in this application also suggests combining the functions of the radio altimeter and the Doppler radar. The manufacturer's literature for this type of equipment indicates that the uncertainty in the measurement of altitude rate is about 0.5 km/hr plus 0.5 percent of the altitude rate. Therefore, the $Q(t_k)$ matrix used for processing altitude and altitude rate is

$$Q(t_k) = \begin{bmatrix} (0.03)^2 & 0 \\ 0 & (0.5 + 0.005|\dot{h}_E|)^2 \end{bmatrix} \tag{15}$$

The errors in altitude and altitude rate are treated as uncorrelated because this relationship is implied in the literature. For example, in some of the more modern systems, the modulation of the carrier is sinusoidal and the altitude is found from the relative phase of the Bessel sidebands and the corresponding transmitted signal. The altitude rate, on the other hand, is measured by the Doppler shift of the carrier frequency.

Air data— An air-data computer which has aerodynamic and thermodynamic sensors is used overland to compute such quantities as altitude and altitude rate, airspeed, true airspeed, angle of attack, sideslip, and Mach number. The discussion at the end of the series of articles in reference 6 indicates that with very accurate calibration equipment, altitude from an air-data computer can be expected to have an *rms* uncertainty of about 0.183 km (600 ft) at 21.336 km at (70,000 ft) altitude. Very little information could be found regarding the accuracy of altitude rate from air-data computers. It was arbitrarily assumed that with the various compensations applied by the air-data computer, the *rms* uncertainty in altitude rate is the same at 10.668 km (35,000 ft) and 21.336 km (70,000 ft) altitude. The value chosen was 1.0 km/hr plus 10 percent of the estimated altitude rate. Therefore, the $Q(t_k)$ matrix for simultaneous processing of altitude and altitude rate was

$$Q(t_k) = \begin{bmatrix} (0.183)^2 & 0 \\ 0 & (1.0 + 0.1|\dot{h}_E|)^2 \end{bmatrix} \tag{16}$$

The altitude and altitude rate errors were assumed uncorrelated for simplicity. In addition, the uncertainty chosen for the altitude rate is sufficiently large so that the system essentially ignores the measurement. The poor measurement of altitude rate causes no difficulty because the guidance system attempts to maintain constant altitude while en route and therefore relies mostly on altitude measurements.

Vertical and heading references— The aircraft is assumed to be equipped with a vertical (or attitude) reference consisting of a vertical gyroscope with gravity sensing of the vertical. Vertical reference of this type, using third-order leveling and corrections for coriolis acceleration, are capable of relatively good accuracy in pitch and roll. In this report, the vertical reference is capable of measuring short period changes (a few seconds) in pitch and roll to an *rms* uncertainty of 0.25°. Over longer periods of time, the *rms* uncertainty is taken as either 0.25° or 0.5°, depending on the quality of the vertical reference. The *rms* errors are assumed to have a Gaussian distribution with a zero mean.

The heading reference can be mechanized in combination with the vertical reference, or, for example, with a directional gyroscope with magnetic sensor slaving, as has been assumed here. As with the vertical reference, the *rms* uncertainty over short periods of time was taken to be 0.25°; over longer periods of time, either 0.25° or 0.5° was assumed, depending on instrument quality. Since the magnetic variation is known to an uncertainty of about 0.1° over most of the earth's surface, a pseudodrift of the gyroscope of 0.1°/hr was assumed between course corrections to simulate the effect of this uncertainty.

Body-mounted accelerometer— An accelerometer is mounted at the center of gravity with its sensitive direction along the aircraft longitudinal axis. This accelerometer is used by the automatic control system to control the aircraft speed during cruise and to measure speed changes during course corrections. The accelerometer output is assumed to have a Gaussian-distributed error with a zero mean and a standard deviation of 0.01 g. Gravity-induced acceleration due to aircraft pitch attitude is compensated for in the on-board computer.

Automatic control system— An automatic control system (autopilot) is assumed to be in operation throughout the flights. Its functions are the following: (1) to maintain the attitude of the aircraft, that is, the pitch, roll, and commanded heading; (2) to hold the prescribed altitude; (3) to perform the required maneuvers to execute the commanded course corrections; and (4) to maintain speed or respond to commanded changes in the aircraft speed during course corrections (autothrottle). This automatic control system was also designed to permit constant rate climb-out and descent maneuvers even though they were not performed in this study. The course correction computations include a pitch change computation for this purpose.

To simplify computations, the control system on all flights was designed to: (1) maintain the cruise altitude to within an error whose standard deviation is 0.183 km (600 ft); (2) maintain the roll angle at the commanded value

to within an error whose distribution is Gaussian with a zero mean and a standard deviation of 2.0°; (3) maintain the heading such that the heading error is limited at $\pm\sqrt{2.0}^\circ$ and has a Gaussian distribution with a zero mean and a standard deviation of $\pm\sqrt{2.0}^\circ$ between these limits; and (4) control the speed to within an error which is Gaussian-distributed with a zero mean and a standard deviation of 5 km/hr.

Aircraft velocity vector wander between measurement data-sets— During the interval between processing two successive measurement data-sets at, say, t_{k-1} and t_k, the aircraft velocity vector wanders from that predicted by the equilibrium transition matrix derived in appendix B. This wander is due to random errors in controlling the effects in velocity of random disturbances in wind, air density, temperature, and so forth, which occur during (t_{k-1}, t_k).

The distribution of the wander error from the commanded velocity can, therefore be calculated from the automatic control system error model, and the acutal wander error is simulated by sampling this distribution.

Appendix C treats these error sources and derives expressions to modify the actual and estimated aircraft states and the R and P covariance matrices to account for the effect of wander from the equilibrium state. Once the computations in appendix C are complete, the Kalman filter computations described in the section on State Estimation are started.

The control system errors are modeled as correlated in time (appendix C). The numerical value of the correlation decay coefficient, α, was unspecified in appendix C. Early in this study it was decided to determine a single choice of α for all of the data runs since there was a large number of other variables to be considered. This choice was made by evaluating the effect of parameter α on system performance. Several runs were made with various values of α and it was found that performance was insensitive to values between 30/hr and 120/hr. As a result, the value α = 60/hr was chosen as being representative.

State Estimation

The objective of the state estimation system is to provide an accurate estimate of the actual aircraft state. To accomplish this objective, a Kalman filter is employed to process simulated measurement data-sets which are derived from the simulated actual aircraft state and statistical descriptions of the measurement noise. A block diagram of the computation flow involved in the state estimation is shown in figure 4.

The block diagram is divided into three portions. The upper portion illustrates the computation flow for the simulation of the aircraft state (actual state), including the computation of the actual add measured data-sets, The lower portion of the block diagram illustrates the computational flow in the reference path simulator. The center portion illustrates the computational flow of the estimation system. The estimation system is composed of an estimated path simulator (analogous to actual and reference path simulators), the Kalman filter, and the computation of the estimated data-set and residual error-set, which is used to compute corrections to the estimated state.

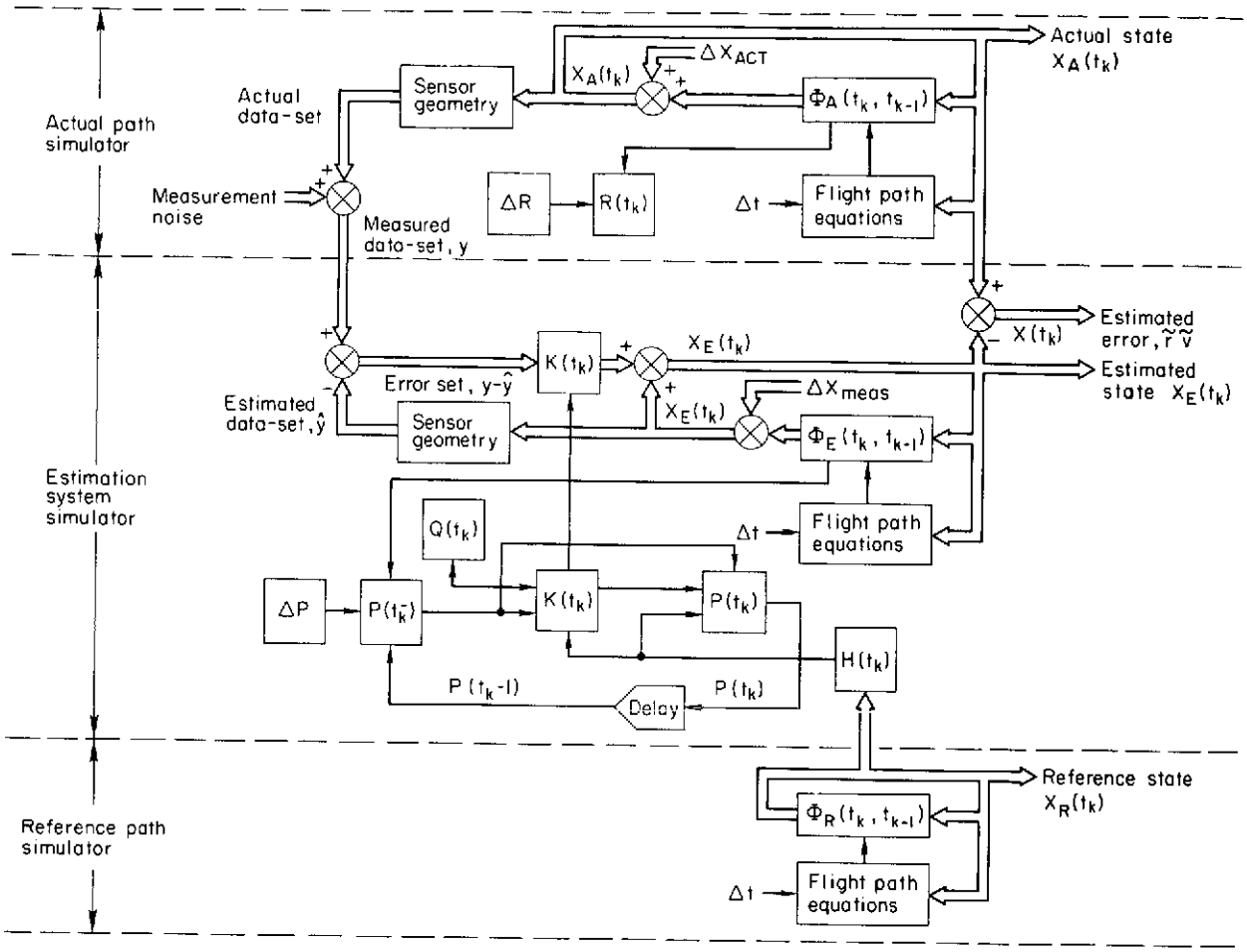

Figure 4.— Block diagram of computational flow for state estimation.

In the following detailed discussion of the computations embodied in the simulated system, the discussion is centered about the Kalman filter, since the simulation of both the actual and reference states involve only simple updating when a data-set is processed. The discussion is divided into five sections. The first four sections deal with the major divisions of the Kalman filter computations and the fifth section deals with computations for estimated performance evaluation. These sections are:

1. Updating the covariance matrices and the states from t_{k-1} to t_k.
2. Computation of the weighting matrix, $K(t_k)$.
3. Updating the covariance matrix, $P(t_k^-)$.
4. Computation of the corrected estimated state.
5. Computation of $\tilde{r}$ and $\tilde{v}$ for performance evaluation.

Updating the covariance matrices and the states from t_{k-1} to t_k— The covariance matrix of the errors in the prior estimated state, $P(t_{k-1})$, the covariance matrix of the prior deviations between the actual and reference states, $R(t_{k-1})$, and the three states X_A, X_R, and X_E are available after

processing the $(k - 1)$ the data-set. It is now desired to process the current data-set at time t_k. To initiate the processing the covariance matrices P and R, the estimated state, the actual state, and the reference state (6×1 vectors) must be updated through prediction from t_{k-1} to the current time t_k. This process is accomplished by use of their respective transition matrices $\Phi_i(t_{k-1}, t_k)$, where $i = A$, R, and E. The transition matrices are found from equations derived in appendix B.

The covariance matrix, $P(t_{k-1})$, is updated in time, using the equation

$$P(t_k) = \Phi_E(t_k, t_{k-1})P(t_{k-1})\Phi_E^T(t_k, t_{k-1}) + \Delta P \tag{17}$$

where the matrix ΔP (derived in appendix C) accounts for the errors in measuring the wander of the velocity vector during the time period $t_k - t_{k-1}$.

The matrix $R(t_k)$ used for performance evaluation is the covariance matrix of the error between the actual and reference states. It is updated using the equation

$$R(t_k) = \Phi_A(t_k, t_{k-1})R(t_{k-1})\Phi_A^T(t_k, t_{k-1}) + \Delta R \tag{18}$$

where ΔR is a covariance matrix that accounts for the effect of random perturbing forces on the actual path of the aircraft between data-set samples.

The actual, estimated, and reference states are updated by their respective transition matrices using the following equations:

$$X_A(t_k) = \Phi_A(t_k, t_{k-1})X_A(t_{k-1}) + \Delta X_A \tag{19}$$

$$X_E(t_k^-) = \Phi_E(t_k, t_{k-1})X_E(t_{k-1}) + \Delta X_E \tag{20}$$

$$X_R(t_k) = \Phi_R(t_k, t_{k-1})X_R(t_{k-1}) \tag{21}$$

where equations (19) and (20) also indicate the addition of the vectors ΔX_A and ΔX_E to produce the updated actual and estimated states. The vectors ΔX_A and ΔX_E are the actual and measured deviations from the paths predicted by the transition matrices $\Phi_A(t_k, t_{k-1})$ and $\Phi_E(t_k, t_{k-1})$, respectively, during the time, $t_k - t_{k-1}$. They are used to account for the random perturbing forces on the aircraft which are not modeled by the transition matrices and have covariance matrices ΔR and ΔP, respectively.

Computation of the weighting matrix, $K(t_k)$— After the updating computations are complete, the Kalman weighting matrix, $K(t_k)$, is computed as follows. First, the measurement Jacobian matrix, $H(t_k)$, is evaluated from partial derivatives of each of the measurement quantities in the particular measurement data-set being sampled. The H matrix has two rows since each measurement data-set consists of two measurement quantities. Expressions for the $H(t_k)$ matrices are derived in appendix D for each (Loran-C, VORTAC/TACAN, etc.) measurement data-set. Next the elements of a covariance matrix of the measurement

errors, $Q(t_k)$, (derived in the Error Models section) is evaluated for the appropriate data-set. Finally, the Kalman weighting matrix, $K(t_k)$, is computed from the expression:

$$K(t_k) = P(t_k^-)H^T(t_k)[H(t_k)P(t_k^-)H^T(t_k) + Q(t_k)]^{-1} \tag{22}$$

where the indicated matrix inversion involves only a 2 × 2 matrix.

Updating the covariance matrix, $P(t_k^-)$— After $K(t_k)$ has been computed, $P(t_k)$ is computed to reflect the reduction of the uncertainty between the actual and estimated states as a result of the information gained from the measurement data-set. The computation is carried out as follows:

$$P(t_k) = [I - K(t_k)H(t_k)]P(t_k^-) \tag{23}$$

where $P(t_k)$ is the corrected matrix. After a delay to the time when the next data-set sample is to be processed, $P(t_k)$ will become $P(t_{k-1})$, and is used in equation (17) as the initial information for the same sequence of updating and processing computations applied to the next measured data-set.

Computation of the corrected estimated state— The estimated state is updated to reflect information gained from processing a measured data-set. To simulate a measured data-set, an actual data-set is computed from the geometry of the aircraft relative to the earth and the actual state variables. Then measurement noise, which is generated according to the variance given in $Q(t_k)$, is added to the actual data-set to produce the measured data-set, y. This process differs from the procedure which would be followed on-board, since the actual state is not known and the measured data-set would be obtained from on-board equipment. The estimated data-set, $\hat{y}$, is computed from the same geometry of the aircraft with respect to the earth as was used above and the estimated state variables. A residual error-set, $y - \hat{y}$, is then computed by taking the difference between measured and estimated data-sets. The estimated state is updated using the following computation:

$$X_E(t_k) = X_E(t_k^-) + K(t_k)(y - \hat{y}) \tag{24}$$

where $X_E(t_k)$ is the updated estimated state.

The text above has given the detailed steps involved in processing a data-set with the Kalman filter to produce an updated estimate of the aircraft state. The difference between the actual state and the estimated state, often called the estimation error, may be considered a measure of estimation system performance since a perfect estimate of the aircraft state would result in zero estimation error.

Computation of $\tilde{r}$ and $\tilde{v}$ for performance evaluation— Figure 4 indicates the computation of the estimation error vector, $\tilde{X}(t_k)$, (6 × 1 vector) which is obtained by subtracting the estimated state from the actual state. The quantities $\tilde{r}$ and $\tilde{v}$ (3 × 1 vectors) are computed by taking the square root of the sum of the squares of the position and velocity terms, respectively, of $\tilde{X}(t_k)$.

This description completes the computational flow illustrated in figure 4 and is the sequence required to process a simulated measurement data-set; this process is repeated for each new measurement data-set.

Flight Path Control

After repeated use of the estimation procedure described above, a reasonably good estimate of the aircraft state should be available from the digital computer; the aircraft speed and heading can then be corrected using the estimated state and the known reference state. In this report, it is desired that corrections to the flight path return the aircraft to the reference path and maintain the reference position and velocity in order to arrive at the destination at a fixed time.

One way to accomplish this goal is by using the two-maneuver correction scheme shown in figure 3. When the aircraft arrives at the scheduled time of the first maneuver, t_1, the fixed time increment, Δt_1, and the estimated state are used to compute a transition matrix, $\Phi_E(t_2,t_1)$, from t_1 to t_2, as illustrated in figure 5. The fixed-time-of-arrival correction equations (see appendix E) are then used to compute Δv from the estimated and reference states.

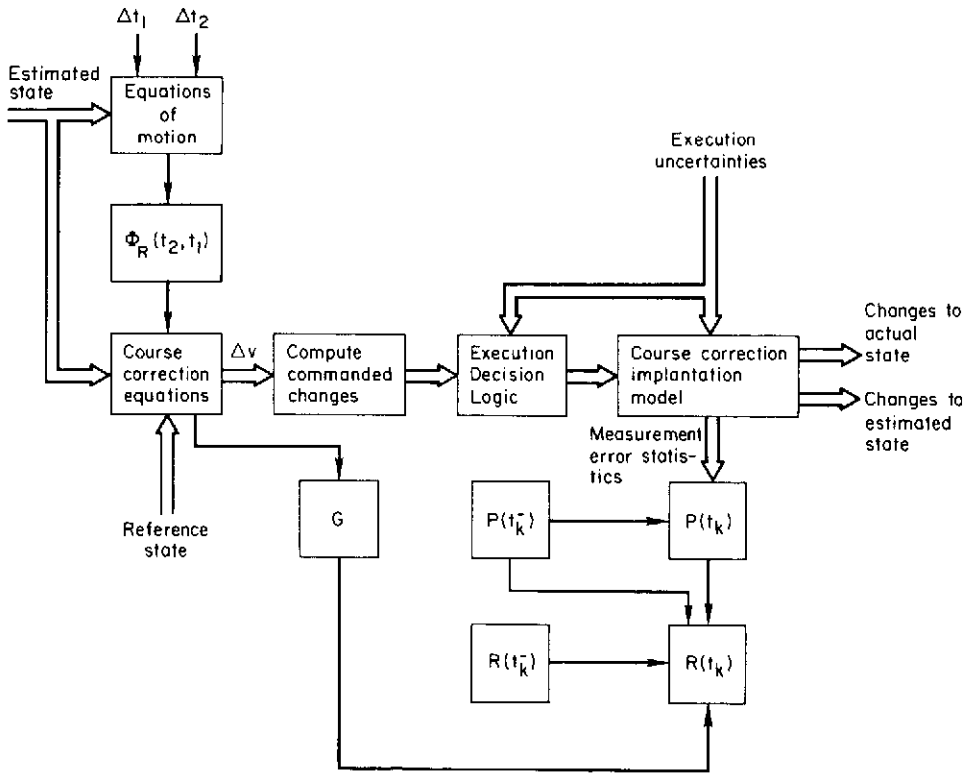

Figure 5.— Block diagram of fixed-time-of-arrival flight path control.

The increment Δv is the commanded change in the velocity vector required for the aircraft to arrive at the desired intercept point on the reference trajectory at time t_2.

This commanded velocity correction is transformed into pitch, heading, and speed corrections and compared to the execution uncertainty for each of these three variables. The execution uncertainty is considered to be the minimum response the control system can make. In pitch and heading, it is the short-term *rms* control error (0.25°) and in speed, it is the *rms* speed control error (5 km/hr). If any one of the commanded changes is less than its respective execution uncertainty, that commanded change is cancelled and only the remaining commands are executed according to the course correction implementation model (appendix E). The resulting changes are added to the actual and estimated states to implement the course correction.

After the course correction, $P(t_k)$ and $R(t_k)$ become $P(t_k^+)$ and $R(t_k^+)$ and must be adjusted for the effects of a course correction. This method is detailed in appendix E, but will be described in general here in order to complete the description of the block diagram in figure 5.

Following a course correction, the estimation errors are increased as a result of errors in measuring the executed course correction. Accordingly, $P(t_k^-)$ is changed, using:

$$P(t_k) = P(t_k^-) + \left[\begin{array}{c|c} 0 & 0 \\ \hline 0 & E(\eta\eta^T) \end{array}\right] \tag{25}$$

where $P(t_k)$ is the new covariance matrix. The 3×3 matrix $E(\eta\eta^T)$ is the covariance matrix (appendix E) of errors in measuring the executed correction. Next, to update the $R(t_k^+)$, a correction matrix, G, formed when Δv was computed in the fixed-time-of-arrival equations, is used along with $P(t_k)$ and $P(t_k^-)$ as follows:

$$R(t_k) = (I + G)[R(t_k^-) - P(t_k^-)](I + G)^T + P(t_k) \tag{26}$$

where $R(t_k)$ is the new matrix which replaces $R(t_k^-)$.

At time t_2, the aircraft will be near the desired reference path and the second maneuver of the two-maneuver course correction sequence must be implemented to aline the aircraft along this path. The second maneuver is executed in the same manner as the first, using the same flow of computations as shown in figure 5, with the following exceptions:

1. The intercept point is the desired destination.

2. The time-to-go to the desired destination replaces Δt.

3. The transition matrix is $\Phi_E(t_d, t_2)$, where t_d is the reference time at the destination.

Initialization of the Reference, Estimated, and Actual States

The initial reference state is found from the desired cruise altitude, the desired reference velocity magnitude, and the initial and final positions; it serves as a basis for the determination of the initial estimated and actual states. The initial reference position and velocity are derived from the position of the starting point, the direction of a great-circle route from this point to the destination, and the cruise speed of the aircraft. The computations are done in the following way: First, unit vectors from the center of the earth to the starting point, ℓ_1, and the final position (destination), ℓ_2, are found from their latitude and longitude. Second, the cruise initial position vector, L_R, is computed from

$$L_R = \ell_1 (R_e + h) \tag{27}$$

where h is the desired cruise altitude and R_e is the radius of the earth. Third, a unit vector, u, perpendicular to the plane of ℓ_1 and ℓ_2, is computed from:

$$u = \frac{\ell_1 \times \ell_2}{|\ell_1 \times \ell_2|} \tag{28}$$

Fourth, the reference angular velocity vector (with respect to the center of the earth) is then

$$\omega = \left(\frac{|V_R|}{R_e + h} \right) u \tag{29}$$

where $|V_R|$ is the desired magnitude of the reference groundspeed. Finally, the initial reference velocity vector is then

$$V_R = \omega \times L_R \tag{30}$$

The best estimated state at $t = 0$ is assumed to be the initial reference state. As a result, deviations between the actual and reference states, and the actual and estimated states, are initially identical. These initial deviations are assumed to be random variables with zero means and covariance matrices $R(0)$ and $P(0)$, respectively, which are also identical as a result of the above assumption.

The matrix $R(0)$ if found by assuming that the Doppler radar and on-board digital computer have a secondary "navigate" mode in which the along-track and cross-track components of velocity and computed position are use by the control system to reduce the effect of random disturbances such as wind and so forth, and to maintain control over the velocity vector from $t = -10$ min to $t = 0$, where navigation and guidance is taken over by the primary system. At this time, $R(0)$ is assumed to be the sum of a diagonal matrix representing the errors in initializing the secondary navigation mode and a second matrix

typical of the ΔR matrices, computed between measurement data-sets and representing the errors in the secondary navigation system from t = -10 min to t = 0. This computation was done by choosing δR as a diagonal matrix, which, when partitioned into 3 × 3 submatrices, is given by

$$\delta R = \begin{bmatrix} I & & 0 \\ & & \\ 0 & & 100\ I \end{bmatrix} \tag{31}$$

where δR is in the ALT, ALONG-TRACK, CROSS-TRACK coordinate system. The second matrix, $\Delta R(0,-10)$, was generated by evaluating the ΔR matrix (appendix C) for an attitude uncertainty of either 0.50° or 0.25° from t = -10 min to t = 0 min. The desired $R(0)$ matrix is then found from

$$R(0) = \Delta R(0,-10) + \delta R \tag{32}$$

The initial actual state deviations from the reference state are generated from $R(0)$ using a random number generator; these samples are added to the reference state to form the actual initial state. The initial deviation used for the sample cases of this study are summarized in table 4.

TABLE 4.— INITIAL DEVIATIONS OF ACTUAL STATE FROM REFERENCE STATE

	Attitude uncertainty, deg	Altitude	Along-track	Cross-track
Supersonic				
Position, km	0.50	1.353	0.209	-1.732
	.25	.722	.208	.924
Velocity, km/hr	.50	-9.065	1.859	29.025
	.25	-5.281	1.924	19.000
Subsonic				
Position, km	.50	.556	.208	-.712
	.25	.376	.208	-.481
Velocity km/hr	.50	-4.370	1.922	16.592
	.25	-3.481	1.923	14.239

It should be noted that the four cases in table 4 are essentially one individual case with identical initial conditions at t = -10 min. The differences at t = 0 are due to the differences in velocity and the attitude uncertainty.

PERFORMANCE EVALUATION

Performance evaluation computations were included as an integral portion of the simulation which was programmed in FORTRAN IV and executed on an IBM 7094 computer. As a result of past experience with state estimation algorithms programmed on this computer, some special precautions were taken to prevent round-off errors from dominating both the simulation results and the

performance evaluation computations. These precautions included double precision vector dot and cross product calculations, forced symmetry of the covariance matrices, and forming the elements of a matrix product by accumulating products according to the sign prior to the final addition to form the elements. In addition, performance calculations were done in double precision. All other computations were done in single precision.

For on-board computation, it seems likely that computers with shorter word lengths than the IBM 7094 would require at least partial control of numerical round-off in the vector and matrix operations. In addition, a method of preserving symmetry of the P and R matrices is recommended. Recent advances with computational techniques have made the "square root" form of the Kalman filter appear attractive for on-board computations. Although some double precision computations may be required with this method, the symmetry, for example, is assured.

Estimated and Actual Flight Paths

Three flight paths were computed: a reference path, an estimated path, and an actual path. The reference flight path is the desired path of the aircraft. The reference state variables can be computed for any elapsed time along this path and are therefore considered to be known variables with which the estimated and actual values can be compared. The estimated flight path was computed and updated in position and velocity by use of a Kalman filter which processed discrete measured data-sets from the various digital subsystems as selected by the on-board computer. After each measurement data-set is processed, the resulting new estimated state is the systems' estimate of the actual state. New estimates are constantly required since both the actual and estimated states are perturbed from the states predicted by their respective transition matrices in the period between measurement data-sets and by the execution of course corrections.

Performance of the state estimation and course correction systems are evaluated by comparing the estimated state with the actual state and by comparing the actual state with the reference state. Comparisons are made individually and statistically. Individual comparisons between the estimated state and the actual state are the errors in the estimate and are denoted $\tilde{r}$ and $\tilde{v}$. The statistical errors in the estimate are denoted $\tilde{r}_{rms}$ and $\tilde{v}_{rms}$. Individual comparison between the actual state and the reference state variables are denoted r and v and the statistical comparisons are denoted r_{rms} and v_{rms}.

Statistical Information for Performance Evaluation

The statistical information for performance evaluation of the state estimation system can be derived from the covariance matrix P. The statistical information for performance evaluation of the combined state estimation, guidance and control systems is provided by the statistics of the actual path deviations from the reference path contained in the covariance matrix R.

These two matrices are 6 × 6 and the statistical data is obtained from them by first partitioning into 3 × 3 submatrices as follows:

$$P = \begin{bmatrix} P_1 & P_2 \\ P_3 & P_4 \end{bmatrix} \tag{33}$$

and

$$R = \begin{bmatrix} R_1 & R_2 \\ R_3 & R_4 \end{bmatrix} \tag{34}$$

From the P submatrices we obtain the following:

$$\tilde{r}_{rms} = (\text{trace } P_1)^{1/2} \tag{35}$$

$$\tilde{v}_{rms} = (\text{trace } P_4)^{1/2} \tag{36}$$

and from the R submatrices we obtain in a similar fashion

$$r_{rms} = (\text{trace } R_1)^{1/2} \tag{37}$$

$$v_{rms} = (\text{trace } R_4)^{1/2} \tag{38}$$

These quantities represent the total statistical position and velocity errors. In the case of $\tilde{r}_{rms}$ and $\tilde{v}_{rms}$, a statistical measure of the total error in the estimated position and velocity is obtained. In the case of r_{rms} and v_{rms}, a statistical measure of the total actual deviations from the reference state are obtained. At this point, it should be made clear that the statistical (or ensemble average) performance of the system is obtained from a single run on the computer and that, should a large number of computer runs be made, it would be expected that ensemble averages of the individual deviations $\tilde{r}$, $\tilde{v}$, r, and v would be given by $\tilde{r}_{rms}$, $\tilde{v}_{rms}$, r_{rms}, and v_{rms}, respectively.

Course Control Performance

Evaluation of course control performance is based on the ability of the system to control position and time errors continuously along the entire reference path. For ease in plotting and computation, the lengths of the reference paths were adjusted slightly so that the time en route would be a more convenient value. As a result, the en route reference times were as follows: (a) supersonic aircraft, San Francisco to New York City, 80 min; (b) supersonic aircraft, New York City to London, 100 min; (c) subsonic aircraft, San Francisco to New York City, 240 min; and (d) subsonic aircraft, New York City to London, 300 min.

Special scales are provided on the figures for evaluation of en route timing performance along the entire reference flight path. These scales allow determination of the en route timing error at any point in time along the reference path by conversion of r_{rms}, r, $\tilde{r}_{rms}$, and $\tilde{r}$ into equivalent time errors. The en route timing errors are denoted as δt_{rms}, δt, $\delta \tilde{t}_{rms}$, and $\delta \tilde{t}$, respectively, and are computed from:

$$\delta t_{rms} = k r_{rms} \tag{39}$$

$$\delta t = k r \tag{40}$$

$$\delta \tilde{t}_{rms} = k \tilde{r}_{rms} \tag{41}$$

$$\delta \tilde{t} = k \tilde{r} \tag{42}$$

where the constant k for the supersonic aircraft is equal to 1.2 sec/km and for the subsonic aircraft, 3.6 sec/km. Each of these time error quantities is the time for the aircraft to travel the total distance given by the respective position error quantity at the reference velocity. In particular, the quantity δt_{rms} is the time required to travel from the *rms* actual position to the reference position at a specific time en route. The quantity δt is the actual en route time error for one member of the ensemble of times represented by δt_{rms}. The quantity $\delta \tilde{t}_{rms}$ is the uncertainty in the knowledge of the time necessary to travel from the actual position to the reference position and means that the en route time error would be known on board the aircraft with an uncertainty given by $\delta \tilde{t}_{rms}$. The quantity $\delta \tilde{t}$ is one member of the ensemble of errors represented by $\delta \tilde{t}_{rms}$.

DISCUSSION OF RESULTS

The navigation system performance of subsonic and supersonic aircraft was evaluated for four cases. Flights were routed over a great-circle route overland from San Francisco to New York City and a great-circle route overwater from New York City to London. Attitude uncertainties (whose major effect is on heading control) of 0.50° and 0.25° were used in conjunction with a fixed-time-of-arrival (FTA) course control system. System performance of the four cases will be discussed in the following six areas: (1) state estimation performance; (2) effect of VORTAC/TACAN data-set samples; (3) effect of course corrections on the *rms* velocity estimation error; (4) individual case estimation performance; (5) control of the actual state; and (6) en route timing errors.

San Francisco to New York City — Subsonic Cruise

In this case, the aircraft reference velocity and altitude are 1,000 km/hr and 10.668 km (35,000 ft). The data-sets processed by the Kalman filter were from VORTAC/TACAN, Doppler radar, and barometric altitude information from an air-data computer. These data-sets were taken every 3 min.

State estimation performance— Control of the actual aircraft state for an effective FTA system is dependent upon the accuracy of estimating the aircraft state at the time the course corrections are executed. State estimation performance with two different attitude uncertainties (0.50° and 0.25°) is shown in figure 6. The figure shows an individual total position estimation error

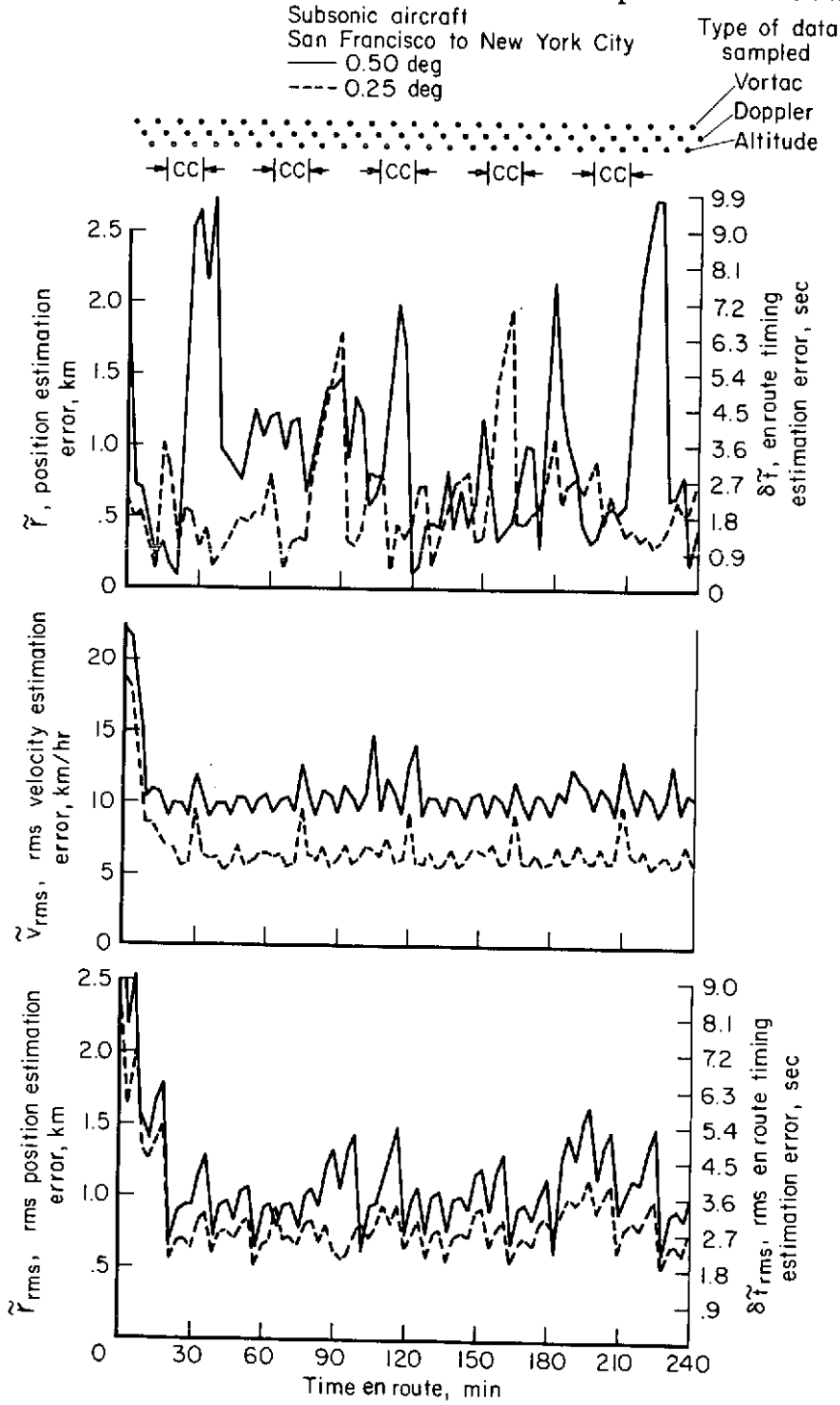

Figure 6.— Comparisons of $\tilde{r}_{rms}$, $\tilde{r}$ and $\tilde{v}_{rms}$ for A.U. = 0.25 and 0.50°.

for the individual ensemble member, $\tilde{r}$ (top), and the statistical total *rms* position and velocity estimation errors, $\tilde{r}_{rms}$ and $\tilde{v}_{rms}$. The *rms* position estimation error for an attitude uncertainty of 0.50° varies from about 0.60 km to about 1.7 km; for an attitude uncertainty of 0.25°, it varies from 0.5 km to 1.2 km.

Total *rms* velocity estimation errors (middle) are nominally of the order of 10 km/hr, with variations from 9 km/hr to 15 km/hr for an attitude uncertainty of 0.50°; for an attitude uncertainty of 0.25°, the total *rms* velocity estimation errors are nominally about 6.5 km/hr with variations from about 5 km/hr to about 10 km/hr.

Effect of VORTAC/TACAN data-set samples— The data presented in all the figures are what existed just after a data-set was processed by the Kalman filter and a new estimate of the aircraft state was obtained. Dots at the tops of certain figures are used to indicate the type and timing of data-set processing. For example, a dot at the coordinates of 30 min time en route and in the VOR row would mean that a VORTAC/TACAN data-set was processed at 30 min time en route. This allows a determination from the figure of the effect on $\tilde{r}_{rms}$, $\tilde{v}_{rms}$, and $\tilde{r}$ of each type of data-set at any time en route along the reference path.

The VORTAC/TACAN data-set samples are the primary source of position information in the ALONG-TRACK and CROSS-TRACK directions. During the initial settling period of the estimation system, the large reductions in $\tilde{r}$ and $\tilde{r}_{rms}$ occur at VORTAC/TACAN samples. Later, $\tilde{r}_{rms}$ is held in the range of 0.5 to 1.5 km largely due to the reduction of $\tilde{r}_{rms}$ to minimum levels at each VORTAC/TACAN sample. For the individual case, $\tilde{r}$ can differ from this trend due to unfortunate combinations of random errors, but as seen in figure 6, most of the minimum points of $\tilde{r}$ occur at VORTAC/TACAN samples.

All of these curves exhibit the ragged appearance characteristic of discrete estimation systems. Amplitude details can be varied by the frequency of processing and by the data type used. These curves do not exhibit a step reduction in estimation error at the time each data-set is processed because only the estimation error existing *after* the data-set was processed is shown. This method of presenting results has the disadvantage of not showing explicitly the improvement made by the processing of each data-set, but experience has shown that the performance after processing a data-set is of far greater interest and the clarity of the figures is greatly enhanced.

Effect of course corrections on the rms velocity estimation error— In figure 6, the increase in the *rms* velocity estimation error, $\tilde{v}_{rms}$, due to uncertainties in the execution of a course correction is shown by a peak in the curve just after the second maneuver of each course correction. This peak is most visible on the curve for an attitude uncertainty of 0.25°. Peaks at the same time can be seen, though less clearly, in the curve for 0.50°. Peaks also occur after the first maneuver of each course correction. But in this case, a Doppler radar data-set was processed by the Kalman filter immediately following the execution of each first maneuver and effectively removed the velocity uncertainty introduced by the course correction; thus the

velocity uncertainty was reduced to approximately the same level existing before the execution of the first maneuver.

Individual case estimation performance— The total position estimation error for the individual case, $\tilde{r}$, is the vector sum of the three error components of the individual position estimation. The individual estimation errors influenced the individual course corrections which were executed on this particular flight. In particular, they are estimation errors which existed at the time of the computation of the individual course correction maneuvers and relate directly to the system's performance in controlling the actual state and the corresponding timing errors.

The individual velocity estimation errors are also involved in the course correction computations but, since their influence is relatively minor compared to that of the position estimation errors, the curves are not shown.

Control of the actual state— The *rms* position estimation error, $\tilde{r}_{rms}$, for an attitude uncertainty of 0.50° is compared in figure 7 (bottom curve) to the

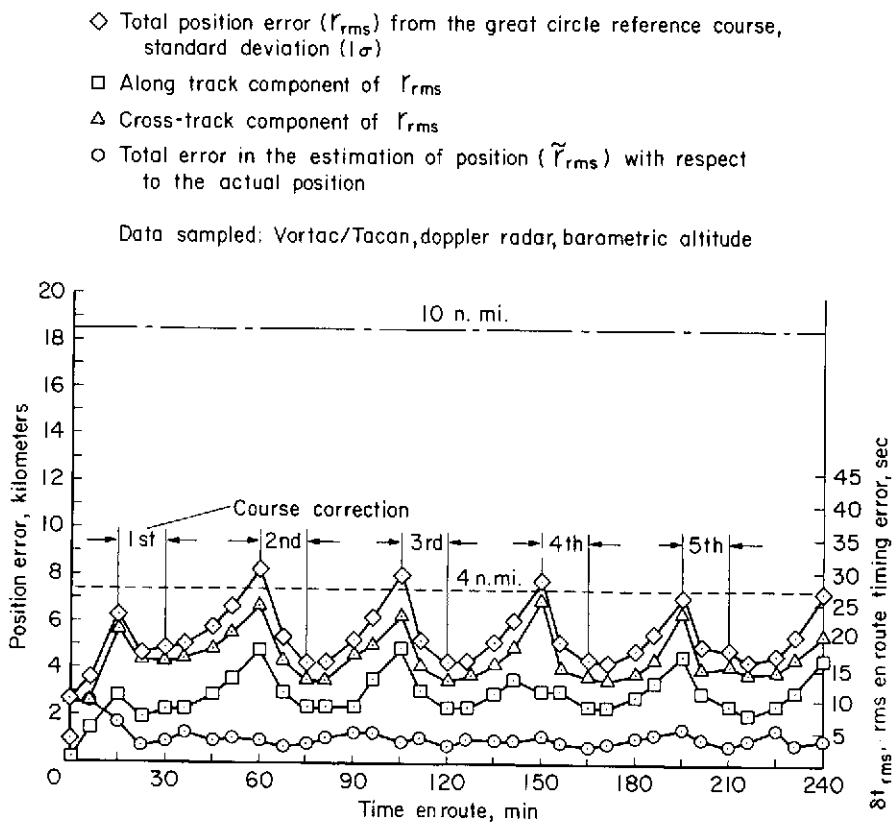

Figure 7.— *rms* errors in position and position estimation subsonic case (1000 km/hr). San Francisco to New York City A.U. = 0.5°.

actual position deviation from the reference position, r_{rms}, (top curve) and the along-track and cross-track components of r_{rms}. Since the vertical component of r_{rms} is small, the total is very nearly the vector sum of the along-track and cross-track components. Data points in figure 7 are plotted at about 6 to 9 min intervals and show that even though the position estimation error is only about 1 km, the minimum actual error, r_{rms}, is about 4 km. This effect occurs at the intercept point (see fig. 3), which occurs at the time of the second maneuver of each course correction and shows that with five course corrections, position estimation performance is about four times better than position control of the actual state. It might be expected that r_{rms} would more closely approach $\hat{r}_{rms}$ at this time, but it does not for three reasons: (1) the course correction computations are based on estimated state information; (2) course corrections are not executed perfectly; and (3) errors in the control system will allow external forces to deviate the aircraft from the computed path to the intercept point. These three error sources cause position errors which, to a first order approximation, increase linearly with time. This effect suggests that position control would be improved by increasing the frequency of course corrections and that the optimum performance (statistically) could be achieved by an adaptive system, in other words, by making a course correction following the processing of each data-set, providing the course correction threshold requirements were met.

It is of theoretical interest to pursue this line of reasoning further. Suppose there were no errors in the course correction computations due to uncertainties in the state estimates; then for conditions corresponding to those of figure 7, it would be expected (statistically) that for $\hat{r}_{rms}$ = 1 km, the *rms* position error would have a lower limit given by

$$r_{rms} = \hat{r}_{rms} + |V_R|\Delta t(0.5/57.3)$$

$$= 1 + (1000)(6/60)(0.5/57.3) \approx 1.9 \text{ km}$$

This position error is based upon the premise that a two-maneuver course correction is made every 6 min. As a practical matter, experience has shown that with the present course correction threshold, course corrections would be made much less frequently than every 6 min. As a result, the 1.9 km value would not be approached. Even so, a value substantially less than 4 km is feasible through a higher frequency of course corrections, such as would be provided through an adaptive system. The effects of increased frequency of course corrections was not investigated explicitly in this study, since it is clear from the foregoing discussion that a significant improvement in performance can be obtained by this means; investigation of this subject was left for further study. Instead, the use of a fixed near-minimum number of course corrections shows much more dramatically the individual effects of the various components of the system and the data-set sampling schedules.

The two horizontal lines in figure 7 at 7.4 km (4 n. mi.) and 18.5 km (10 n. mi.) are present separation standards (cross-track) within the United States (ref. 9). When the aircraft has distance measuring equipment, the 7.4 km (4 n. mi.) standard applies. The cross-track component of r_{rms} meets this separation standard on a 1-σ basis.

The quantity r_{rms}, which is indicative of actual state control, is compared for attitude uncertainties of 0.25° and 0.50° in figure 8 (bottom curve).

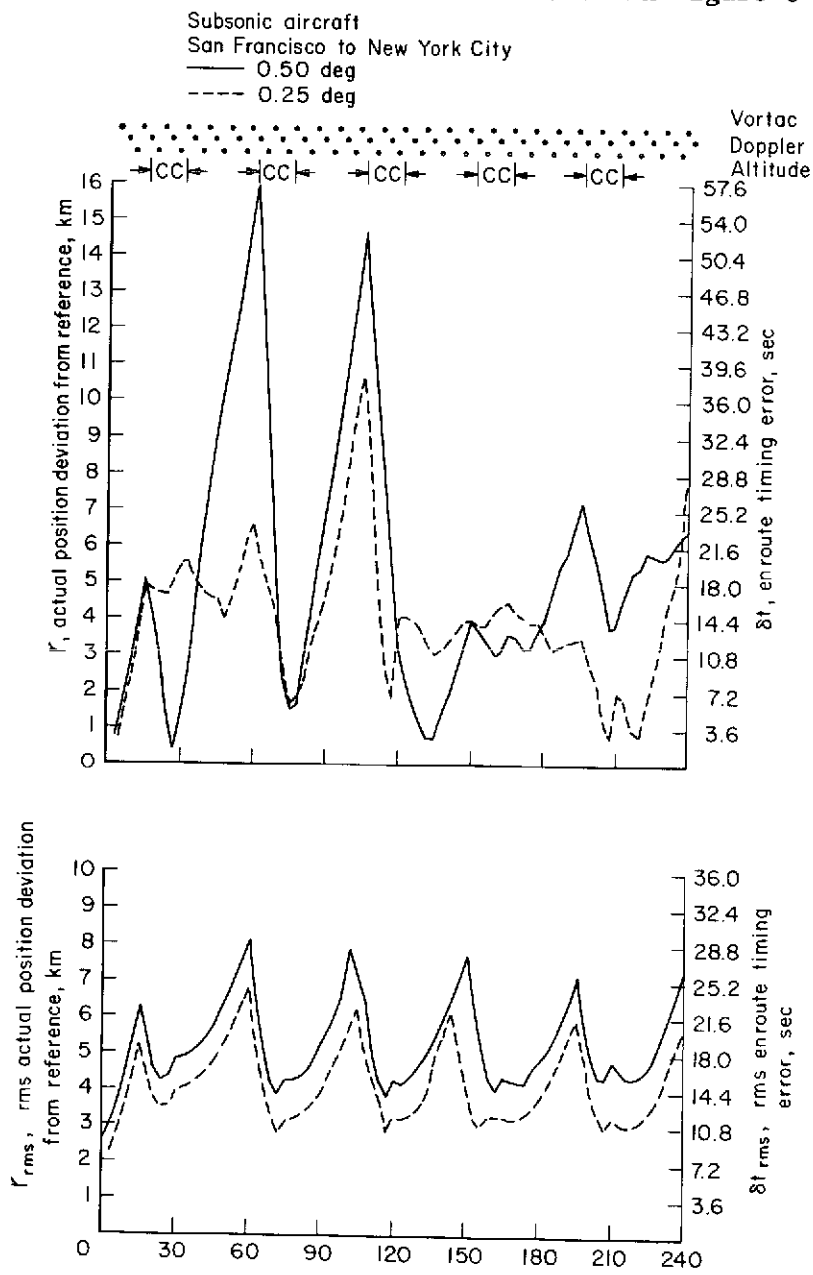

Figure 8.— Comparison of r_{rms} and r for A.U. = 0.25 and 0.50°.

Also shown is the total individual case actual position deviation from the reference, r, for each of the two attitude uncertainties. Figures such as this one are useful in judging the effectiveness of a particular number of course corrections in meeting specific cross-track error requirements. In this particular case, the lower curve shows that the *rms* deviation of the actual path from the reference path varied from about 3.8 km to about 8.3 km for 0.50° altitude uncertainty and from about 2.8 km to about 6.8 km for the

0.25° case. The upper curve, r, (individual case) is of interest because it dramatically demonstrates the wide variation in actual flight path deviations with a given control system accuracy and a small number of course corrections. It also calls attention to the discrepancy in the statistical (*rms*) performance and the actual performance which can occur; the *rms* plot indicates quite adequate control, whereas in the individual case, control errors were significantly larger. This effect is due primarily to unfortunate combinations of random errors occurring in the control system. Better control of the individual case could be obtained by: (a) using an adaptive correction schedule which would make a course correction whenever the groundspeed or heading change required exceeded a given threshold; or (b) using the existing fixed schedule and imposing an upper threshold on the estimated deviation which, when exceeded, would cause an additional correction to be implemented.

En route timing errors— The course correction system used in this report is intended to reduce en route timing errors at all points along the reference path to acceptable values. Figures 6, 7, and 8 have scales on them so that en route timing errors may be found at any point along the reference path. The definition of en route timing error used herein is the time it takes to travel from the actual aircraft position to the reference position at a particular time and at the reference velocity.

The approximate range of the *rms* en route timing errors, δt_{rms}, and the *rms* uncertainty in these errors, $\delta \tilde{t}_{rms}$, are given in the table below:

Attitude uncertainty, deg	δt_{rms}, sec	$\delta \tilde{t}_{rms}$ sec
0.50	13.5 - 30.0	1.8 - 6.0
0.25	10.5 - 24.5	1.8 - 4.1

The table shows that the major effect of the attitude uncertainty is on δt_{rms} and results from decreasing control system performance with increasing attitude uncertainty.

San Francisco to New York City - Supersonic Cruise

In this case, the aircraft is supersonic with a reference velocity of 3,000 km/hr. The flight path is from San Francisco to New York City along a great-circle path at an altitude of 21.336 km (70,000 ft).

State estimation performance— In figure 9, $\tilde{r}_{rms}$, $\tilde{v}_{rms}$, and $\tilde{r}$ are shown for attitude uncertainties of 0.50° and 0.25°. The data-set sample rate is 1/min.

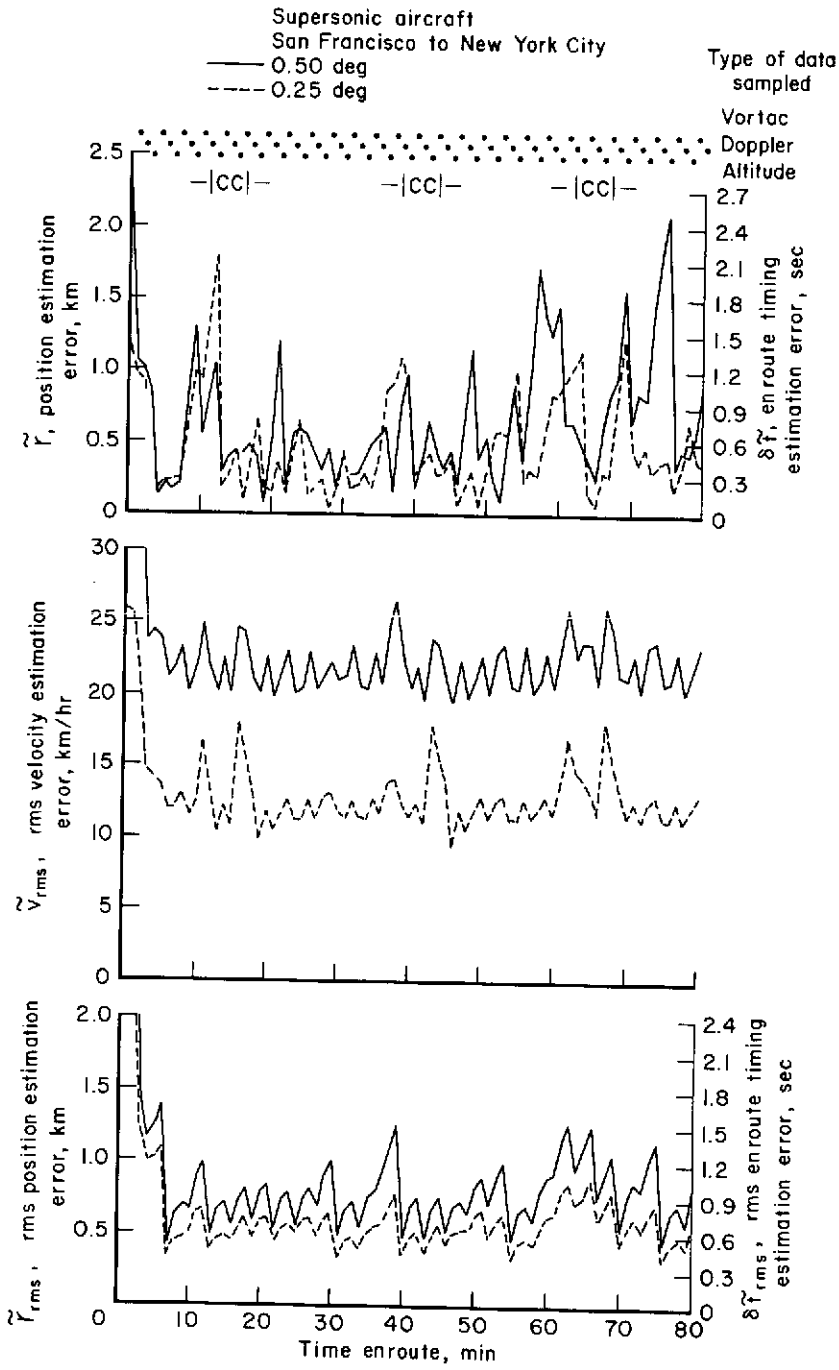

Figure 9.— Comparisons of $\tilde{r}_{rms}$, $\tilde{r}$ and $\tilde{v}_{rms}$ for A.U. = 0.25 and 0.50°.

The approximate ranges of the *rms* position estimation error, $\tilde{r}_{rms}$, and the velocity estimation error, $\tilde{v}_{rms}$, are shown in the following table.

Attitude uncertainty, deg	$\tilde{r}_{rms}$, km	$\tilde{v}_{rms}$, km/sec
0.50	0.35 - 1.25	19.5 - 26.5
0.25	0.35 - 0.90	9.0 - 18.5

As can be seen from this table, the effect of the attitude uncertainty is primarily on $\tilde{v}_{rms}$.

Effect of VORTAC/TACAN data-set samples on state estimation— When figure 9 is compared to figure 6, which shows the corresponding data for the subsonic case, it is found that in general, the effects of VORTAC/TACAN data-set samples on $\tilde{r}_{rms}$ and $\tilde{v}_{rms}$ are much the same as in figure 6. In addition, there is a reduction of $\tilde{r}_{rms}$ over that of the subsonic case. This reduction is due to the shorter time intervals between data-set samples, which lessen the effects of external disturbances since velocity and acceleration disturbances have less time to affect the aircraft position. The reduction in position uncertainty is also influenced by the higher angular rate of change of the slant range vector from the VORTAC/TACAN stations to the aircraft. When the $\tilde{v}_{rms}$ curves in figure 9 are compared to those in figure 6, it is seen that there is an upward shift in figure 9 by a factor of about 2.25. One might expect this factor to be 3.0, since the aircraft reference velocity was increased by a factor of 3.0 and the Doppler radar velocity measurement error model is a linear function of the aircraft reference velocity. This improved performance of the velocity estimation is directly related to the improved position estimation which was explained above.

Effect of course corrections on the rms velocity estimation error— The velocity estimation error for an attitude uncertainty of 0.50° and 0.25° is shown in figure 9. These two curves each show a peak at the times of both the first and second maneuvers of each course correction. In general, the first peak is more pronounced than in figure 6, even though a Doppler radar data-set sample is processed by the Kalman filter immediately following the first maneuver. The smaller reduction is a considerably different result than that obtained in the subsonic case because the velocity uncertainty in the Doppler radar along-track component was three times larger than for the subsonic aircraft and will, therefore, have less weight in forming the new state estimate in the Kalman filter computations.

Individual case estimation performance— The total estimation error, $\tilde{r}$, for an individual case is shown for the two attitude uncertainties. As expected, most of the minimum points of $\tilde{r}$ occur at VORTAC/TACAN data-set samples.

Control of the actual state— The total *rms* position estimation error, $\tilde{r}_{rms}$, is compared in figure 10 to the total actual *rms* position deviation

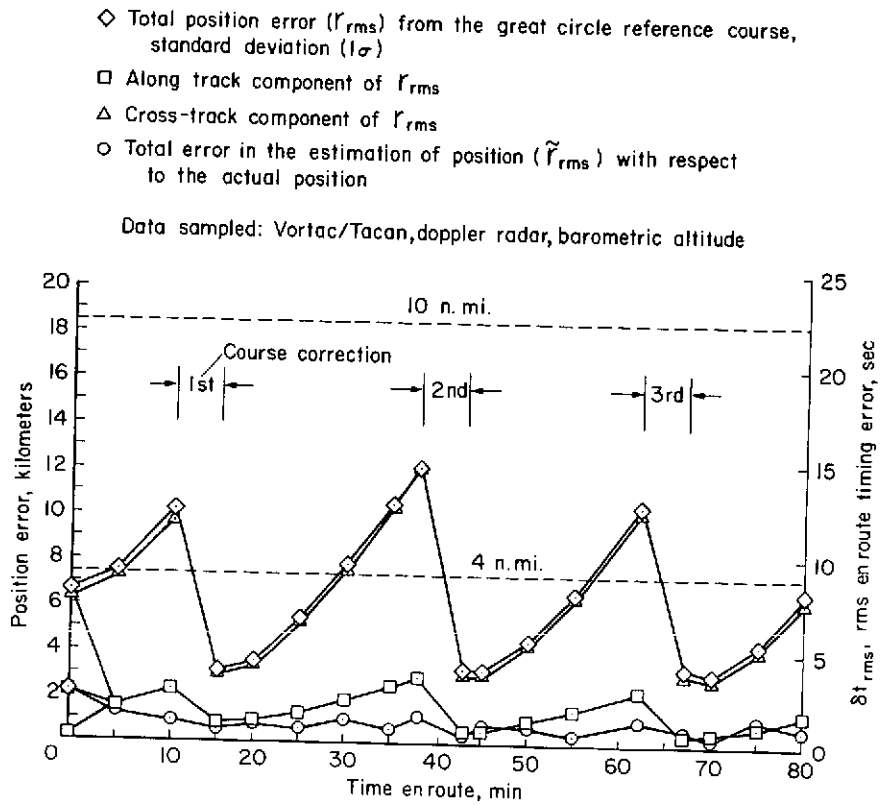

Figure 10.— *rms* errors in position and position estimation. Supersonic case (3000 km/hr) A.U. = .5° San Francisco to New York City.

from the reference, r_{rms}, and the along-track and cross-track components of r_{rms}. This figure shows a decrease in the along-track component of r_{rms} when a comparison is made with the subsonic case in figure 7. The larger error in figure 7 is due primarily to the time interval between course corrections, being 30 min in figure 7 and from 19 to 22 min in figure 10. The quantity v_{rms} between course corrections is roughly the same, since the model for the actual along-track velocity deviation from the reference is not strongly influenced by the reference velocity.

The estimation error, $\tilde{r}_{rms}$, is the *rms* deviation of the actual state from the estimated state. Therefore, although the actual state may deviate from the reference state by several kilometers, the knowledge of this deviation has an uncertainty given by $\tilde{r}_{rms}$ and is of the order of 1 km.

The three course corrections executed on this flight were considered to be a practical minimum number for the purposes of this report. To meet the 7.4 km (4-n.-mi.) maximum cross-track deviation requirement with an attitude uncertainty of 0.50° would require four or five evenly spaced course corrections. Also, as illustrated in figure 11, with an attitude uncertainty of 0.25°, three course corrections were slightly less than adequate. Figure 11

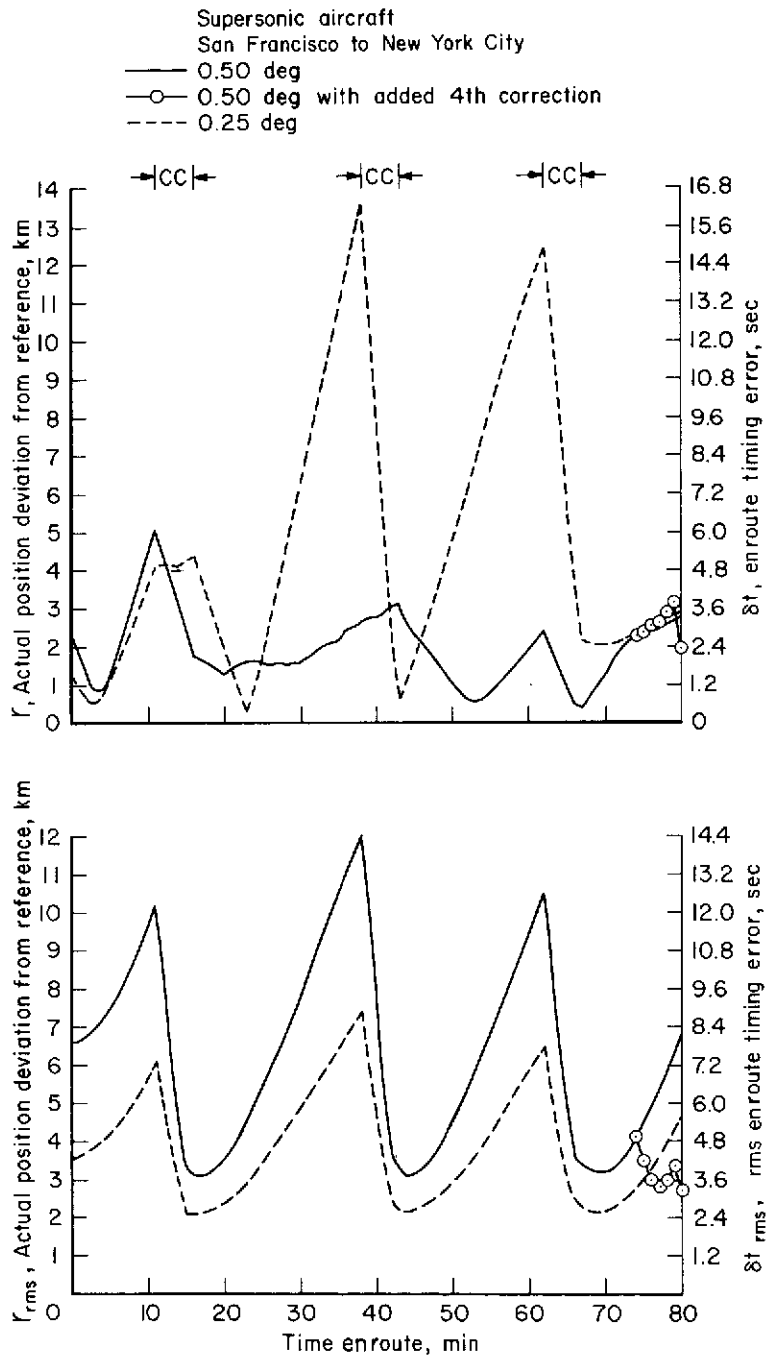

Figure 11.— Comparison of r_{rms} and r for A.U. = 0.25 and 0.50°.

also compares r_{rms} and r for 0.50° and 0.25°. This figure allows a comparison of the results for the two attitude uncertainties and a comparison of r and r_{rms} for each attitude uncertainty. These results show that the *rms* deviation of the actual path from the reference path varied from about 3.1 km to about 12.1 km for the 0.50° attitude uncertainty, and from about 2.1 km to about 7.4 km for the 0.25° attitude uncertainty.

En route timing errors— The general en route timing performance can be seen from figures 9, 10, and 11. Using the en route timing scale, one can find the total *rms* time error, the along-track and cross-track time error, and the total uncertainty in the time error at any time along the reference path. In general, there would be no difficulty in adhering to fixed time schedules along the entire flight path to within a few seconds. On this supersonic San Francisco to New York flight, the approximate range of the *rms* en route timing error, δt_{rms}, and the *rms* uncertainty in the knowledge of this error, $\delta \hat{t}_{rms}$, are given below.

Attitude uncertainty, deg	δt_{rms}, sec	$\delta \hat{t}_{rms}$, sec
0.50	3.7 - 14.5	0.6 - 1.6
0.25	3.7 - 8.9	0.4 - 1.1

This table shows, as in the subsonic case, that the major effect of increasing the attitude uncertainty is to increase the range of δt_{rms}.

If it is desired to reduce the en route timing error to a minimum at some point along the reference path, a course correction can be added at the proper time in advance of this point so that r_{rms} will be a minimum at the desired time. Figure 11 shows a flight where a course correction was added at 74 min to ensure that the en route timing error at 80 min would be small. In this figure, r, the individual case total position error, and r_{rms} are plotted showing the 0.50° attitude uncertainty situation; curves are plotted both with (circled data points) and without the added correction, so that a comparison can be made between the results obtained. This comparison illustrates some of the versatility of the system. Not only have the en route timing errors at any point along the reference path been maintained at a reasonable level, but these errors can be reduced to a minimum at any desired time by adding a new correction or by adjusting the time of execution of an existing course correction.

New York City to London - Subsonic Cruise

In this case, the aircraft is cruising at a reference velocity of 1,000 km/hr at an altitude of 10.668 km (35,000 ft). The data-sets processed

by the Kalman filter were from Loran-C, Doppler radar, and a radio altimeter.

State estimation performance— The effect of the attitude uncertainty on position and velocity estimation errors is shown in figure 12. After the

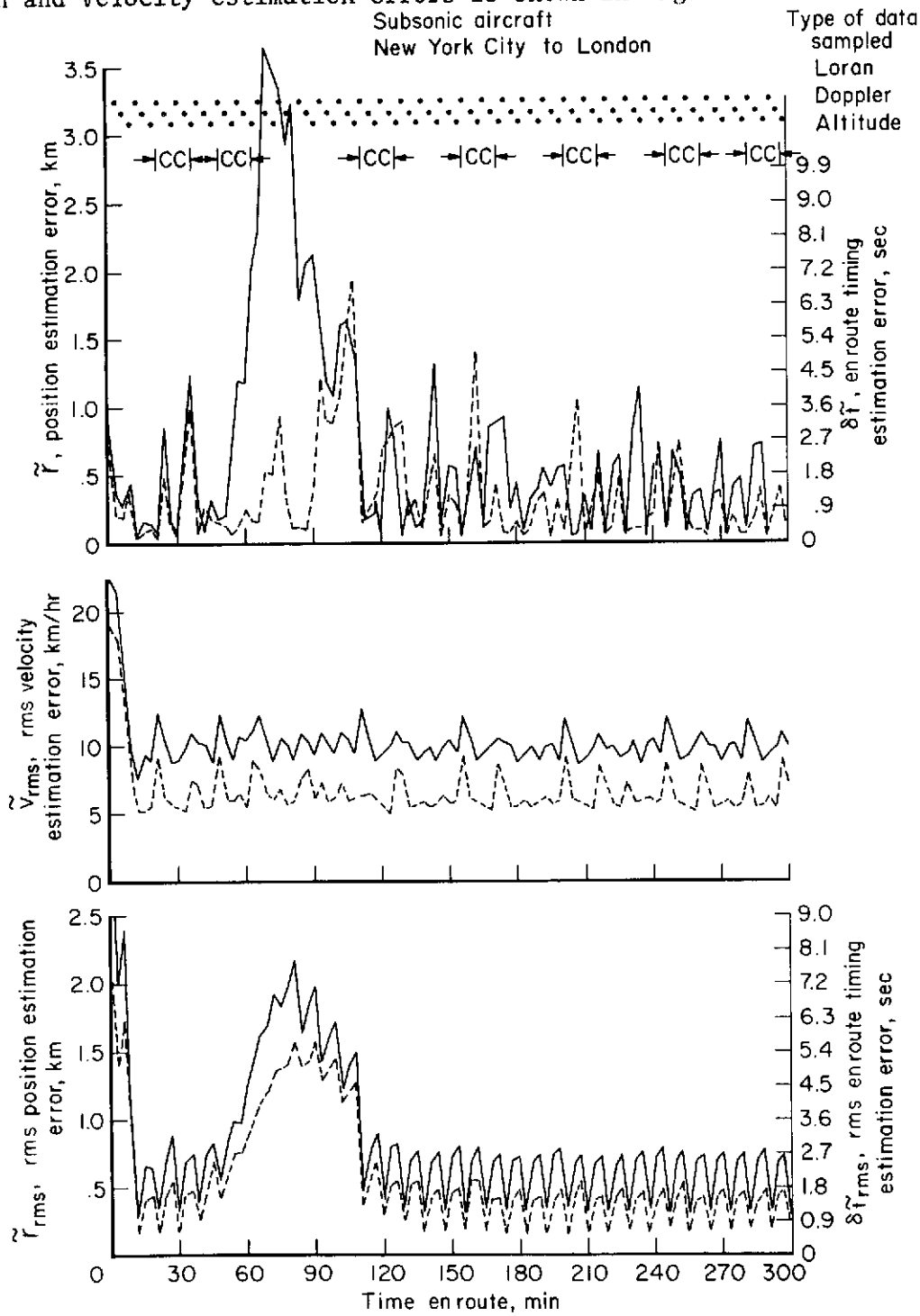

Figure 12.— Comparison of $\tilde{r}_{rms}$, $\tilde{r}$ and $\tilde{v}_{rms}$ for A.U. = 0.25 and 0.50°.

initial Kalman filter settling period, the approximate range of the *rms* position estimation error, $\tilde{r}_{rms}$, and the *rms* velocity estimation error, $\tilde{v}_{rms}$ is shown in the table below.

Attitude uncertainty deg	$\tilde{r}_{rms}$, km	$\tilde{v}_{rms}$, km/sec
0.50	0.30 - 2.2	8.5 - 13.0
0.25	0.15 - 1.6	5.0 - 9.0

The table shows that uncertainty in the attitude reference has a more pronounced effect on velocity uncertainty than on position uncertainty.

Effect of Loran-C data-set samples— The accuracy of the Loran-C position fixes is dependent upon the relative locations of the aircraft and the three-station transmitting triad. When the accuracy of the Loran-C position fixes is poor, the aircraft is said to be in an area of poor coverage. In the plot of $\tilde{r}_{rms}$ in figure 12, there is a large hump during the period from about 50 min to about 110 min time en route. This hump occurs because the aircraft is in an area of poor coverage during this period of time. The poor coverage does not have any noticeable effect on $\tilde{v}_{rms}$ because velocity estimation depends mainly on the Doppler radar. An on-board system could make some improvement in estimation performance in the poor coverage area by modifying the sampling schedule to increase the number of Loran-C data-sets in this region.

Effect of course corrections on the rms velocity estimation error— The effect of course correction execution errors are seen at both the first and second maneuvers of each course correction for the 0.50° case. The peak in $\tilde{v}_{rms}$ at the second maneuver is generally reduced from that of the first maneuver because the vertical velocity uncertainty component is reduced by the processings of altitude and altitude rate information by the Kalman filter immediately following the second maneuver. For the 0.25° case, the reduction is much less and the opposite effect is seen in the third and seventh course corrections. This effect is apparently caused by the fact that the vertical velocity uncertainty is always less for this case and the effect of processing altitude and altitude rate makes a relatively small improvement in the overall velocity uncertainty. For the third and seventh course corrections, $\tilde{v}_{rms}$ was dominated at the first maneuver by good Loran-C fixes.

Individual case estimation performance— The individual case estimation error, r, during the period of poor Loran-C coverage shows a peak estimation error of about 4.25 km, but is unusually large throughout the time period from about 60 min to 111 min. Thus, the performance in position estimation in the area of poor coverage is consistent with the error which would be expected considering the uncertainty in the position fixes which existed at the time.

Control of the actual state— The *rms* position estimation for an attitude uncertainty of 0.50° is compared in figure 13 to the total actual position deviation from the reference position, r_{rms}, and the along-track and cross-track components of r_{rms}. This figure, as expected, shows that estimation is better than control.

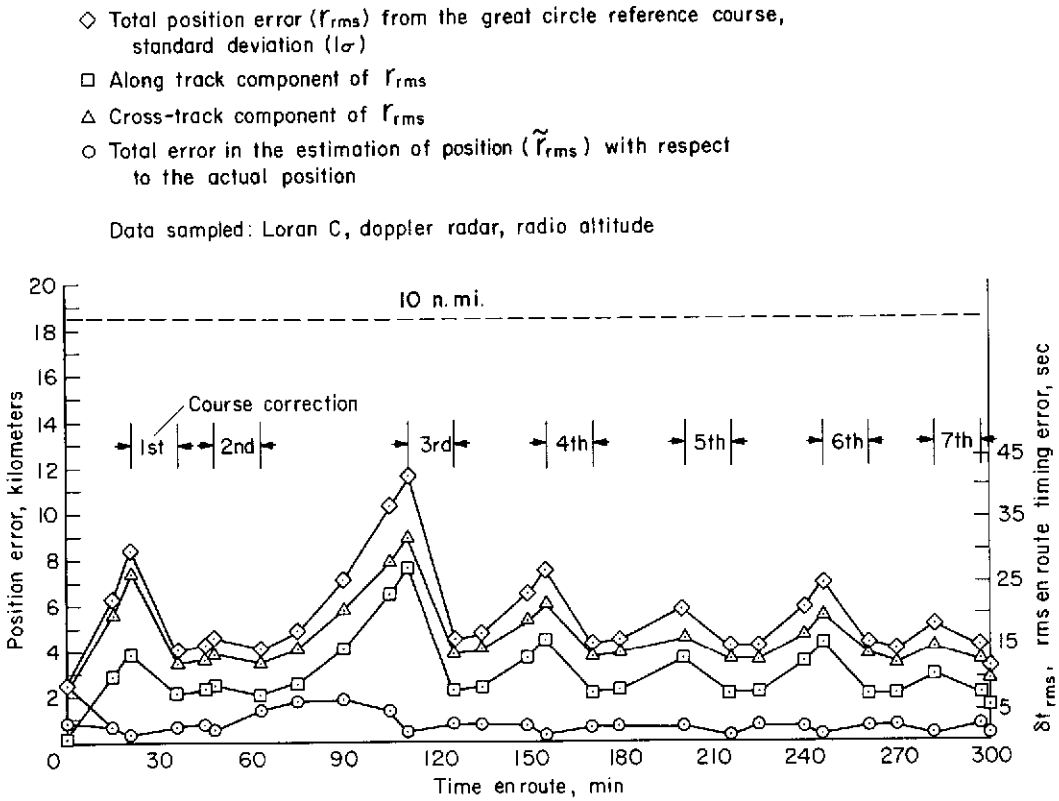

Figure 13.— *rms* errors in position and position estimation, subsonic case (1000 km/hr). New York City to London. A.U. = 0.5°.

Present standards for the North Atlantic corridor for lateral deviation from the route centerline is 111.1 km (60 n. mi.), except for reductions to 18.5 km (10 n. mi.) when within 211.1 km (114 n. mi.) of a navigation aid. En route timing (along-track) separation standards are apparently ill-defined, but are on the order of 20 min between aircraft (ref. 9).

Figure 13 shows that the seven course correction schedule keeps the actual path (r_{rms}) within 12 km, which is well within the most stringent distance standard of 18.5 km (10 n. mi.).

The flight of the aircraft through an area of poor Loran-C coverage was known to occur and previous results had shown that with evenly spaced course corrections in this area, the course control could be expected to be poorer than when made outside this area. In fact, the poorer course correction performance was observed to result in occasional large actual deviations from the reference path in excess of 27 km. This is not an excessive deviation.

Nevertheless, it was decided to investigate the effect of delaying the second course correction on the overall performance. Figure 14, which compares r_{rms}

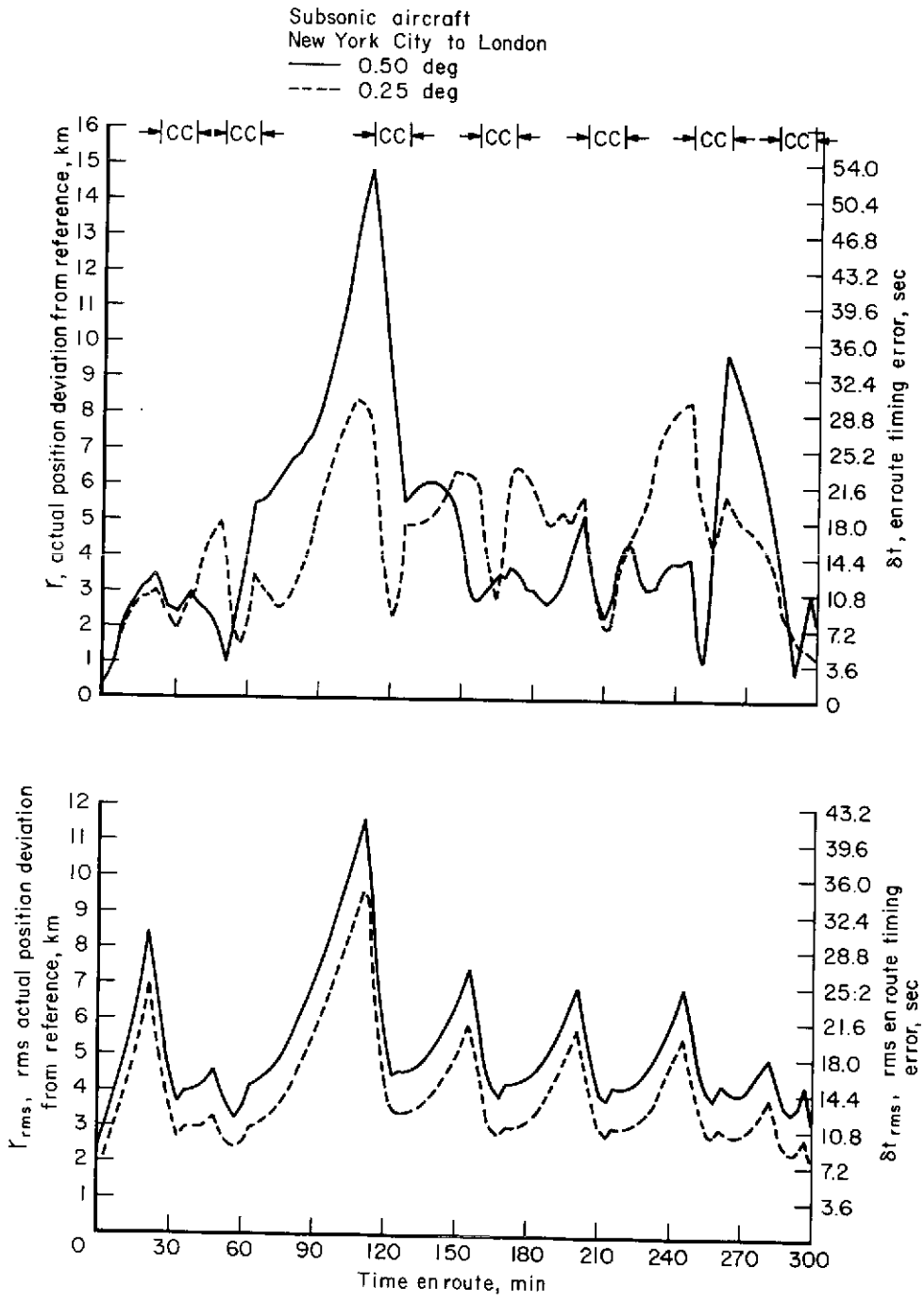

Figure 14.— Comparison of r_{rms} and r for A.U. = 0.25 and 0.50°.

and r for the two attitude uncertainties, shows the results of delaying the second course correction to avoid a correction in the area where position uncertainty was about three times as large as in adjoining areas. This figure shows that although avoiding corrections during a period of larger position uncertainty did keep the system from making poor corrections, there was a penalty due to the relatively long spacing between the corrections in the poor coverage area as compared to the spacing in the other areas. This penalty, as shown by both r_{rms} and r, is a relatively large deviation of the actual position from the reference position, but still results in better performance than that observed when corrections were made with a relatively high position uncertainty.

At 246 min, the first maneuver of the sixth course correction is initiated and illustrates what can happen to r (for the 0.5° *rms* attitude error individual case) when there is an unfortunate combination of moderate estimation error and relatively large course correction execution errors. The result in this case was that the first maneuver implemented a course correction which caused the actual path to cross the reference path, resulting in an increase in the actual position error from 4 km to 9.6 km before the second maneuver began to return the actual path back to the reference path.

The *rms* deviation of the actual path from the reference path varied from 3.4 km to 11.6 km for an attitude uncertainty of 0.50° and from 2.4 km to 9.6 km for the 0.25° case.

En route timing errors— The en route timing errors can be read from the time scales on figures 12, 13, and 14. The individual case in figure 14 shows that due to the poor Loran-C coverage, there was a maximum en route timing error, of about 54 sec. The approximate range of the *rms* en route timing error, δt_{rms}, and the *rms* uncertainty in the timing error, $\delta \dot{t}_{rms}$, for the two attitude uncertainties are given in the table below.

Attitude uncertainty, deg	δt_{rms}, sec	$\delta \dot{t}_{rms}$, sec
0.50	12.2 - 41.8	1.3 - 8.0
0.25	8.6 - 34.6	0.5 - 5.8

As in previous tables, it is clear that en route timing errors are better estimated than controlled. Also, while there is a general reduction of δt_{rms} and $\delta \dot{t}_{rms}$ as a result of reducing the attitude uncertainty, the magnitude of the reductions in comparison to the range indicates the effect is relatively minor. The table shows very good en route timing performance when compared to the en route timing separation standards, which are on the order of 20 min.

The scheduling of a course correction to minimize the error at the reference destination time of 300 min is shown in figure 14. This process results in an error of about 8 sec for the attitude uncertainty of 0.50° in the individual case.

New York City to London - Supersonic Cruise

For this case, the aircraft is cruising at a reference velocity of 3000 km/hr at an altitude of 21.336 km (70,000 ft). The data-set samples processed by the Kalman filter were from Loran-C, Doppler radar, and a radio altimeter.

State estimation performance— The effect of the two attitude uncertainties on the *rms* position, $\tilde{r}_{rms}$, and velocity, $\tilde{v}_{rms}$, estimation error and on the position estimation error for an individual case is shown in figure 15.

The approximate range of these variables for the two attitude uncertainties are given in the table below.

Attitude uncertainty, deg	$\tilde{r}_{rms}$, km	$\tilde{v}_{rms}$, km
0.50	0.2 - 1.5	18.0 - 29.0
0.25	0.13 - 1.2	6.3 - 19.0

This table shows that the effect of attitude uncertainty is quite pronounced on $\tilde{v}_{rms}$ but that there is little effect on $\tilde{r}_{rms}$. In addition, the range of $\tilde{v}_{rms}$ is much greater than in the subsonic case because of the greater speed of the supersonic aircraft.

Effect of Loran-C data-set samples— In figure 15, the hump due to poor Loran-C coverage, which was so evident in the subsonic case, is somewhat reduced for the supersonic aircraft. This behavior results from the time periods between data-set samples being 1 min instead of 3 min in the subsonic case, so that errors have less time to accumulate.

Effect of course corrections on the rms velocity estimation error— The effect of course correction execution errors is seen at both the first and second maneuvers of each course correction. The peaks in $\tilde{v}_{rms}$ at each maneuver are much more evident (particularly when the attitude uncertainty is 0.25°) than for the subsonic aircraft shown in figure 12. This effect is due to the sensitivity of the course correction execution errors to the aircraft velocity.

Individual case estimation performance— The individual case position estimation error, $\tilde{r}$, during the period of poor Loran-C coverage shows a situation where the 0.25° attitude uncertainty produced estimates which were worse in some instances than those for the 0.50° case (fig. 15). In individual

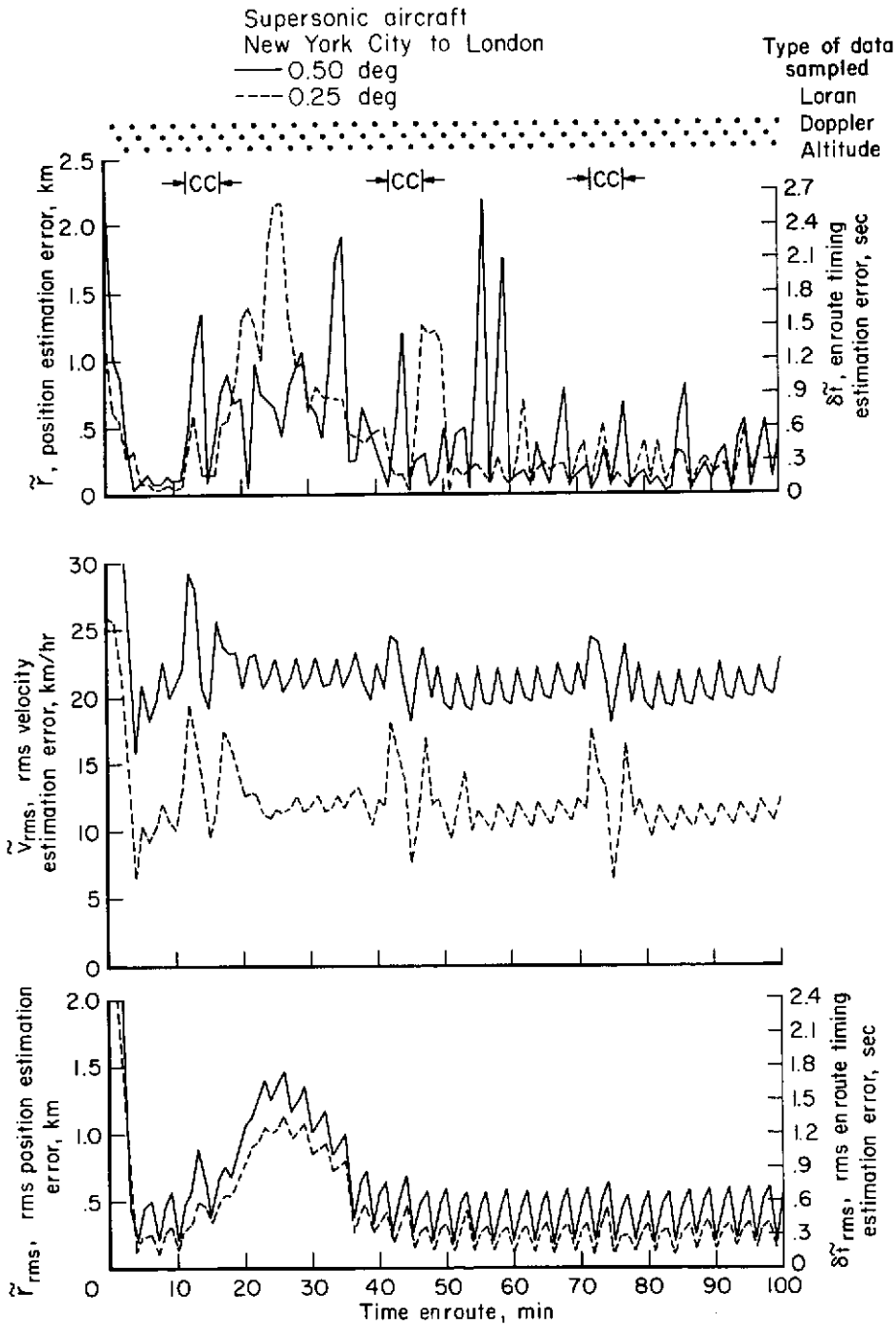

Figure 15.— Comparisons of $\tilde{r}_{rms}$, $\tilde{r}$ and $\tilde{v}_{rms}$ for A.U. = 0.25 and 0.50°.

cases, these events are to be expected and, in general, can be attributed to a series of unfavorable random numbers being generated by the simulation program and to the Kalman filter weighting matrix giving more weight to these errors in the 0.25° attitude uncertainty case than in the 0.50° attitude uncertainty case, as would be expected.

Control of the actual state— The *rms* position estimation error for an attitude uncertainty of 0.50° is compared in figure 16 with the total position

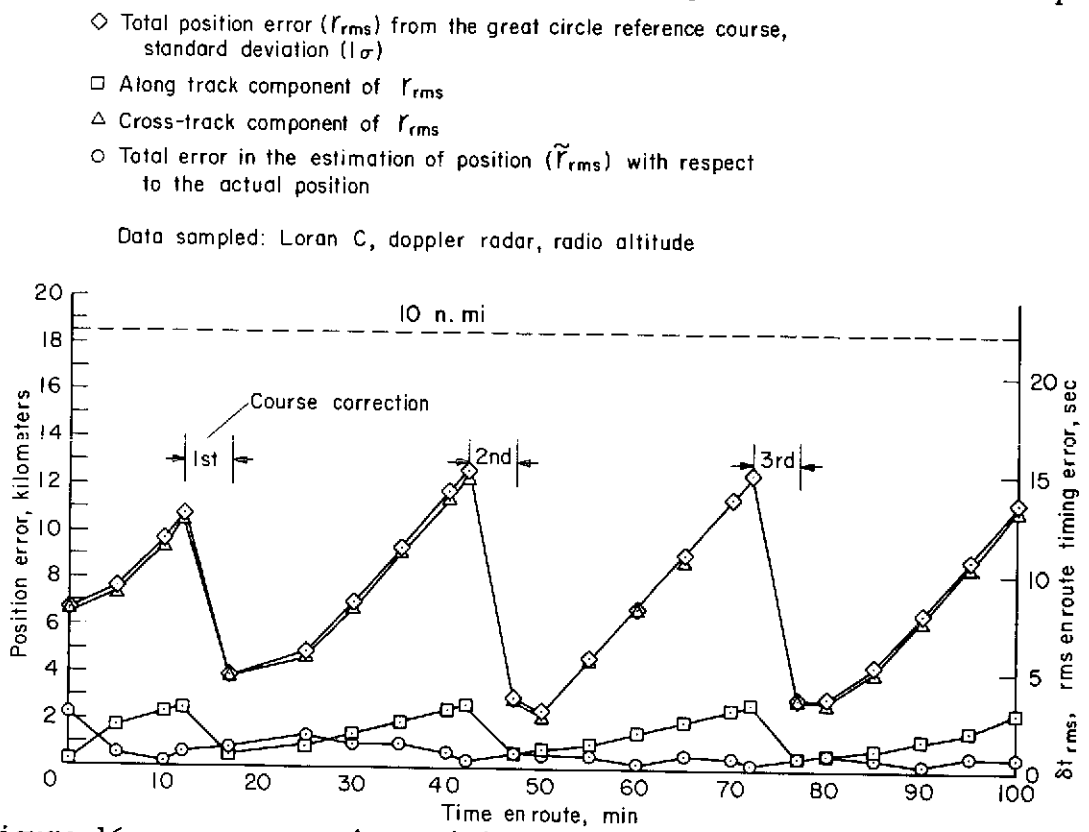

Figure 16.— *rms* errors in position and position estimation, supersonic case (3000 km/hr). New York City to London A.U. = .5°.

deviation from the reference, r_{rms}, and the along-track and cross-track components of r_{rms}. This figure shows that the execution of only three course corrections is sufficient to keep the aircraft position errors within 18.5 km (10 n. mi.) (1 σ). In the along-track direction, the *rms* position error is expected to be less than about 2.9 km and in the cross-track direction, less than 12.5 km.

Comparison of figure 16 with figure 13 shows that for the supersonic case, the along-track position control is much better than the cross-track position control but that, in the subsonic case, the control performance was about the same for both. The reasoning which explains the observed performance is as follows: the buildup in position error between course corrections is due principally to velocity errors following the previous course correction and, to the first order,

$$(\Delta X_{AT})_{rms} = (\Delta T_{k,k-1}) \times rms \text{ speed control error}$$

and

$$(\Delta X_{CT})_{rms} = V(\Delta T_{k,k-1}) \times rms \text{ heading control error}$$

where ΔX_{AT} and ΔX_{CT} are the *rms* along-track and cross-track errors, V is the aircraft speed, and $\Delta T_{k,k-1}$ is the time interval between the second maneuver of correction of k-1 and the first maneuver of correction k.

For both subsonic and supersonic cases, the *rms* speed control error (5 km/hr) and heading control error (attitude uncertainty) are assumed to be the same. Thus the buildup in along-track error is due solely to the course correction scheduling ($\Delta T_{k,k-1}$) while the cross-track error buildup is due to the contribution of groundspeed and the correction schedule, $V\Delta T_{k,k-1}$, or equivalently, the distance between corrections.

For the supersonic case, $\Delta T_{k,k-1}$ was generally smaller than for the subsonic case; for this reason, better along-track control performance is obtained for this case. However, the distance between corrections is slightly longer for the supersonic case, with the result that the cross-track control performance is slightly poorer. This effect can be seen by comparing figures 13 and 16.

In figure 17, r_{rms} and r are compared to show the effects of the two attitude uncertainties. This figure also allows the comparison of r_{rms} with r for each of the attitude uncertainties considered. The upper curve shows r for an individual case; the second maneuver of the second course correction (0.25° attitude uncertainty) had such large execution errors that the actual deviation from the reference reached 26.4 km before the first maneuver of the third course correction was executed to return the actual path to the reference path. This correction was necessarily large and implied another large correction at the time of the second maneuver. If a larger number of course corrections had been scheduled, the chance of such large deviations from the reference would have been reduced. In general, the *rms* deviation of the actual path from the reference path varied from about 2.9 km to about 12.7 km for the 0.50° attitude uncertainty and from about 1.9 km to about 7.6 km for the 0.25° attitude uncertainty.

En route timing errors— The en route timing errors can be read from the time scales on figures 15, 16, and 17. Because of the large course correction execution errors at the second maneuver of the second correction, the individual case en route time error in figure 17 reached a maximum of about 32 sec.

The approximate range of the *rms* en route timing error, δt_{rms}, and the *rms* uncertainty in the timing error, $\delta \tilde{t}_{rms}$, for the attitude uncertainties are given in the table below

Attitude uncertainty, deg	δt_{rms}, sec	$\delta \tilde{t}_{rms}$, sec
0.50	3.6 - 15.1	0.20 - 1.7
0.25	2.3 - 9.1	0.15 - 1.4

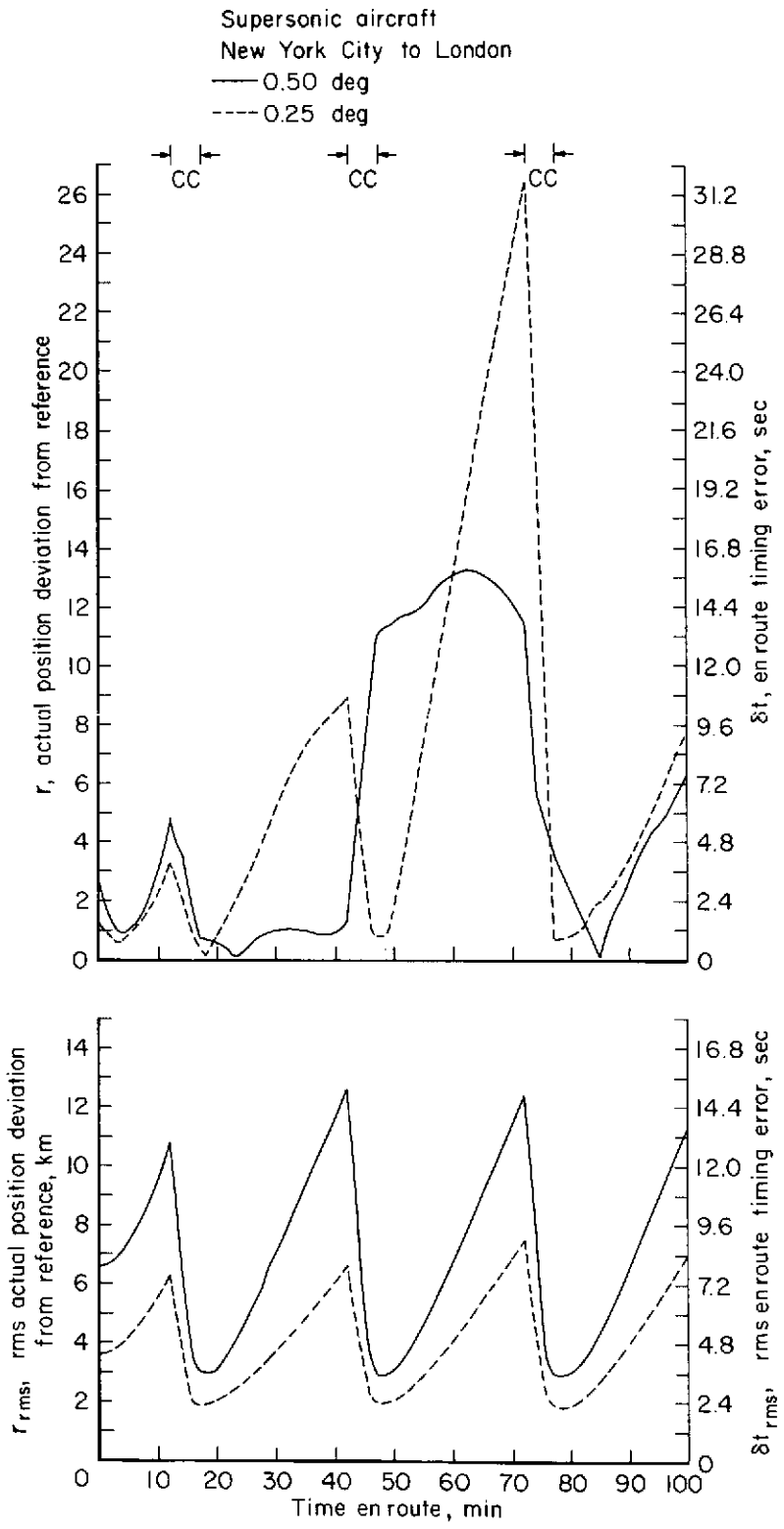

Figure 17.— Comparison of r_{rms} and r for A.U. = 0.50 and 0.25°.

As in the subsonic case, the table shows the en route timing errors are better estimated than controlled. In addition, the table shows a substantial improvement in the time control, δt_{rms}, when the attitude uncertainty is reduced. Comparison of δt_{rms} with the subsonic case shows that improved control is achieved due to the better along-track position control in the supersonic case.

Replacing VORTAC/TACAN With Loran-C

Loran-C was available during about the last 25 percent of the San Francisco to New York City flights. In figure 18, the effect of replacing VORTAC/TACAN data-set samples starting at 64 min is shown. The quantity r_{rms} is

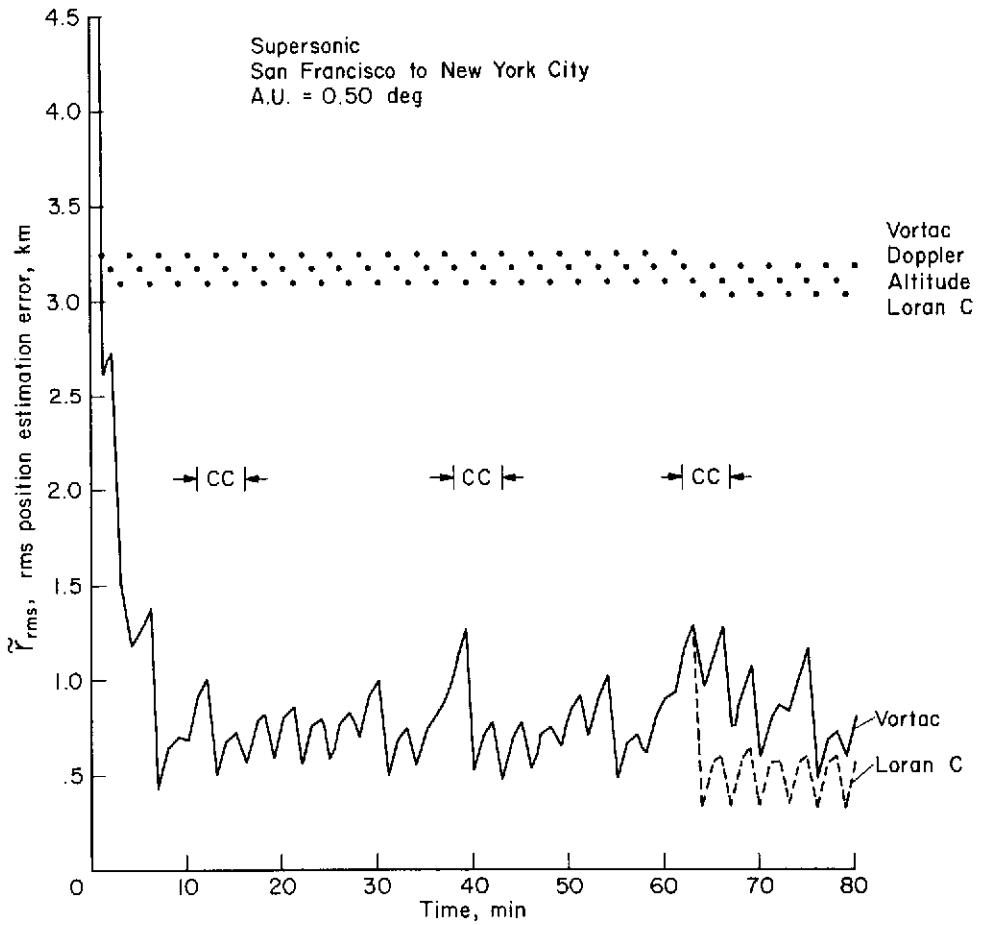

Figure 18.— Comparison of *rms* estimation error using Loran-C and VORTAC/TACAN after 64 min.

compared both before and after the change to Loran-C. This comparison shows a definite reduction in r_{rms} occurs after 64 min time en route, thus demonstrating the superiority of the Loran-C position fixes.

Effect of Increased Data-Set Sample Rate Before Course Corrections

A short investigation was made to determine what improvement, if any, to system performance could be achieved by reducing the position estimation error just prior to the execution of a course correction. Two methods were used on the supersonic San Francisco to New York City flight. The two methods were: (1) retaining the normal sequence of data-set types but doubling the sample rate just prior to the first maneuver and retaining this rate until after the second maneuver for each course correction; and (2) using the same strategy as in (1), but making every other data-set a VORTAC/TACAN data-set and alternating the remaining data-sets between Doppler radar and the radio altimeter. The results obtained showed that neither of these two methods had more than a negligible effect on overall system performance (r_{rms}), even though the position estimation error ($\tilde{r}_{rms}$) was slightly reduced. This effect was observed because the limiting factor in system performance is the course control achievable by the fixed-course-correction-schedule strategy. The dominance of control errors over the effect of estimation error on overall system performance means an improvement in position estimation will have no more than a negligible effect on overall statistical performance. Some individual cases could be expected to show improvement, as was seen in the case where a course correction was made when the aircraft was in an area of poor Loran-C coverage. The only effective way to take advantage of better state estimation to improve system performance would be to improve the course control. One method, described earlier, for improving performance would be an adaptive system which makes corrections at every opportunity, providing the course correction threshold is satisfied.

The effect of reduced velocity estimation error was not investigated because early investigations into data-set sample mixing had shown that it could not be improved more than a negligible amount by: (1) increasing the Doppler radar measurement frequency; or (2) keeping the number of data-sets the same and increasing the ratio of Doppler radar measurements to the other measurements.

Effect of the Correlation Decay Coefficient, α

The correlation decay coefficient, α, in the system dynamics model (appendix C) was chosen to be 60/hr in all the data presented so far. To demonstrate that this choice was not critical, the New York City to London supersonic flight was repeated with α = 30 and 120/hr. Since it was assumed that r_{rms} would show the most change resulting from different choices of α, this quantity was compared for α = 30, 60, and 120 in figure 19. The figure shows that the results are not sensitive to the choice of α.

Summary of Course Correction Changes

The individual case commanded changes in both speed and direction; these are given in table 5 for each maneuver of each course correction. The

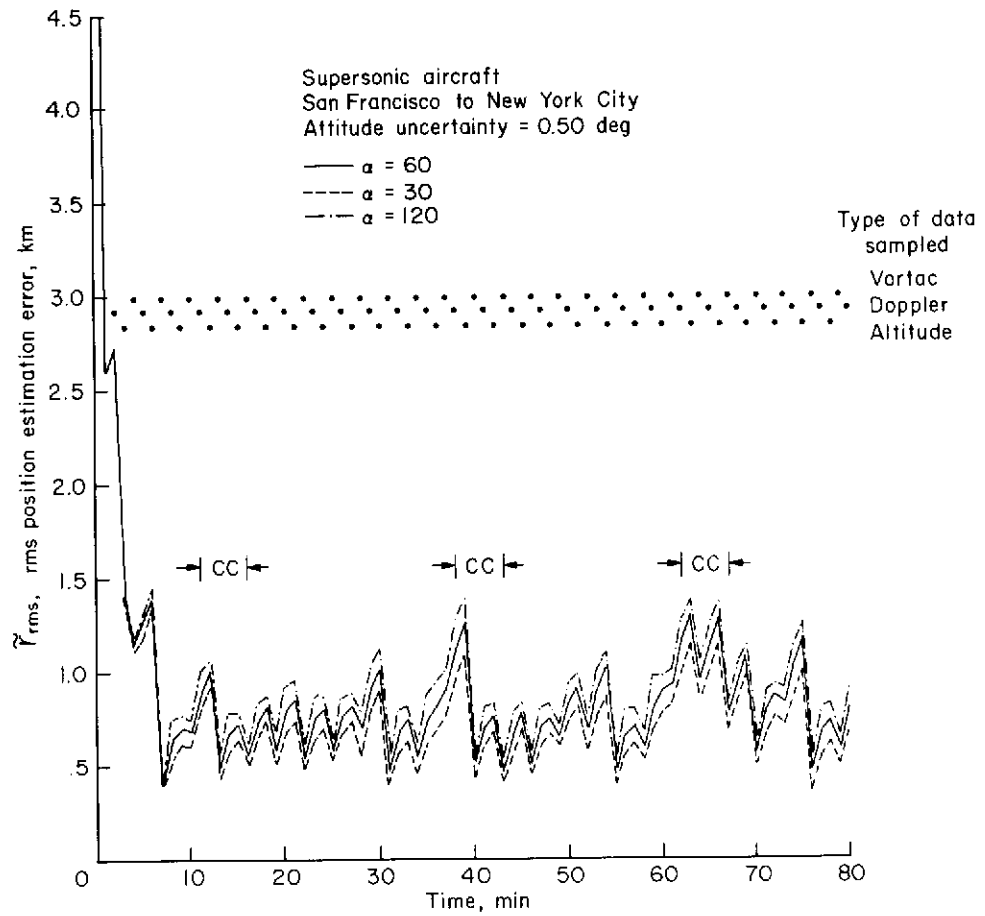

Figure 19.— Comparison of *rms* position estimation error for α = 30, 60, 120.

corresponding statistical changes are also presented for comparison. The summation of magnitudes and the algebraic summation of changes in velocity magnitude and direction are also given for each attitude uncertainty.

When the statistical entries in table 5 are compared for attitude uncertainties of 0.50° and 0.25° for a particular maneuver, it is seen that for 0.25°: (1) the changes in magnitude are only slightly less; and (2) the changes in direction are of the order of 0.6 times that obtained for the 0.50° case.

The speed corrections are nearly the same at each maneuver for the two attitude uncertainties because they depend, to a first order approximation, only on along-track position errors and are independent of estimation and attitude (heading control) uncertainties, as was shown in the "Course Corrections" section of the text. It was also shown in the same section that heading corrections are, to a first order approximation, only a function of the cross-track error. Thus, it is seen that the major influence of heading (attitude)

TABLE 5.— COURSE CORRECTION CHANGES

(a) New York City To London

Course correction	Maneuver	Supersonic aircraft								Subsonic aircraft							
		Commanded velocity corrections (individual case)				*rms* commanded velocity corrections				Commanded velocity corrections (individual case)				*rms* commanded velocity corrections			
		A.U.[a] = 0.5		A.U. = 0.25		A.U. = 0.5		A.U. = 0.25		A.U. = 0.5		A.U. = 0.25		A.U. = 0.5		A.U. = 0.25	
		Δs[b]	$\Delta\psi$[c]	Δs	$\Delta\psi$	Δs	$\Delta\psi$	Δs	$\Delta\psi$	Δs	$\Delta\psi$	Δs	$\Delta\psi$	Δs	$\Delta\psi$	Δs	$\Delta\psi$
1	1st	-12.30	1.49	-12.08	1.09	39.92	2.11	36.97	1.21	-11.24	0.43	-11.38	0.28	27.44	0.62	27.38	0.51
	2nd	11.18	-1.00	12.59	.00	32.06	1.73	28.28	1.00	16.82	0.53	20.12	.00	18.51	.42	18.44	
2	1st	-7.92	1.74	-19.39	-2.21	39.20	3.12	37.44	11.50	.00	1.44	12.34	2.04	15.04	.32	15.04	.16
	2nd	12.24	-2.22	27.07	3.23	33.47	2.70	31.45	1.34	.00	-1.06	.00	-2.57	13.80	.28	13.79	.18
3	1st	38.95	-2.64	41.37	-7.17	41.12	3.08	39.77	1.79	11.48	-3.11	-41.52	-1.02	42.51	.78	42.53	.52
	2nd	-23.82	3.73	-42.11	6.29	34.95	2.67	33.51	1.58	-13.32	2.35	43.44	0.82	31.95	.66	31.87	.44
4	1st									.00	1.72	17.61	1.46	27.58	.53	27.56	.35
	2nd									7.44	0.00	-22.68	-1.26	20.72	.46	20.68	.30
5	1st									.00	2.34	-21.01	-1.32	27.31	.48	27.31	.36
	2nd									12.50	-1.25	16.80	1.83	20.61	.43	20.60	.30
6	1st									.00	3.17	-33.89	-2.39	27.05	.50	27.06	.34
	2nd									-5.81	-3.58	27.06	2.02	20.98	.46	20.98	.30
7	1st									9.87	-.92	.00	.00	19.77	.38	19.76	
	2nd									9.20	3.43	09.84	-.76	22.63	.55	22.62	.29
Summation of magnitudes		106.41	12.82	154.61	19.99	220.72	15.41	207.42	8.42	97.68	25.33	277.69	17.77	335.90	6.87	355.62	4.63

[a] A.U. = *rms* Attitude (heading control) uncertainty, deg.
[b] Δs = Change in groundspeed, km/hr.
[c] $\Delta\psi$ = Change in heading, deg.

TABLE 5.— COURSE CORRECTION CHANGES - Concluded

(b) San Francisco To New York City

Course correction	Maneuver	Supersonic aircraft								Subsonic aircraft							
		Commanded velocity corrections (individual case)				*rms* commanded velocity corrections				Commanded velocity corrections (individual case)				*rms* commanded velocity corrections			
		A.U.[a] = 0.5		A.U. = 0.25		A.U. = 0.5		A.U. = 0.25		A.U. = 0.5		A.U. = 0.25		A.U. = 0.5		A.U. = 0.25	
		Δs[b]	$\Delta\psi$[c]	Δs	$\Delta\psi$	Δs	$\Delta\psi$	Δs	$\Delta\psi$	Δs	$\Delta\psi$	Δs	$\Delta\psi$	Δs	$\Delta\psi$	Δs	$\Delta\psi$
1	1st	-5.83	1.67	0.00	0.76	36.29	2.00	34.57	1.13	-10.63	3.08	-11.52	2.44	21.89	0.48	21.87	0.07
	2nd	0.00	-.91	.00	.41	28.38	1.67	26.11	.96	6.29	.00	5.27	.50	14.88	.31	14.86	.25
2	1st	14.41	.00	7.60	-4.46	43.26	2.63	40.04	1.60	36.77	-4.72	27.61	-1.55	28.91	.49	28.67	.40
	2nd	.00	.47	-13.52	2.86	37.07	2.25	33.49	1.40	-36.64	2.22	-24.38	-1.44	21.62	.43	21.40	.34
3	1st	.00	-.85	83.17	2.54	36.29	2.34	33.86	1.42	12.54	4.72	-17.09	4.12	29.14	.48	28.98	.34
	2nd	-8.08	.00	-86.18	-2.05	30.75	2.01	28.06	1.25	-7.97	-1.22	18.70	-3.23	22.01	.40	21.83	.29
4	1st									12.39	-1.09	13.89	0.25	28.78	.46	28.72	.31
	2nd									-5.98	.00	.00	-.82	21.97	.40	21.87	.27
5	1st									.00	2.30	14.61	.00	28.82	.31	28.81	.28
	2nd									-11.83	-2.18	-19.91	.25	22.75	.38	22.66	.25
Summation of magnitudes		28.32	3.90	190.47	13.08	212.04	12.90	196.13	7.76	141.04	21.58	152.98	14.60	240.77	4.14	239.67	3.10

[a] A.U. = *rms* Attitude (heading control) uncertainty, deg.
[b] Δs = Change in groundspeed, km/hr.
[c] $\Delta\psi$ = Change in direction (heading), deg.

uncertainty is on the cross-track position control; changes in heading uncertainty result in nearly linear corresponding changes in the cross-track components of r_{rms} and v_{rms}.

The commanded changes (individual case) are signed values to indicate the direction of the change. These commanded changes exhibit some randomness in magnitude when the first and second maneuvers of each course correction are compared. The signs of the heading and speed commands for the second maneuver will almost always be opposite to those of the first maneuver. This effect is observed because, ideally, the first maneuver of the course correction causes the aircraft to intercept a nearby point on the reference trajectory, matching both position and time at that point. The second maneuver then matches the reference velocity vector at the intercept point. This strategy requires relatively large changes at the first maneuver and makes a second maneuver mandatory in order to remove most of the speed and heading changes applied at the first maneuver. The advantage of this strategy is that timing relative to a reference path is controlled at any time along the reference path. This en route time control advantage is obtained by using speed (thrust) changes in the correction maneuvers in addition to the heading changes necessary to control the cross-track position errors.

Increasing the number of course corrections, either by a fixed-schedule or by use of an adaptive control system, will improve the en route time and position performance of the system. When this process is accomplished, it can be expected that there will be an increase in the number of individual (speed or heading) commanded changes which will be so small that they will be below the threshold of the course correction system and will be skipped. In effect, it is these speed and heading thresholds in the automatic control system which establish the lower limit of position and en route time control which can be achieved. In this report, individual commanded changes which were below their respective thresholds and were skipped by the automatic control system are shown as zeros in table 5.

Each column in table 5 has a summation of the magnitudes of the values appearing in that column. This summation is an indication of the total throttle activity required for time control. The required thrust changes for each maneuver are proportional to Δs. It can be seen in table 5 that, for each case, the *rms* speed changes are approximately the same for every speed correction; hence, *rms* thrust changes are about the same each time the speed is corrected.

Comparison of the results in table 5 for the two attitude uncertainties indicates that the total *rms* Δs requirements are independent of attitude uncertainty. It can also be seen from the individual cases that the speed change in the second maneuver approximately cancels the speed change of the first maneuver at each course correction. The cancelled portion is due to the time correction and the residual speed change is due to correction of the initial error in speed from the reference speed.

The summation of the magnitudes of the heading changes indicates the total heading control activity used to control the cross-track position. The

attitude uncertainty has a pronounced effect on the heading control activity, as expected.

RESULTS AND CONCLUSIONS

The results of this study show that a navigation system such as the one described in this report has excellent en route time control capability throughout the entire flight of subsonic or supersonic aircraft traveling along either of the great-circle routes considered. It is shown that good system performance throughout the entire flight requires both good state estimation and good control over the actual state.

The results summarized below are taken from the digital simulation after sufficient time has been allowed for the system to "settle out." All summary data presented in this section will be for an attitude uncertainty of 0.50°

Summary of Results

The basic assumptions which were made for the transcontinental flight are summarized in the table below

	Supersonic	Subsonic
Altitude	21.336 km (70,000 ft)	10.668 km (35,000 ft)
Speed	3,000 km/hr	1,000 km/hr
Course correction schedule (see table 1)	Every 30 min (3 course corrections)	Every 45 min (5 course corrections)
Data types	TACAN/VORTAC, Doppler, radio, barometric altimeter	
Data sampling	Sequential, once every min	Sequential, once every 3 min

Similarly, the assumptions which were made for the trans-Atlantic flight are summarized in the following table.

	Supersonic	Subsonic
Altitude	21.336 km (70,000 ft)	10.668 km (35,000 ft)
Speed	3,000 km/hr	1,000 km/hr
Course correction schedule (see table 1)	Variable — approximately every 25 min (3 corrections)	Variable — approximately every 45 min (7 corrections)
Data types	Loran-C, doppler radar, radio altimeter	
Data sampling	Sequential, once every min	Sequential, once every 3 min

The results obtained for the transcontinental and the trans-Atlantic flights are presented in terms of an approximate range for the following variables: (a) *rms* en route timing error, δt_{rms}; (b) *rms* uncertainty in the en route timing error, $\delta \tilde{t}_{rms}$; (c) *rms* deviation from the reference path, r_{rms}; (d) *rms* position estimation error, $\tilde{r}_{rms}$; and (e) *rms* commanded speed correction. These variables are tabulated below for an attitude uncertainty of 0.50°

	δt_{rms}, sec	$\delta \tilde{t}_{rms}$, sec	r_{rms}, km	$\tilde{r}_{rms}$, km	Δs_{rms}
Transcontinental flight					
Supersonic	3.7 - 14.5	0.6 - 1.6	3.1 - 12.1	0.35 - 1.25	28.4 - 43.3
Subsonic	13.5 - 30.0	1.8 - 6.0	3.8 - 8.3	0.50 - 1.65	14.9 - 29.1
Trans-Atlantic flight					
Supersonic	3.6 - 16.4	0.20 - 1.7	2.9 - 12.7	0.20 - 1.50	32.1 - 41.1
Subsonic	12.2 - 41.8	1.3 - 8.0	3.4 - 11.6	0.15 - 2.30	13.8 - 42.5

Conclusions

1. The maximum *rms* actual position deviation from the reference position is dependent upon the number and spacing of the course corrections.

2. The system performance is limited by the execution errors in the control system and external forces in the physical environment. Thus, the realizable minimum values of r_{rms} at the intercept point on the reference path is significantly larger than $\tilde{r}_{rms}$ and the aircraft trajectory is better estimated than it can be controlled.

3. The minimum *rms* value of $\tilde{r}_{rms}$ can be reduced slightly by increasing the data-set sample rate just prior to making the course corrections.

4. A minimum *rms* actual position deviation from the reference (and *rms* actual en route timing error) may be moved to any desired point along the reference flight path by changing the course correction schedule so that a minimum *rms* deviation occurs at the desired time.

5. Loran-C position fixes are more accurate than those obtained from VORTAC/TACAN position fixes.

6. The system performance is relatively insensitive to the choice of value used for the correlation decay coefficient, α, in the dynamic system model within the range from 30 to 120/hr.

7. The supersonic aircraft guidance and navigation system in this report could meet the lateral separation standards presently specified by the FAA over the continental United States by an increase in the number of course corrections from three to four or five. The en route timing error standard was easily met. Thirty sec or less was obtained with the schedule used in this study.

8. Along a great-circle route in the North Atlantic, the performance of the guidance and navigation system in both the lateral and longitudinal

directions was such that the lateral position error was less than 13 km and the en route timing error was less than 42 sec on all flights.

9. It is postulated that a modification to the course control strategy would provide an adaptive control system capable of substantially improved performance.

Ames Research Center
National Aeronautics and Space Administration
Moffett Field, Calif., 94035, May 10, 1973

APPENDIX A

EFFECT OF GEOMETRY ON LORAN-C POSITION UNCERTAINTY

To obtain a position fix, a Loran-C receiver is used to obtain two simultaneous time difference readings from a master and two slave stations in a particular group or chain of stations identified by a basic and a specific pulse repetition rate. The time difference readings define two hyperbolic lines-of-position (LOP's) whose point of intersection is the desired position fix. The accuracy of this fix is dependent upon the geometric location of the receiver with respect to the master and two slave stations and on the receiver itself. The geometric location of the stations used in this report is that of January 17, 1969 (reference 5), and is shown in figure 2 in the text. When a particular station group is chosen, the effect on position accuracy due to that particular geometry with respect to the receiver is fixed and arises because of the hyperbolic nature of the LOP's and the fact that the two LOP's do not, in general, cross at right angles.

The errors in measuring the two time differences in the time of arrival of the pulses from the selected master and two slaves, say x and y, are assumed to have Gaussian distributions with variances σ_x^2 and σ_y^2.

The position fix is desired in terms of latitude and longitude and it is therefore necessary to find the components of σ_x^2 and σ_y^2 in these spherical coordinates. The method for finding these variances is given in reference 10 but was modified somewhat to obtain the results given in reference 3 for an intermediate orthogonal coordinate system (W,Z). The results in terms of equivalent distance units are:

$$\sigma_w^2 = \frac{C^2}{4 \sin \delta}\left[\frac{\sigma_x^2}{\sin^2 \eta_x}\cos^2 \delta + \frac{2\rho_{xy}\sigma_x\sigma_y \cos \delta}{\sin \eta_x \sin \eta_y} + \frac{\sigma_y^2}{\sin^2 \eta_y}\right] \tag{A1}$$

$$\sigma_z^2 = \frac{C^2\sigma_x^2}{4 \sin^2 \eta_x} \tag{A2}$$

$$\rho_{wz} = \frac{\dfrac{\sigma_x \cos \delta}{\sin \eta_x} + \dfrac{\rho_{xy}\sigma_y}{\sin \eta_y}}{\left[\dfrac{\sigma_x^2}{\sin^2 \eta_x}\cos^2 \delta + \dfrac{\sigma_y^2}{\sin^2 \eta_y} + \dfrac{2\rho_{xy}\sigma_x\sigma_y \cos \delta}{\sin \eta_x \sin \eta_y}\right]^{1/2}} \tag{A3}$$

where C is the velocity of light in kilometers/microsecond and η_x and η_y are one-half of the angles between a line drawn from the point of LOP intersection to the master station and a line from the same point to slave station x and to slave station y, respectively. (See sketch (Aa).) The LOP crossing angle,

δ, is given by

$$\delta = \eta_x + \eta_y \tag{A4}$$

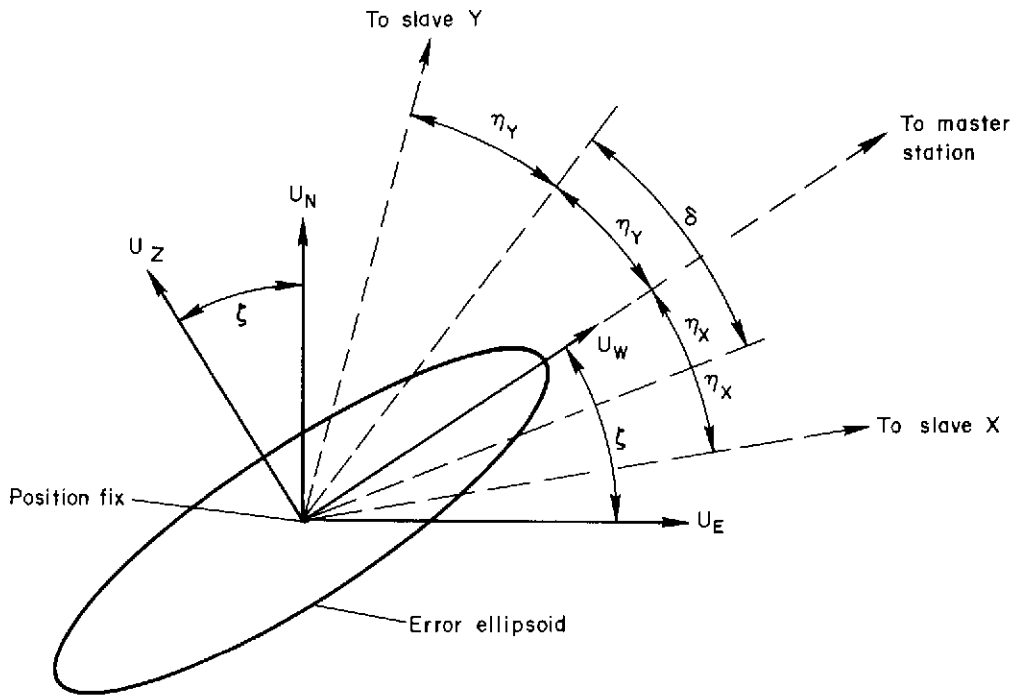

Sketch (Aa)

The correlation coefficient, ρ_{xy}, is due to both time differences being measured with respect to the same master station pulse. Reference 10 gives 0.3 as the usual value chosen for ρ_{xy}.

The results in equations (A1), (A2), and (A3) can be expressed as a covariance matrix, Q, which represents an error ellipsoid in the W, Z coordinate system. Thus

$$Q = \begin{bmatrix} \sigma_w^2 & \rho_{wz}\sigma_w\sigma_z \\ \rho_{wz}\sigma_z\sigma_w & \sigma_z^2 \end{bmatrix} \tag{A5}$$

Essentially following references 3 and 10, the major axis of the error ellipsoid lies along a line from the position fix (LOP crossing point) to the master station, with its center located at the position fix. Let two unit vectors, U_W and U_Z, lie along the major axis and the minor axis, respectively, of the error ellipsoid as shown in sketch Aa. This sketch shows the relationship of the error ellipsoid to the station geometry and includes:

(1) two unit vectors, U_N and U_E, which are directed to the north and east, respectively, from the position fix; (2) typical directions to the master and two slave stations; and (3) the angles η_x and η_y, which in equation (A4) define the LOP crossing angle, δ. From this sketch, the angle, ζ, between the W, Z coordinate system and latitude, longitude coordinate system (U_E, U_N) is found from

$$\cos \zeta = U_W \cdot U_E = U_Z \cdot U_N \tag{A6}$$

This angle allows transformation of the error ellipsoid into the latitude, longitude coordinate system using a transformation matrix of the form

$$b = \begin{bmatrix} \cos \zeta & -\sin \zeta \\ \sin \zeta & \cos \zeta \end{bmatrix} \tag{A7}$$

The covariance matrix of the position fix uncertainty in terms of distance squared in the latitude, longitude coordinate system (ϕ, λ) is given by:

$$Q^*_{\phi\lambda} = bQb^T$$

Given the magnitude of the radial distance from the center of the earth to the aircraft, $|R|$, and an estimate of the latitude, ϕ, a transformation matrix A is formed which transforms $Q^*_{\phi\lambda}$ into angular units (radians) squared. Thus,

$$Q_{\phi\lambda} = AQ^*_{\phi\lambda}A^T$$

where

$$A = \frac{1}{|R|} \begin{bmatrix} \sec \phi & o \\ o & 1 \end{bmatrix}$$

The matrix $Q_{\phi\lambda}$ is used as the measurement uncertainty matrix for Loran-C in the Kalman filter and in the generation of the random errors for simulating the output of the Loran-C coordinate converter; the output of this converter is latitude and longitude, given two time differences from a master and two slave stations.

APPENDIX B

TRANSISTION MATRIX FOR THE EQUILIBRIUM FLIGHT PATH

A general transition matrix $\phi(t_o + \tau, t_o)$ will be derived which allows the aircraft state at time $t = t_o + \tau$ to be found from the aircraft state at $t = t_o$ along an equilibrium path. The general form of this transition matrix will be such that it will be applicable to all three aircraft states used in this report (i.e., the reference, actual, and estimated states), requiring only that the transition matrix be evaluated from the appropriate state variables. Thus, the computation to find the estimated aircraft state at $t = t_o + \tau$ is simply

$$\hat{\chi}(t_o + \tau) = \Phi(t_o + \tau, t_o)\hat{\chi}(t_o) \tag{B1}$$

where

$$\hat{\chi}(t_o) = \begin{bmatrix} R(t_o) \\ \\ V(t_o) \end{bmatrix}$$

In this study, the basic form of equation (B1) will be used to predict the equilibrium path from one data-set sample to the next and for predicting the effect of added velocity increments in computing course corrections. The prediction is in error due to unknown randomly occurring forces during the interval, such as automatic control system errors and wind disturbances.

The equilibrium kinematics are defined by the assumptions that

1. The angular momentum of the aircraft with respect to the earth is conserved.
2. Altitude rate is constant over the period τ. Equivalently, the aircraft is assumed to be flying in a plane (great-circle) with respect to the earth, with constant altitude rate, and a groundspeed-altitude relation that conserves angular momentum.

The equilibrium path—The motion of the aircraft is described in two coordinate systems: (1) a right-handed Cartesian system rotating with the earth, in which the Z-axis passes through the North Pole and is the axis of rotation, the X-axis coincides with the meridian of zero longitude, and the Y-axis is at 90° east longitude; and (2) a system consisting of a unit vector, $\hat{i}_r$, which lies along the instantaneous position vector, $R(t)$; a unit vector, $\hat{i}_p$, which is perpendicular to $\hat{i}_r$ in the plane of motion and in the direction of motion; and a unit vector, $\hat{i}_q$, perpendicular to both $\hat{i}_r$ and $\hat{i}_p$, and given

by $\hat{i}_r \chi \hat{i}_p$. These coordinate systems are shown in the following sketch (Ba).

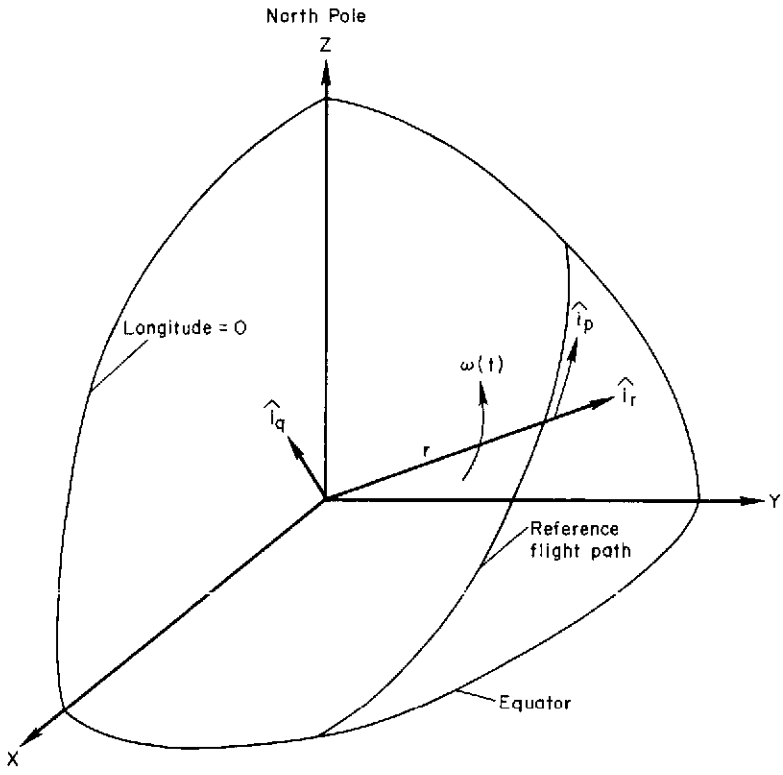

Sketch (Ba)

The position and velocity of the aircraft may now be defined as

$$R = r\hat{i}_r$$

$$V = V_p\hat{i}_p + \dot{r}\hat{i}_r \tag{B2}$$

Since the altitude rate is assumed to be constant during the period τ, then

$$\dot{r}(\tau) = \dot{r}(t_o) = \dot{r}_o$$

$$r(\tau) = r_o + \dot{r}_o\tau \tag{B3}$$

Because the angular momentum

$$R\chi V = rV_p\hat{i}_q$$

is conserved, then

$$\frac{d}{d\tau} i_q = 0$$

and

$$V_p(\tau)r(\tau) = V_p(t_o)r(t_o) = V_{po}r_o \tag{B4}$$

or

$$V_p(\tau) = V_{po}r_o/(r_o + \dot{r}_o\tau)$$

The vectors $\hat{i}_r(\tau)$ and $\hat{i}_p(\tau)$ are found as follows: Since $\hat{i}_q = o$, the aircraft motion remains in the plane defined by R_O and V_O, hence $\hat{i}_O(\tau)$, $\hat{i}_p(\tau)$, $\hat{i}_{ro}$, and $\hat{i}_{po}$ are all in the same plane. Sketch (B-b) shows the relationship of these two sets of orthogonal unit vectors after rotation in the plane of motion through the angle θ.

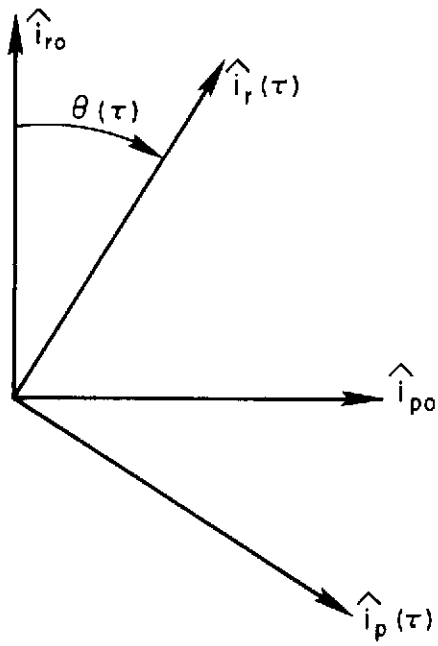

Sketch (Bb)

From this sketch, an expression relating the two sets of unit vectors may be written as follows:

$$\begin{bmatrix} \hat{i}_r(\tau) \\ \hat{i}_p(\tau) \end{bmatrix} = \begin{bmatrix} \cos\theta(\tau) & \sin\theta(\tau) \\ -\sin\theta(\tau) & \cos\theta(\tau) \end{bmatrix} \begin{bmatrix} \hat{i}_{ro} \\ \hat{i}_{po} \end{bmatrix} \tag{B5}$$

The unknown angle, $\theta(\tau)$, is evaluated from

$$\dot{\theta}(\tau) = V_p(\tau)/r(\tau)$$

which, after integrating, using equations (B3) and (B4), gives

$$\theta(\tau) = \frac{V_{po}\tau}{r_o + \dot{r}_o\tau} = \eta\tau \tag{B6}$$

The state at $t = t_o + \tau$ may now be expressed in terms of the initial state and the time increment, τ. Combining equations (B2), (B3), (B5), and (B6), we obtain:

$$\begin{aligned} R(\tau) &= \frac{1}{\eta}\left[\omega_o \cos\eta\tau - \frac{\dot{r}}{r}\sin\eta\tau\right] R_o + \frac{1}{\eta}\sin\eta\tau V_o \\ V(\tau) &= \left[\mu\eta\tau\cos\eta\tau - (\mu + \eta)\sin\eta\tau\right]\left[R_o + \frac{1}{\omega_o}\left(\frac{\dot{r}}{r_o}\sin\eta\tau + \eta\cos\eta\tau\right)\right] V_o \end{aligned} \tag{B7}$$

where $$\omega_o = \frac{V_{po}}{r_o},\quad \mu = \frac{\dot{r}^2}{v_{po}r_o},\quad \text{and}\quad \eta = \frac{V_{po}}{r_o + \dot{r}_o\tau}$$

In transition matrix form, with R_o and V_o given in terms of the Cartesian coordinates shown in the first sketch in this appendix, equation (B7) becomes

$$\begin{bmatrix} R(\tau) \\ V(\tau) \end{bmatrix} = \Phi(t_o + \tau, t_o) \begin{bmatrix} R_o \\ V_o \end{bmatrix} \tag{B8}$$

where

$$\phi(t_o + \tau, t_o) = \left[\begin{array}{c|c} \frac{1}{\eta}\left(\omega_o \cos \eta\tau - \frac{\dot{r}}{r_o} \sin \eta\tau\right) I & \left(\frac{1}{\eta} \sin \eta\tau\right) I \\ \hline \left[\mu\eta\tau \cos \eta\tau - (\mu + \eta) \sin \eta\tau\right] I & \frac{1}{\omega_o}\left(\frac{\dot{r}}{r_o} \sin \eta\tau + \eta \cos \eta\tau\right) I \end{array}\right] \tag{B9}$$

where I is the 3×3 identity matrix. The quantities in ϕ are functions of initial conditions and time and are evaluated for the estimated, actual and reference paths using the respective initial conditions for the path in question.

APPENDIX C

COMPUTATION OF ΔX_A, ΔX_E, AND THE MATRICES ΔR AND ΔP FOR WANDER FROM THE PREDICTED PATH

The Kalman filter is used to process measurement data-sets every Δt hours. Between any two of these measurement data-sets, say at t_{k-1} and t_k, the aircraft velocity vector wanders in pitch, heading, and velocity magnitude from that predicted by the transition matrix for conditions at t_{k-1}. This non-deterministic wander from the predicted path is due to random disturbances such as changes in the wind, air density, temperature, and so forth. The on-board automatic control system is assumed to be capable of limiting the excursions due to these disturbances but, because of errors in the measurement devices and errors in the automatic control system itself, the aircraft does not follow the desired (commanded) flight path. In addition, because of the instrument and estimation errors, it was assumed that the on-board system would not have a precise measure of deviations from the commanded flight path. Thus, only an estimate of the actual flight could be made. Furthermore, because of the dynamics of the aircraft, its automatic control system, and time constants in the measurement devices, the deviations from the commanded flight path were modeled as time correlated error sources, as were the instrument errors. The statistical model of the deviations of the actual state from the reference state will be considered in two parts: (1) nonstationary; and (2) stationary. Nonstationary statistics result when a course correction is executed. At this time, the Kalman filter processes a final data-set and the updated aircraft state is used in the course correction computation to find incremental changes in speed, heading, and pitch. The automatic control system is directed to change rapidly the aircraft heading and pitch by the incremental values and then change the speed by the commanded incremental value. During the short period of time the speed is being changed, the uncertainties in heading, pitch, and roll are equal to the short period instrument errors of the vertical and heading reference. Since the long period errors have a time constant of 60 sec, the error in the control system implementation of the incremental changes is assumed negligible. Following the completion of the course correction maneuver, the uncertainties in the new pitch, roll, heading, and speed increase as the long time constant errors come into play. That is, the control system must now maintain total pitch, roll, heading, and speed rather than implement an incremental change as was done in the course correction.

The long period errors are assumed to be characterized by the following differential equation:

$$\begin{bmatrix} \dot{\sigma}_\theta' \\ \dot{\sigma}_\psi' \\ \dot{\sigma}_\phi' \\ \dot{\sigma}_s' \end{bmatrix} = -\alpha \begin{bmatrix} \sigma_\theta' \\ \sigma_\psi' \\ \sigma_\phi' \\ \sigma_s' \end{bmatrix} + \alpha \begin{bmatrix} \sigma_\theta \\ \sigma_\psi \\ \sigma_\phi \\ \sigma_s \end{bmatrix} \tag{C1}$$

where σ_θ, σ_ψ, σ_ϕ, and σ_s are the long period constants taken from table 2 in the text. A solution to equation (C1) is

$$\begin{bmatrix} \sigma_\theta' \\ \sigma_\psi' \\ \sigma_\phi' \\ \sigma_s' \end{bmatrix} = \begin{bmatrix} \sigma_\phi \\ \sigma_\psi \\ \sigma_\phi \\ \sigma_s \end{bmatrix} (1 - e^{-\alpha\tau}) \tag{C2}$$

where τ is equal to $n\Delta t$ — the number of Δt intervals occurring since the last course correction. When 10 Δt intervals have passed ($n = 10$), the statistics of the deviations are considered to have exponentially reached stationary[1] values. Under these conditions, the primed values on the left side of equation (C2) are replaced by the unprimed values on the right.

The error sample generation process used to obtain the actual state deviations from the reference state at t_k is essentially four identical first order filters driven by individual random noise sources whose variance is determined by equation (C2). The well-known discrete form of the sample generation process which simulates the effect of a first order filter is given below:

$$\begin{bmatrix} \Delta\theta \\ \Delta\psi \\ \Delta\phi \\ \Delta_s \end{bmatrix}_k = \begin{bmatrix} \Delta\theta \\ \Delta\psi \\ \Delta\phi \\ \Delta_s \end{bmatrix}_{k-1} e^{-\alpha\Delta\tau} + (1 - e^{-2\alpha\Delta\tau})^{1/2} \begin{bmatrix} \sigma_\theta' U_1 \\ \sigma_\psi' U_2 \\ \sigma_\phi' U_3 \\ \sigma_s' U_4 \end{bmatrix} \tag{C3}$$

[1]This assumption is not strictly true in the case of the heading error standard deviation which is actually increasing at 0.1°/hr due to a pseudo-gyroscope drift discussed in the text.

where the U_i $(i = 1, 2, 3, 4)$ are Gaussian, zero mean, unit variance, random numbers which are independent of each other and uncorrelated in time. Equation (C3) generates error samples which are correlated in time with previous samples and is an expression normally used with stationary statistics; that is, the variances of the samples generated by this expression are constant when the variances given by equation (C2) have reached stationary values. In addition, these pitch, heading, and speed samples are measured in an ALT, ALONG-TRACK, CROSS-TRACK coordinate system defined by the reference state at t_k. The roll angle, $\Delta\phi$, has little significance in the simulation results, but was carried along for completeness. The limiting action of the automatic control system was simulated by examining the heading deviation, $\Delta\psi$, given by equation (C3) and, if larger than $\pm\sqrt{2.0}°$, was reduced to the nearest $\pm\sqrt{2.0}°$.

The samples obtained from equation (C3) represent the deviation of the actual trajectory from the reference trajectory. The samples represent changes in the aircraft trajectory because of variations in such factors as wind, air density, control system errors, and so forth. If it were not for these deviations, the aircraft would fly along the reference path by virtue of the fact that nominal corrections have already been applied to the aircraft speed, heading, and pitch attitude by the on-board computer.

In this study, a vector, ΔX_A, is used to modify the existing actual state so that it corresponds to the actual state indicated by the error samples obtained from equation (C3). This procedure is implemented immediately before the processing of a data-set by the Kalman filter.

Derivation of ΔX_A

To compute the ΔX_A, used in the text, an expression is required for the new actual velocity vector in terms of the error samples which have already been found. Thus, the new actual velocity is given by

$$V_A^*(t_k) = |V_A|(t_k) \begin{bmatrix} \Delta\theta \\ 1 \\ \Delta\psi \end{bmatrix}_{t_k} \tag{C4}$$

where

$$|V_A|(t_k) = |V_A|(t_k^-) + \Delta s(t_k) \tag{C5}$$

is the new groundspeed obtained by adding the speed change $\Delta s(t_k)$ to the speed predicted by the transition matrix from conditions at t_{k-1}.

Let the predicted actual state at t_k^- be expressed by

$$X_A^*(t_{k^-}) = \begin{bmatrix} X^*_{A1} \\ X^*_{A2} \end{bmatrix}_{t_{k^-}} \tag{C6}$$

and let the desired ΔX_A in the same coordinate system be given by

$$\Delta X_A^*(t_k) = \begin{bmatrix} \Delta X^*_{A1} \\ \Delta X^*_{A2} \end{bmatrix}_{t_k} \tag{C7}$$

The required change in velocity can now be written as

$$\Delta X^*_{A2}(t_k) = V_A^*(t_k) - X^*_{A2}(t_{k^-}) \tag{C8}$$

The position deviation from that predicted by the transition matrix from conditions at t_{k-1} is obtained by assuming that this change is parallel to the new velocity vector in the ALT and CROSS-TRACK directions, but equal to Δt times Δs in the ALONG-TRACK direction. Thus

$$\Delta X^*_{A1}(t_k) = \Delta t \begin{bmatrix} |V_A|\Delta\theta \\ \Delta s \\ |V_A|\Delta\psi \end{bmatrix}_{t_k} \tag{C9}$$

All of the elements of equation (C7) have been determined in the reference ALT, ALONG-TRACK, CROSS-TRACK coordinate system. To find ΔX_A, all that remains is to transform equation (C7) into the X, Y, Z coordinate system. Thus the required matrix operation is

$$\Delta X_A(t_k) = \begin{bmatrix} T & 0 \\ 0 & T \end{bmatrix} \Delta X_A^*(t_k) \tag{C10}$$

where T is the known 3×3 transformation matrix.

Derivation of the Matrix ΔR

Equation (18) in the text shows the addition of a matrix ΔR after the transition matrix has been used to update $R(t_{k-1})$ to $R(t_k)$. The quantity ΔR is added to account for the increase in uncertainty in the deviation between the actual and reference trajectories following course correction maneuvers as given by equation (C2). Equation (C2) produces nonstationary variances following each course correction and reaches a stationary value after 10 data-sets have been processed. It is this increase in the variance for each Δt that must be accounted for by ΔR.

Returning to equation (C2), the change in the left side as a function of n is given by

$$\begin{bmatrix} \delta\sigma_\theta \\ \delta\sigma_\psi \\ \delta\sigma_s \end{bmatrix} = \begin{bmatrix} \sigma_\theta \\ \sigma_\psi \\ \sigma_s \end{bmatrix} (1-e^{-\alpha\Delta t})(e^{-\alpha\eta\Delta t}) \tag{C11}$$

Now, translating into equivalent ALT, ALONG-TRACK, and CROSS-TRACK velocities and positions we have

$$\delta\chi^* = \begin{bmatrix} \delta\sigma_\theta |V_A| \Delta t \\ \delta\sigma_s \Delta t \\ \delta\sigma\psi |V_A| \Delta t \\ \delta\sigma_\theta |V_A| \\ \delta\sigma_s \\ \delta\sigma_\psi |V_A| \end{bmatrix} (1 - e^{-\alpha\Delta t})(e^{-\alpha\eta\Delta t}) \tag{C12}$$

The matrix R_w^* is given by

$$R_w^* = E(\delta\chi^* \delta\chi^{*t}) = (R_w^*)^{1/2}(R_w^*)^{1/2} \tag{C13}$$

where both R_w^* and $(R_w^*)^{1/2}$ are diagonal matrices and the elements of $(R_w^*)^{1/2}$ are the square roots of the elements of R_w^*. Thus, the diagonal elements of $(R_w^*)^{1/2}$ are the elements of the 6×1 vector $\delta\chi^*$; all other elements are zero.

To find ΔR it is first necessary to transform $R(t_{\bar{k}})$ into the reference ALT, ALONG-TRACK, CROSS-TRACK coordinate system to obtain $R^*(t_{\bar{k}})$. Define

$$D(t_k) \text{ and } D(t_{\bar{k}}) = \text{diagonal matrices whose elements are the square roots of the diagonal elements of } R^*(t_k) \text{ and } R^*(t_{\bar{k}}), \text{ respectively.} \tag{C14}$$

Now,

$$\begin{aligned} \Delta R^* &= D^2(t_k) - D^2(t_{\bar{k}}) \\ &= D(t_{\bar{k}}) + R_w^{*1/2} - D^2(t_{\bar{k}}) \\ &= R_w^* + 2D(t_{\bar{k}})R_w^{*1/2} \end{aligned} \tag{C15}$$

The matrix ΔR is found by using the transformation matrix, T, and transforming ΔR^* as follows:

$$\Delta R = \begin{bmatrix} T & O \\ O & T \end{bmatrix} \Delta R^* \begin{bmatrix} T & O \\ O & T \end{bmatrix}^T \tag{C16}$$

Derivation of the Matrix ΔP

During the interval (t_{k-1}, t_k) between measurements, the uncertainty in the state estimate obtained at t_{k-1} increases because of random changes in the wind, air density, and so forth. This increase is assumed to satisfy equation (C1) with the following solution:

$$\begin{bmatrix} \Delta\sigma_\theta \\ \Delta\sigma_s \\ \Delta\sigma_\psi \end{bmatrix} = \begin{bmatrix} \sigma_\theta - (P^*_{44})^{1/2}/|V_E| \\ \sigma_s - (P^*_{55})^{1/2} \\ \sigma_\psi - (P^*_{66})^{1/2}/|V_E| \end{bmatrix} (1-e^{-\alpha\Delta t}) \tag{C17}$$

where the σ's are the same as those in equation (B1) and the $(P^*_{jj})^{1/2}$, $j = 4$, 5, and 6, are the square roots of the diagonal elements of the P matrix, which has been transformed into the actual ALT, ALONG-TRACK, CROSS-TRACK coordinate system.

In equation (C17), the column vector on the right is the driving uncertainty. It is obtained by subtracting the rms uncertainty in the current estimate of the aircraft pitch, speed, and heading from the corresponding

rms instrument uncertainty. These instrument uncertainties are the values to which the pitch, speed, and heading uncertainties would eventually rise if no further aircraft state estimates were obtained through the processing of navigation information. The matrix P_w is the covariance of the increase given by equation (C17). Therefore, following the method used to find ΔR, we have

$$P_w = P_w^{1/2} P_w^{1/2} = E \begin{bmatrix} \Delta\sigma_\theta |V_E| \Delta t \\ \Delta\sigma_s \Delta t \\ \Delta\sigma_\psi |V_E| \Delta t \\ \Delta\sigma_\theta |V_E| \\ \Delta\sigma_s \\ \Delta\sigma_\psi |V_E| \end{bmatrix} \begin{bmatrix} \sigma_\theta |V_E| \Delta t \\ \Delta\sigma_s \Delta t \\ \Delta\sigma_\psi |V_E| \Delta t \\ \Delta\sigma_\theta |V_E| \\ \Delta\sigma_s \\ \Delta\sigma_\psi |V_E| \end{bmatrix}^T \tag{C18}$$

from which

$$P_w^{1/2} = \left(1 - e^{-\alpha\Delta t}\right) \left[\begin{array}{ccc:ccc} \Delta\sigma_\theta |V_E| \Delta t & 0 & 0 & & & \\ 0 & \Delta\sigma_s \Delta t & 0 & & 0 & \\ 0 & 0 & \Delta\sigma_\psi |V_E| \Delta t & & & \\ \hdashline & & & \Delta\sigma_\theta |V_E| & 0 & 0 \\ & 0 & & 0 & \Delta\sigma_s & 0 \\ & & & 0 & 0 & \Delta\sigma_\psi |V_E| \end{array}\right] \tag{C19}$$

Now, using the same approach used to find ΔR, define

$DP(t_k)$ and $DP(t_{\bar{k}})$ = diagonal matrices whose elements are the square roots of the diagonal elements of $P(t_k)$ and $P^*(t_{\bar{k}})$, respectively. (C20)

Then,

$$\begin{aligned}\Delta P^* &= DP^2(t_k) - DP^2(t_{\bar{k}}) \\ &= [DP(t_{\bar{k}}) + P_w^{1/2}]^2 - DP^2(t_{\bar{k}}) \\ &= P_w + 2DP(t_{\bar{k}})P_w^{1/2}\end{aligned} \tag{C21}$$

The required ΔP is then found by first transforming ΔP^* from the actual ALT, ALONG-TRACK, CROSS-TRACK system into the reference ALT, ALONG-TRACK, CROSS-TRACK system using the actual angular deviations from the reference (found earlier) to compute a transformation matrix T_A. Once this process is accomplished, a second transformation is made to the X, Y, Z coordinate system using the transformation matrix T. Thus,

$$\Delta P = \begin{bmatrix} TT_A & O \\ O & TT_A \end{bmatrix} \Delta P^* \begin{bmatrix} TT_A & O \\ O & TT_A \end{bmatrix}^T \tag{C22}$$

Derivation of ΔX_E

The vector ΔX_E is computed in a manner completely analogous to the procedure used to compute ΔX_A. Therefore, only the differences will be emphasized here.

The angular deviations from the actual path must be found using the updated elements of $DP(t_k)$ which are also the square roots of the diagonal elements of $P^*(t_k)$. The deviation angles are then found from

$$\begin{bmatrix} \tilde{\theta} \\ \tilde{\beta} \\ \tilde{\psi} \end{bmatrix} = \begin{bmatrix} P_{44}^{*\,1/2}(t_k)/|V_E|U_1 \\ P_{55}^{*\,1/2}(t_k)U_2 \\ P_{66}^{*\,1/2}(t_k)/|V_E|U_3 \end{bmatrix} \tag{C23}$$

where the U_i, $i = 1$, 2, and 3, are Gaussian, zero mean, unit variance, random number samples. The estimated quantities are produced by adding to the samples in equation (C2) the deviation obtained from equation (C23). Thus,

$$\begin{bmatrix} \Delta\hat{\theta} \\ \Delta\hat{s} \\ \Delta\hat{\psi} \end{bmatrix} = \begin{bmatrix} \Delta\theta \\ \Delta s \\ \Delta\psi \end{bmatrix} + \begin{bmatrix} \tilde{\theta} \\ \tilde{s} \\ \tilde{\psi} \end{bmatrix} \tag{C24}$$

From this point, the derivation follows that of ΔX_A exactly, except that the estimated quantites found in equation (C24) are used instead of the actual quantites found in equation (C2). When all the elements of $\Delta X_E^*(t_k)$ have been found as in equations (C7) through (C9), then a transformation matrix T_E is found from the error angles in equation (C23). The required transformation equivalent to the expression in (C10) is

$$\Delta X_E(t_k) = \begin{bmatrix} TT_E & 0 \\ 0 & TT_E \end{bmatrix} \Delta X_E^*(t_k) \tag{C25}$$

APPENDIX D

DERIVATION OF THE MEASUREMENT JACOBIAN MATRICES FOR LORAN-C, VORTAC/TACAN, DOPPLER RADAR, AND RADIO AND BAROMETRIC ALTIMETERS

Each time a data-set is processed by the Kalman filter, a measurement Jacobian or H matrix is required which relates changes in each measured quantity to changes in each of the state variables. These matrices, which are evaluated on the reference trajectory, are derived in the following sections. The basic coordinate system defined by the unit vectors $\hat{i}$, $\hat{j}$, and $\hat{k}$ is the usual geographic system rotating with the earth, as shown in sketch (Da).

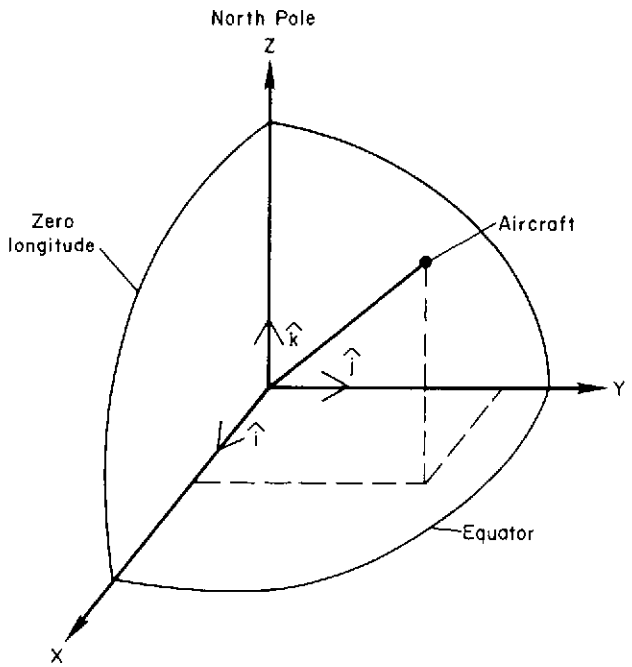

Sketch (Da)

LORAN-C

Loran-C position fixes are obtained by simultaneously measuring two time differences between radio signals received from a three-station triad. These time differences are then fed to a coordinate converter which, knowing the position coordinates of the three-station triad, computes the latitude and longitude of the aircraft. The measurement Jacobian matrix, H_L, is of the form:

$$H_L = \begin{bmatrix} \frac{\partial(Lat)}{\partial X} & \frac{\partial(Lat)}{\partial Y} & \frac{\partial(Lat)}{\partial Z} \\ \frac{\partial(Long)}{\partial X} & \frac{\partial(Long)}{\partial Y} & \frac{\partial(Long)}{\partial Z} \end{bmatrix} \tag{D1}$$

Each element of H_L is evaluated from:

$$Lat = \sin^{-1} \frac{Z}{R} \tag{D2}$$

$$Long = \tan^{-1} \frac{Y}{X} \tag{D3}$$

$$R = (X^2 + Y^2 + Z^2)^{1/2} \tag{D4}$$

Taking partial derivatives, we have:

$$H_L = \frac{1}{R^2 d^2} \begin{bmatrix} -XZd & -YZd & d^3 \\ -R^2 Y & R^2 X & 0 \end{bmatrix} \tag{D5}$$

where

$$d = (X^2 + Y^2)^{1/2} \tag{D6}$$

VORTAC/TACAN

For both VORTAC and TACAN, it is assumed that slant range and bearing to the ground station from the aircraft are measured simultaneously.

In sketch (Db), a typical configuration is shown. The slant range vector is from the ground station to the aircraft and the bearing angle, β, is measured from true north to the projection of the slant range vector onto the tangent plane at the ground station. In practice, bearing is measured from magnetic north, but the difference between true north and magnetic north is known at each station, and it is therefore assumed that this correction is stored in the computer to correct the measured bearing to true north. Also, when the on-board equipment measures the magnitude of the slant range vector, the on-board computer is assumed to have stored a predetermined bias correction which is applied prior to any further computations.

The following definitions are made for the geometric elements shown in this sketch:

1. The symbol β is the bearing from the VORTAC/TACAN ground station to the airborne receiver, measured clockwise from true north to the vector R_R.

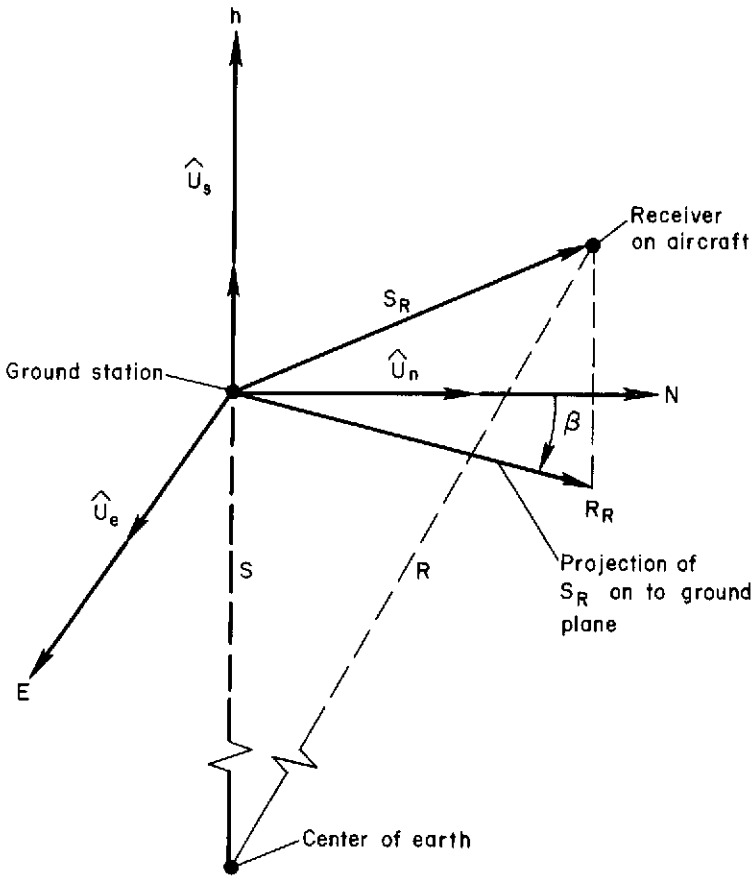

Sketch (Db)

2. The symbol S is a vector from the center of the earth to the ground station and is a constant vector for the particular VORTAC/TACAN station.

3. The symbol R is the current vector from the center of the earth to the on-board receiver.

4. The symbol S_R is the slant range vector from the ground station to the on-board receiver. It is the vector difference of R and S; that is, $S_R = R - S$.

5. The three unit vectors $\hat{U}_n$, $\hat{U}_e$, and $\hat{U}_s$ constitute a rectangular coordinate system. The unit vector $\hat{U}_s$, lies along the S vector. The unit vector, $\hat{U}_n$, lies perpendicular to S and in the direction of true north. The third unit vector, $\hat{U}_e$, which is perpendicular to both $\hat{U}_s$ and $\hat{U}_n$, completes the right-handed orthogonal coordinate system and lies to the east. These unit vectors are constant for a particular ground station and are computed from the following relationships:

$$\hat{U}_s = \frac{S}{|S|} \tag{D7}$$

$$\hat{U}_e = \frac{\hat{U}_s \times \hat{k}}{|\hat{U}_s \times \hat{k}|} \tag{D8}$$

$$\hat{U}_n = \frac{\hat{U}_e \times \hat{U}_s}{|\hat{U}_e \times \hat{U}_s|} \tag{D9}$$

6. The symbol R_R is the projection of the slant range vector, S_R, onto the ground plane defined by the unit vectors $\hat{U}_n$ $\nabla\sim\Phi$ $\hat{U}_e$.

The measurement Jacobian matrix, H_V, is of the form:

$$H_V = \begin{bmatrix} \frac{\partial \beta}{\partial X} & \frac{\partial \beta}{\partial Y} & \frac{\partial \beta}{\partial Z} \\ \frac{\partial |S_R|}{\partial X} & \frac{\partial |S_R|}{\partial Y} & \frac{\partial |S_R|}{\partial Z} \end{bmatrix} \tag{D10}$$

To find the required partial derivatives of the bearing angle, β, the component of the slant range in the northerly and easterly directions are found using the slant range vector and the unit vectors, $\hat{U}_n$ and $\hat{U}_e$, as follows:

$$N = S_R \cdot \hat{U}_n = R_R \cos \beta \tag{D11}$$

$$E = S_R \cdot \hat{U}_e = R_R \sin \beta \tag{D12}$$

from which

$$R_R^2 = N^2 + E^2 \tag{D13}$$

The partial derivative of β with respect to N is found by taking the partial derivative of both sides of equation (D11) which yields

$$\frac{\partial \beta}{\partial N} = \frac{1}{E}\left(\frac{\partial R_R}{\partial N} \cos \beta - 1\right) \tag{D14}$$

To evaluate $\partial R_R / \partial N$, both sides of equation (D13) are differentiated with the result

$$\frac{\partial R_R}{\partial N} = \frac{N}{R_R} \tag{D15}$$

so that

$$\frac{\partial \beta}{\partial N} = \frac{1}{E}\left(\frac{N}{R_R}\cos\beta - 1\right) = \frac{-E}{R_R^2} = \frac{-\sin\beta}{R_R} \tag{D16}$$

Using equations (D12) and (D13), the partial derivative of β with respect to E is found in a manner analogous to that just described. This process results in the expression

$$\frac{\partial \beta}{\partial E} = \frac{N}{R_R^2} = \frac{\cos\beta}{R_R} \tag{D17}$$

Since β lies in a plane perpendicular to the local vertical at the ground stations, it has no component along $\hat{U}_s$. Therefore

$$\frac{\partial \beta}{\partial h} = 0 \tag{D18}$$

The upper row of H_v is a row matrix of the coefficients of the gradient of the scalar bearing angle, β, in the $\hat{i}$, $\hat{j}$, $\hat{k}$ coordinate system. Since the gradient of a scalar is invariant under a unity orthogonal transformation, the gradient of β in the $\hat{i}$, $\hat{j}$, $\hat{k}$ system may be found by transforming the gradient of β in the $\hat{U}_n$, $\hat{U}_e$, $\hat{U}_s$ system into the $\hat{i}$, $\hat{j}$, $\hat{k}$ system. The required transformation matrix is the transpose of a matrix composed of the unit column vectors $\hat{U}_n$, $\hat{U}_e$, and $\hat{U}_s$, which have already been found. Thus,

$$\left[\frac{\partial \beta}{\partial X}\ \frac{\partial \beta}{\partial Y}\ \frac{\partial \beta}{\partial Z}\right] = \left[\frac{\partial \beta}{\partial N}\ \frac{\partial \beta}{\partial E}\ \frac{\partial \beta}{\partial h}\right]\left[\hat{U}_n\ \hat{U}_e\ \hat{U}_s\right]^T \tag{D19}$$

is the required matrix equation for the upper row of H_V.

To find the elements for the lower row of H_V, the slant range may be expressed as

$$S_R = |R - S| = [(X - S_1)^2 + (Y - S_2)^2 + (Z - S_3)^2]^{1/2} \tag{D20}$$

where

$$R = X\hat{i} + Y\hat{j} + Z\hat{k} \tag{D21}$$

and

$$S = S_1\hat{i} + S_2\hat{j} + S_3\hat{k} \tag{D22}$$

The partial derivatives of the slant range, $|S_R|$, with respect to, X, Y, and Z are:

$$\frac{\partial|S_R|}{\partial x} = \frac{X - S_1}{|S_R|} \tag{D23}$$

$$\frac{\partial|S_R|}{\partial Y} = \frac{Y - S_2}{|S_R|} \tag{D24}$$

$$\frac{\partial|S_R|}{\partial Z} = \frac{Z - S_3}{|S_R|} \tag{D25}$$

Thus, the lower row of H_v is given by

$$\left[\frac{\partial|S_R|}{\partial X} \; \frac{\partial|S_R|}{\partial Y} \; \frac{\partial|S_R|}{\partial Z}\right] = \frac{1}{|S_R|}\left[(X - S_1) \; (Y - S_2) \; (Z - S_3)\right] \tag{D26}$$

Doppler Radar

A Doppler radar system is assumed which measures the ground speed, $|V|$, and the angle (drift angle, γ) of the ground track from the longitudinal axes of the airframe projected in the horizontal plane. These measurements are independent of the aircraft position.

The Jacobian measurement matrix, H_D, of the velocity and drift angle is defined as:

$$H_D = \begin{bmatrix} \frac{\partial|V|}{\partial\dot{x}} & \frac{\partial|V|}{\partial\dot{y}} & \frac{\partial|V|}{\partial\dot{z}} \\ \\ \frac{\partial\gamma}{\partial\dot{x}} & \frac{\partial\gamma}{\partial\dot{y}} & \frac{\partial\gamma}{\partial\dot{z}} \end{bmatrix} \tag{D27}$$

The groundspeed is the speed of the aircraft along the reference trajectory so that

$$|V|^2 = \dot{x}^2 + \dot{y}^2 + \dot{z}^2 \tag{D28}$$

The elements of the upper row of H_D are found by taking the partial derivatives of $|V|$ with respect to each of the velocity components. The resulting upper row is

$$\left[\frac{\partial|V|}{\partial\dot{x}} \quad \frac{\partial|V|}{\partial\dot{y}} \quad \frac{\partial|V|}{\partial\dot{z}}\right] = \frac{1}{|V|}\begin{bmatrix}\dot{X} & \dot{Y} & \dot{Z}\end{bmatrix} \tag{D29}$$

To evaluate the partial derivatives in the lower row of H_D, we define a new orthogonal coordinate system in which the unit vector $\hat{U}_2$ is tangent to the ground track, a second unit vector $\hat{U}_1$ is along the local vertical at the aircraft, and a third unit vector is perpendicular to $\hat{U}_1$ and $\hat{U}_2$, such that a right-handed system is formed. The relationship of the ground-speed and drift angle to the $\hat{U}_1$, $\hat{U}_2$, and $\hat{U}_3$ coordinate system is shown in sketch (Dc).

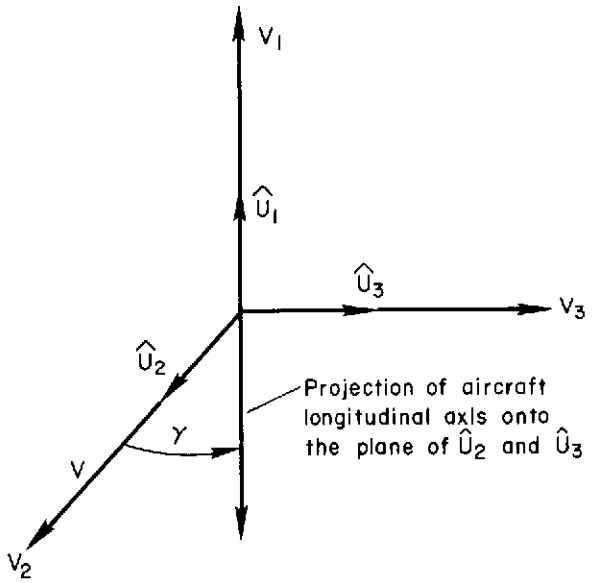

Sketch (De)

The unit vectors $\hat{U}_1$, $\hat{U}_2$, and $\hat{U}_3$ are found from the following relationships:

$$\hat{U}_1 = \frac{R}{|R|} \tag{D30}$$

$$\hat{U}_3 = \frac{V\times R}{|V\times R|} \tag{D31}$$

$$\hat{U}_2 = \frac{\hat{U}_1\times\hat{U}_3}{|\hat{U}_1\times\hat{U}_3|} \tag{D32}$$

Following the same general arguments as were used to find the partial derivatives of the VORTAC/TACAN bearing, we find the lower row of H_D in the $\hat{U}_1$, $\hat{U}_2$, $\hat{U}_3$ coordinate system to be:

$$\begin{bmatrix} \frac{\partial \gamma}{\partial V_1} & \frac{\partial \gamma}{\partial V_2} & \frac{\partial \gamma}{\partial V_3} \end{bmatrix} = \frac{1}{|V|} \begin{bmatrix} 0 & 1 & 0 \end{bmatrix} \tag{D33}$$

Again following the argument used with the VORTAC/TACAN bearing, the required transformation matrix is the transpose of a matrix which has as its columns the unit vectors $\hat{U}_1$, $\hat{U}_2$, and $\hat{U}_3$. Therefore, the final lower row in the H_D matrix is found using equation (D33) and this transformation matrix as follows:

$$\begin{aligned} \begin{bmatrix} \frac{\partial \gamma}{\partial \dot{x}} & \frac{\partial \gamma}{\partial \dot{y}} & \frac{\partial \gamma}{\partial \dot{z}} \end{bmatrix} &= \frac{1}{|V|} [0 \ 1 \ 0][\hat{U}_1 \ \hat{U}_2 \ \hat{U}_3]^T \\ &= \frac{1}{|V|} \hat{U}_2{}^T \end{aligned} \tag{D34}$$

Radio and Barometric Altimeters

The radio altimeter and the barometric altimeter (which is compensated for in air data computer) both produce altitude and altitude rate information.

The altitude is given by the magnitude of a vector from the center of the earth to the aircraft, R, minus the radius of the earth, R_o:

$$h = |R| - R_o = (X^2 + Y^2 + Z^2)^{1/2} - R_o \tag{D35}$$

The altitude rate $\dot{h}$ is the component of the velocity along the R vector, that is

$$\dot{h} = \frac{R \cdot V}{|R|} = \frac{X\dot{X} + Y\dot{Y} + Z\dot{Z}}{|R|} \tag{D36}$$

The Jacobian matrix H_A is defined as

$$H_A = \begin{bmatrix} \frac{\partial h}{\partial X} & \frac{\partial h}{\partial Y} & \frac{\partial h}{\partial Z} & 0 & 0 & 0 \\ \frac{\partial \dot{h}}{\partial X} & \frac{\partial \dot{h}}{\partial Y} & \frac{\partial \dot{h}}{\partial Z} & \frac{\partial \dot{h}}{\partial \dot{X}} & \frac{\partial \dot{h}}{\partial \dot{Y}} & \frac{\partial \dot{h}}{\partial \dot{Z}} \end{bmatrix} \tag{D37}$$

or

$$H_A = \frac{1}{|R|}\left[\begin{array}{c|c|c|c|c|c} X & Y & Z & 0 & 0 & 0 \\ \hline \dot{X} - \dot{h}\frac{X}{|R|} & \dot{Y} - \dot{h}\frac{Y}{|R|} & \dot{Z} - \dot{h}\frac{Z}{|R|} & X & Y & Z \end{array}\right] \qquad \text{(D38)}$$

APPENDIX E

FIXED-TIME-OF-ARRIVAL COURSE CORRECTIONS

Course corrections are intended to return the aircraft to the reference path and to arrive there at a specific time. These corrections, which will be based on the aircraft estimated state, are computed from a course correction law. This course correction law is a fixed-time-of-arrival law which allows computation of a commanded change in speed, Δs, a commanded change in aircraft heading, $\Delta\psi$, and a commanded change in aircraft pitch, $\Delta\theta$. In this implementation, the commanded changes in the first correction maneuver will be required to accomplish the desired correction of position error in a fixed length of time, Δt. At the end of the time Δt, a second correction maneuver will be required to aline the aircraft velocity vector along the desired reference path.

Derivation of Δv

The expression for computing the commanded course correction, Δv, will be derived in this section. This Δv is the vector change in velocity which will cause the predicted position error to be zero at some time Δt following the execution of the correction. If the correction is the first maneuver in the course correction, then Δt is a fixed interval of time. If the correction is the second maneuver, then Δt is the time-to-go to the destination.

Assuming the course correction is to take place at time t_k, a transition matrix $\phi(t_k + \Delta t, t_k)$ is computed from the equations of motion, the reference state, and the estimated altitude rate. Let $\Phi(t_k + \Delta t, t_k)$ be partitioned in to 3×3 submatrices as follows:

$$\Phi(t_k + \Delta t, t_k) = \begin{bmatrix} \Phi_1 & \Phi_2 \\ \Phi_3 & \Phi_4 \end{bmatrix} \tag{E1}$$

Also, let the column vector, $\hat{x}$, which is defined at the estimated deviation from the reference state, be partitioned into two 3×1 submatrices:

$$\hat{x}(t_k) = \begin{bmatrix} \hat{x}_1(t_k) \\ \hat{x}_2(t_k) \end{bmatrix} \tag{E2}$$

where $\hat{x}_1$ is the position portion and $\hat{x}_2$ is the velocity portion. Using the upper half of the partitioned transition matrix, the predicted position error at $t_k + \Delta t$ may be computed from

$$\hat{x}_1(t_k + \Delta t) = \left[\Phi_1(t_k + \Delta t, t_k) \,\vdots\, \Phi_2(t_k + \Delta t, t_k)\right] \begin{bmatrix} \hat{x}_1(t_k) \\ \\ \hat{x}_2(t_k) \end{bmatrix} \tag{E3}$$

where $\Phi_1(t_k + \Delta t, t_k)\hat{x}_1(t_k)$ and $\Phi_2(t_k + \Delta t, t_k)\hat{x}_2(t_k)$ both predict position error at $t_k + \Delta t$. The first matrix product predicts position error due to position error at t_k and the second matrix product predicts the position error due to velocity error at t_k.

Equation (E3) may be used to find the commanded velocity correction by noting that the required velocity increment, when added to $\hat{x}_2(t_k)$, will cause the position error to be zero at $t_k + \Delta t$. Thus, equation (E3) becomes

$$0 = \left[\Phi_1(t_k + \Delta t, t_k) \,\vdots\, \Phi_2(t_k + \Delta t, t_k)\right] \begin{bmatrix} \hat{x}_1(t_k) \\ \\ \hat{x}_2(t_k) + \Delta v \end{bmatrix} \tag{E4}$$

The desired value of the velocity correction is found by solving equation (E4) for Δv. The result is

$$\begin{aligned} \Delta v &= -\left[\Phi_2^{-1}(t_k + \Delta t, t_k)\Phi_1(t_k + \Delta t, tk) \,\vdots\, I\right]\hat{x}(t_k) \\ &= B\hat{x}(t_k) \end{aligned} \tag{E5}$$

Implementation of the Δv Correction

Having determined Δv from equation (E5), the equivalent changes in heading, $\Delta\psi$, pitch, $\Delta\theta$, and the speed correction, Δs, can be computed.

To find the angular changes $\Delta\psi$ and $\Delta\theta$, a coordinate system is defined in which the unit vector $\hat{u}_x$ lies along the estimated velocity vector V_E, the unit vector $\hat{u}_y$ is perpendicular to the plane of $\hat{u}_x$ and the radius vector from the center of the earth, and the unit vector $\hat{u}_z$ is directed upward, perpendicular to the plane of $\hat{u}_x$ and $\hat{u}_y$, so as to form a right-handed coordinate system. This coordinate system is shown in sketch, (Ea) which also shows the vector Δv and its components Δv_x, Δv_y, and Δv_z, as well as the desired final velocity V_f in the coordinate system just defined.

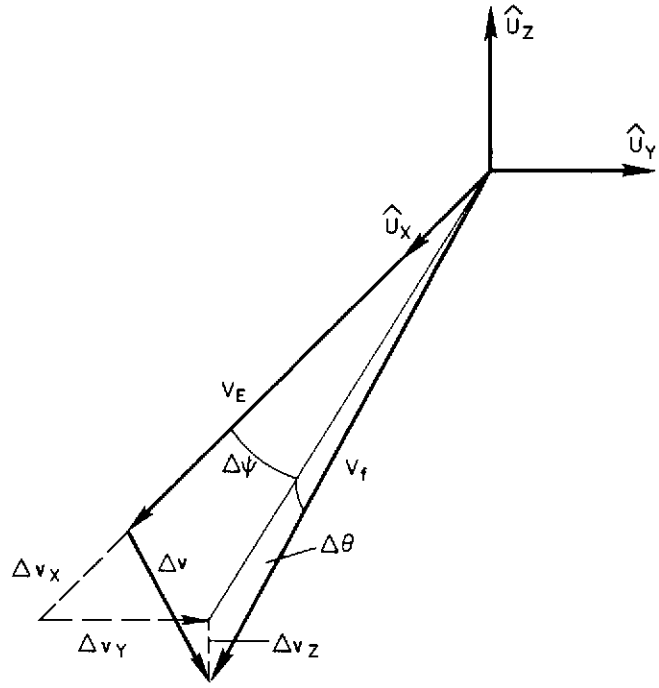

Sketch (Ea)

In this sketch, the angle between V_E and V_f in the $\hat{u}_x$, $\hat{u}_y$ plane is the change in heading, $\Delta\psi$, and is found from the expression

$$\tan \Delta\psi = \frac{\Delta v_y}{|V_E| + \Delta v_x} \tag{E6}$$

where

$$\left[\Delta v_x \ \Delta v_y \ \Delta v_z\right] = \Delta v^T \left[\hat{U}_x \ \hat{U}_y \ \hat{U}_z\right] \tag{E7}$$

Similarly, the pitch change angle, $\Delta\theta$, is found from

$$\tan \Delta\theta = \frac{\Delta v_z}{|V_E| + \Delta v_x} \tag{E8}$$

The speed correction (assuming the pitch and heading changes are executed first) is given by

$$\Delta s = |V_f| - |V_E| = |V_E + \Delta v| - |V_E| \tag{E9}$$

Course Correction Execution Error Statistics

A new coordinate system, $\hat{u}_x{}^1$, $\hat{u}_y{}^1$, $\hat{u}_z{}^1$, is defined which is the same as that shown in the preceding sketch, except that $\hat{u}_x{}^1$ lies along V_f. This coordinate system is shown in sketch (Eb). In addition, the actual executed velocity, V_e, is shown along with the random error in measuring the changes in the pitch and heading angles, $\delta\theta$ and $\delta\psi$.

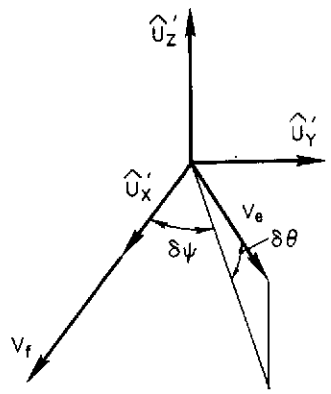

Sketch (Eb)

The vectors V_f and V can be expressed in matrix notation using the technique developed in reference 11. Thus, after defining δs to be the error in measuring Δs we have

$$V_f = |V_f| M \begin{bmatrix} 1 \\ 0 \\ 0 \end{bmatrix} \tag{E10}$$

and

$$V_e = \left(|V_f| + \delta s\right) M \begin{bmatrix} \cos\delta\theta \cos\delta\psi \\ \cos\delta\theta \sin\delta\psi \\ \sin\delta\theta \end{bmatrix} \tag{E11}$$

where M is a transformation matrix which relates the $\hat{u}_x{}^1$, $\hat{u}_y{}^1$, $\hat{u}_z{}^1$ coordinate system to the reference ALT, ALONG-TRACK, CROSS-TRACK coordinate system. The angles $\delta\theta$ and $\delta\psi$ are small angles, so that the following approximations are made:

$$\left.\begin{aligned} \cos \delta\theta &= 1 \\ \cos \delta\psi &= 1 \\ \sin \delta\theta &= \delta\theta \\ \sin \delta\psi &= \delta\psi \end{aligned}\right\} \tag{E12}$$

Equation (E12) now becomes

$$V_e = (|V_f| + \delta s)M \begin{bmatrix} 1 \\ \delta\psi \\ \delta\theta \end{bmatrix} \tag{E13}$$

The error in making the course correction is

$$\begin{aligned} \eta &= V_e - V_f \\ &= (|V_f| + \delta s)M \begin{bmatrix} 1 \\ \delta\psi \\ \delta\theta \end{bmatrix} - |V_f|M \begin{bmatrix} 1 \\ 0 \\ 0 \end{bmatrix} \\ &= |V_f|M \begin{bmatrix} 0 \\ \delta\psi \\ \delta\theta \end{bmatrix} + \delta s M \begin{bmatrix} 1 \\ \delta\psi \\ \delta\theta \end{bmatrix} \end{aligned} \tag{E14}$$

The covariance matrix of the errors in making the correction is found by taking the expected value of $\eta\eta^T$. Thus

$$E(\eta\eta^T) = E(|V_f|^2)M \begin{bmatrix} 0 & 0 & 0 \\ 0 & \sigma_\psi{}^2 & 0 \\ 0 & 0 & \sigma_\theta{}^2 \end{bmatrix} M^T + \sigma_s{}^2 M \begin{bmatrix} 1 & 0 & 0 \\ 0 & \sigma_\psi{}^2 & 0 \\ 0 & 0 & \sigma_\theta{}^2 \end{bmatrix} M^T \tag{E15}$$

where the following definitions have been made:

$$\left.\begin{aligned} E(\delta\theta^2) &= \sigma_\theta^2 \\ E(\delta\psi^2) &= \sigma_\psi^2 \\ E(\delta s^2) &= \sigma_s^2 \end{aligned}\right\} \tag{E16}$$

In addition, it has been assumed that $\delta\theta$, $\delta\psi$, and δs are independent random variables with zero means and that δs is independent of V_f.

To evaluate $E(|V_f|^2)$, note that

$$|V_f|^2 = (V_E + \Delta v)\cdot(V_E + \Delta v) \tag{E17}$$

After expanding, taking the expected value of both sides, and noting that V_E is a constant vector, we have

$$E(|V_f|^2) = |V_E|^2 + 2E(V_E\cdot\Delta v) + E(\Delta v\cdot\Delta v) \tag{E18}$$

The course correction vector, Δv, is assumed to be spherically distributed with zero mean. While this assumption is not particularly good, it does not lead to a significant error because of the dominance of the estimated velocity vector V_E. The main reason for making the assumption is its simplification of the expressions given below.

With the above assumption, the expected value of each component of Δv will have a zero mean. Therefore,

$$E(V_E\cdot\Delta v) = 0 \tag{E19}$$

To simplify, let the following definition be made:

$$E(\Delta v\cdot\Delta v) = \Delta v_{rms}^2 \tag{E20}$$

Equation (D19) now becomes

$$E(|V_f|^2) = |V_E|^2 + \Delta v_{rms}^2 \tag{E21}$$

where Δv_{rms} is the *rms* computed correction. The quantity Δv_{rms} can be found by noting that

$$\Delta v_{rms}^2 = Trace\ E(\Delta v\ \Delta v^T) \tag{E22}$$

Using equation (E5), equation (E22) becomes

$$\Delta v_{rms}^2 = Trace\ BE(\hat{x}\hat{x}^T)B^T \tag{E23}$$

In reference 1, it is shown that

$$E(\hat{x}\hat{x}^T) = R(t_k^-) - P(t_k^-) \tag{E24}$$

so that

$$\Delta v_{rms}^2 = Trace\ B\left[R(t_k^-) - P(t_k^-)\right]B^T \tag{E25}$$

where the matrix $R(t_k)$ is a covariance matrix of the errors in the deviations of the actual state from the reference state and $P(t_k)$ is a covariance matrix of the errors between the actual and estimated states. Using the above expressions, equation (E16) may now be written as:

$$E(\eta\eta^T) = \left\{|V_E|^2 + Trace\ B\left[R(t_k^-) - P(t_k^-)\right]B^T\right\}M\begin{bmatrix}0 & 0 & 0\\ 0 & \sigma_\psi^2 & 0\\ 0 & 0 & \sigma_\theta^2\end{bmatrix}M^T$$

$$+ \sigma_s^2 M\begin{bmatrix}1 & 0 & 0\\ 0 & \sigma_\psi^2 & 0\\ 0 & 0 & \sigma_\theta^2\end{bmatrix}M^T \tag{E26}$$

Correction of $P(t_k)$ and $R(t_k)$

Following a course correction, the covariance matrices P and R must be corrected for the random errors which were generated by the course correction process. The basic expressions for this correction are derived in reference 1 and will not be repeated here. Instead, the final results will be discussed.

The expression for correcting the $P(t_k^-)$ matrix for the added errors resulting from a course correction is:

$$P(t_k) = P(t_k^-) + \begin{bmatrix}0 & 0\\ 0 & E(\eta\eta^T)\end{bmatrix} \tag{E27}$$

where all submatrices are 3×3.

To correct $R(t_k^-)$, first let

$$G = \begin{bmatrix} 0 \\ --- \\ B \end{bmatrix} \tag{E28}$$

where B is 3×6 and G is 6×6. Then the expression for $R(t_k)$ is given by:

$$R(t_k) = (I + G)\left[R(t_k^-) - P(t_k^-)\right](I + G)^T + P(t_k) \tag{E29}$$

REFERENCES

1. McLean, John D.; Schmidt, Stanley F.; and McGee, Leonard A.: Optimal Filtering and Linear Prediction Applied to a Midcourse Navigation System for the Circumlunar Mission. NASA TN D-1208, 1962.

2. Anon.: U. S. Coast Guard, Wash., D.C.: The Loran-C System of Navigation. Jansky and Bailey, Inc., Feb. 1962.

3. DeGroot, L. E.: Navigation and Control From Loran-C. Navigation. J. Inst. Navig., vol. 11, no. 3, autumn 1964, pp. 213-227.

4. Razin, Sheldon: Explicit (Noniterative) Loran Solution. Navigation J. Inst. Navig., vol. 14, no. 3, fall 1967, pp. 265-269.

5. Anon.: DOD Flight Information Publication: Planning International Rules and Procedures and IFR-Supplement, United States. The Aeronautical Chart and Information Center USAF, St. Louis, Missouri, Jan. 17, 1969.

6. Pritchard, John S.: The VOR/DME/TACAN System, Its Present State and Its Potential. IEEE Trans. Aerosp. Navig. Electron., vol. ANE-12, no.1, Mar. 1965, pp. 6-10.

7. Dodington, Sven H.: Recent Improvements in Today's DME, IEEE Trans. Aerosp. Navig. Electron., vol. ANE-12, no. 1, Mar. 1965, pp. 67.

8. Height Measurement In Supersonic Aircraft, Cape, B,: Some Aspects of Pressure Measurement Techniques; and Garfield, W.L.: Radio Altimetry; J. Inst. Navig., vol. 19, no. 1, Jan. 1966, pp. 68-75.

9. Anon.: DOT, Air Traffic Service Federal Aviation Administration: En Route Air Traffic Control. FAA 7110.9, Oct. 1, 1967.

10. O'Day, James.; Sattinger, Irvin; Scott, Robert; and Sullivan, Joseph: Study and Analysis of Selected Long-Distance Navigation Techniques. Vol. 11. Final Report, FAA Contract (ARDS-436), Navigation and Guidance Laboratory, Inst. Sci. Technol., Univ. of Michigan, Mar. 1963.

11. White, John S.; Callas, George P.; and Cicolani, Luigi S.: Application of Statistical Filter Theory to the Interplanetary Navigation and Guidance Problem. NASA TN D-2697, 1965.

NASA-Langley, 1973 — 21 A-3505